HYDRODYNAMIC INTERACTIONS IN POLYMER DYNAMICS

Thesis by
John Edward Bauer

In Partial Fulfillment of the Requirements
for the Degree of
Doctor of Philosophy

California Institute of Technology
Pasadena, California

1992

(Defended September 24, 1991)

ACKNOWLEDGEMENTS

My time at Caltech has provided me with the opportunity for growth in many areas. While the growth in my understanding of chemical engineering, and research in general, has been substantial, those are by no means the only areas – – perhaps not even the most important. For these "lessons" I have had many teachers.

First, of course, I must thank my advisor, John Brady, for his patience and advice as I often struggled to find my own way in my research. This appreciation is tempered by the regret that we were never able to communicate comfortably. I believe we both have suffered from this, since I never felt I was able to reach my full potential in my work. I also thank the other members of my research group: Thanh Phung, Jeff Morris, Julia Lester, Lou Durlofsky, Phil Lovalenti, Prabhu Nott and Willem Boersma. Most of all, I wish to thank Roger Bonnecaze and Ivan Claeys for all their helpful discussions, providing insight into fluid mechanics and life in general; my conversations with them were always enjoyable.

Life as a graduate student is often difficult, and I doubt I could have gotten through without the wonderful companionship of the other members of what I have grown to consider as (excuse the hyperbole) the "Fabulous First-Year Five": Frank Doyle, Sarah Galt, Eric Hanczyc, and Dave Loren. We spent many hours together, both studying and relaxing, and this made the first year at Caltech more than bearable, it made it enjoyable. I am further indebted to Dave and Eric for their encouragement in my fledgling efforts to play softball and basketball. Indeed, one of my proudest moments at Caltech was the first time I drove to the basket and made a layup. Those non-ChE's, Matt Gursky and Chuck Krill, also made my first year (and later years) easier.

In subsequent years, Tammy and I had a lot of fun with Bob and Marcia Todd, going camping, playing golf, watching U of M football games, and just playing

cards or talking together. I also owe Bob a tremendous debt for his patience as my unofficial golf instructor. No doubt I saved thousands of dollars in private lessons just by playing an "occasional" nine holes with him.

In my "final" years at Caltech, I was again blessed with the company of Frank and Matt as we regularly "pumped iron" in the Caltech weight room. The great camaraderie I feel I developed with them more than made up for the occasional strained muscle. I must also thank Diana Rodriguez for the hospitality of many parties at Newport Beach. Tammy and I always enjoyed our time with her.

I must thank my parents, Dorothy and Raymond, both of whom I love very much. In addition to giving me the necessary genes for this accomplishment, they also instilled in me a love of science, a respect for hard work, the understanding that I am responsible for my actions, and much more. I cannot feel pride in my accomplishments without also feeling pride in what they have done for me.

Most importantly, I must thank my wonderful wife, Tammy. When I came to Caltech, I thought that my Ph.D. would be the most important thing I would gain here. I have never been more wrong. Throughout our time here, Tammy has always been loving, caring, and supportive. She was understanding when I had to work late, never complained although my small stipend made fancy vacations impossible, and always let me cry on her shoulder when things were not going well. During my last months at Caltech, when I thought about quitting because I perceived everything as conspiring against me, she never slapped me and told me to stop feeling sorry for myself. Instead she stood by me, held my hand, and reassured me that I could do it. As usual, she was right. In the end, the greatest lesson I learned at Caltech was not about science or chemical engineering. I learned how insignificant such things are when compared with the joy of going through life, learning and growing, together with someone as wonderful as she.

ABSTRACT

A modification to the traditional bead–spring model of polymers is proposed, which properly accounts for the full hydrodynamic interactions between the beads. The new model uses the Stokesian dynamics simulation technique to calculate far-field, many-body effects as well as near-field lubrication and excluded-volume effects. No preaveraging of the interactions is required. In addition to the **xF**, "spring" contribution to the stress, the Stokesian dynamics model calculates hydrodynamic and direct Brownian contributions to the stress.

Orientations and stresses obtained from the Stokesian dynamics dumbbell were compared to predictions of the Rouse dumbbell (no hydrodynamic interaction) and the Zimm dumbbell (Rotne-Prager hydrodynamic interaction). Infinite-dilution behaviors were examined in steady, simple shear and oscillatory shear flows. In steady shear the Stokesian dynamics model provides no improvement over the Zimm model. Both give qualitatively similar results for shear and normal stresses. The hydrodynamic stress is constant and equal to the Einstein viscosity contribution from each bead. The Brownian stress is negligible. The analysis reveals how hydrodynamic interaction causes shear thinning. The interaction between the beads tilts the dumbbell towards the shear axis, reducing the **xF** contribution to the shear stress. The oscillatory-shear results are similar to the steady-shear results, except that the hydrodynamic stress results in a non-zero high-frequency viscosity. Hydrodynamic and Brownian stresses will provide greater contributions to the rheology of multibead chains, in which many-body effects are more important. This is true of both steady shear and oscillatory shear.

Simulations of non-dilute suspensions of Stokesian dynamics dumbbells were compared with results for suspensions of spheres at the same volume fractions. The **xF** stress reaches a maximum at a bead volume fraction of 0.15, above which hydrodynamic forces dominate the solution rheology. The interparticle forces have little effect on the magnitudes of the hydrodynamic and Brownian stresses. The interparticle forces become very dependent upon initial configuration at high volume fractions. It is hypothesized that there exists a critical volume fraction, above which the polymer distribution function will always be dependent upon the initial configuration and the shear history.

Table of Contents

LIST OF TABLES AND FIGURES

TABLES

FIGURES

Note: Unless otherwise stated, all figures are for results from the Stokesian dynamics dumbbell model.

1. INTRODUCTION

The past quarter century has seen a striking increase in the use of plastics in our society. While consumer products such as cooking utensils, chairs and appliances were once constructed with wood, metal or ceramic, today they are constructed primarily from polymeric materials. Unfortunately, our understanding of polymers has not grown with our production of them. Their enormous molecular weights and twisted or branched structures lead to non-Newtonian rheological behavior, and the study of non-Newtonian fluids is a science still in its infancy. Polymer solutions and melts exhibit such unusual properties as shear-dependent viscosity and normal-stress differences. For these reasons a better understanding of polymer flow behavior would be of immense use in industry. Polymer production requires that the polymer be pumped, stirred, extruded, etc., and the present level of understanding makes the design of these processes difficult. A better understanding also would be appreciated from a purely scientific point of view, since it could provide insight into the nature of non-Newtonian flow in general.

This study suggests an improvement that can be made in the modeling of polymers. Because a polymer is made up of hundreds or even thousands of monomers, often it is not practical to examine each monomer and each bond in detail. For this reason a simplified micromechanical model often is used. The most popular choice is the bead–spring model, in which the polymer molecule is represented by a collection of beads connected by "springs." The bead–spring model will be used in this analysis. The aspect of polymer behavior addressed in this study is the relative importance of excluded-volume effects, hydrodynamic effects, and interparticle ("spring") and Brownian forces on the rheological behavior of a polymer in solution during flow. Particular attention is paid to an improved method of determining hydrodynamic interaction within the polymer. This is accomplished through dynamic simulation of a single polymer chain in a viscous, incompressible solvent subjected to either steady or oscillatory shear flow. Three different models will be used to describe the polymer molecule – – the Rouse model, the Zimm model, and the new Stokesian dynamics model. The Rouse model provides analytical, theoretical predictions, while the Zimm and Stokesian dynamics models provide results through numerical simulations on computer. An analysis of the resulting microstructures will be used to determine the viscosities predicted by each model. The Rouse and Zimm models calculate only the interparticle-force contribution to the stress. The Stokesian dynamics model provides the hydrodynamic and direct Brownian contributions to the stress, in addition to the interparticle-force contribution. Except for a few comparisons under oscillatory shear, the study is restricted to comparison of the 2 bead – 1 spring (dumbbell) versions of each model. Section 2.1 gives a brief history of the evolution of the treatment of hydrodynamic interaction in dilute-solution polymer theory, outlining the landmark work of Rouse, Zimm, Kirkwood and Riseman, and also recent work by Öttinger. The approximations used and resulting limitations are examined. Section 2.2 discusses Stokesian dynamics, a simulation method that allows, for the first time, accurate consideration of the full hydrodynamics problem. General aspects of the method are discussed, as well as the details of calculating the hydrodynamic interaction. The averaging methods with which macroscopic properties are extracted from the microscale results are explained. Section 3 discusses the equilibrium state for the models and also discusses the two flows that were examined, along with more detailed theory particular to each case. Section 4 compares the results of the Stokesian dynamics simulations to the results of the Zimm-model simulations and the predictions of the Rouse model discussed in §3. Particular attention is paid to finding ranges of flow parameters in which particular contributions to the stress are dominant, and when certain contributions may be neglected. Hydrodynamic interaction induces shear-thinning behavior in the polymer models by changing the microstructural orientation of the polymer. At higher shear rates this orientational change reduces the polymer contribution to the stress. In oscillatory shear, the more complete hydrodynamical description of the Stokesian dynamics model has the opposite effect. Inclusion of the hydrodynamic stress leads to a prediction of a non-zero high-frequency viscosity, which is absent in the Rouse and Zimm models.

Section 5 presents some preliminary results for suspensions of Stokesian dynamics dumbbells at concentrations above infinite dilution, subjected to steady shear flow. These results are obtained through the use of a fixed volume containing 20 dumbbells, periodically replicated throughout space. Just as the isolated-dumbbell results are used to gain insight into infinitely-dilute polymer solutions, these "suspensions" of dumbbells provide insight into the behavior of non-dilute solutions of polymers. The non-dilute results are compared to the infinitely dilute, or single-chain, Stokesian dynamics results of §4. A very brief overview of the changes to the simulation (e.g., application of periodic boundaries) is presented. It is found that the contribution to the stress from the interparticle springlike forces reaches a maximum at a dumbbell volume fraction of about 0.15, above which the rheology of the solution is dominated by hydrodynamic forces. This contradicts experimental results (e.g. Ferry, 1980) that indicate concentrated-solution rheology is dominated by the interparticle forces. This indicates a shortcoming in the dumbbell model: it cannot address the multiple length scales that are important in non-dilute solutions. The results are also compared with the results of Phung (1991) for suspensions of spheres not connected by interparticle forces. The presence of the interparticle forces has little effect on the shear-rate dependence of the hydrodynamic and Brownian stresses. An argument is made for the existance of a critical concentration, ϕ^*, above which the distribution of the polymer chains as time $t \to \infty$ will be dependent upon the initial configuration and flow history.

Aside from its prediction of a non-zero high-frequency viscosity, the Stokesian dynamics model has no advantages over the Zimm model for the dumbbell case. The more accurate hydrodynamic interactions in the Stokesian dynamics model produce an orientational distribution that is nearly identical to the much simpler Rotne-Prager interaction in the Zimm model. The calculations of the hydrodynamic and Brownian stresses are time-consuming, and these stresses turn out to be, respectively, essentially constant and negligibly small. The study of the Stokesian dynamics dumbbell does point out two improvements to be made to the bead-spring model. First, since the hydrodynamic stress is nearly constant, it can be superposed to the Rouse or Zimm results. This gives both these models the correct high-frequency behavior without altering the qualitative features of the low- and moderate-frequency regimes. Second, the zero Brownian-stress contribution points to an improvement that can be made to the traditional bead-spring model stress calculation. In the classic bead-spring model, no consideration is given to the angular distribution of the end-to-end vector of the dumbbell. As is known from the theory of rodlike polymers, the entropy associated with the orientational distribution of the end-to-end vector can generate a large contribution to the stress.

While it provides no advantages in the infinitely-dilute dumbbell case, the Stokesian dynamics model offers distinct advantages in studies of multibead chains and studies of concentrated polymer solutions. Unlike the dumbbell case, many-body effects are important in these cases, and 2-body hydrodynamic-interaction descriptions such as Rotne-Prager cannot capture the physics of many-bead arrangements. Excluded-volume effects also become important, particularly in the concentrated-solution case. Stokesian dynamics, with its complete evaluation of the excluded-volume constraint, is a powerful tool for concentrated-solution analysis. Models that lack excluded volume are missing a major force affecting the rheology of concentrated solutions.

Although this study examines properties only for uniform molecular-weight distributions, the method is not restricted to this. Stokesian dynamics can address polydispersity as well.

2. BACKGROUND

2.1 Treatment of Hydrodynamic Interaction in Dilute Polymer Theory

The two most familiar names in the field of polymer modeling are Rouse and Zimm. Both used the bead–spring model as the basis for their studies, but differed in one very important area – – hydrodynamic interaction. Rouse did not consider any interaction, while Zimm was the first investigator to include hydrodynamic interactions in the bead–spring model. Zimm's additions were based on the work of Kirkwood and Riseman (1948), which involved "preaveraging" the interactions based on the equilibrium, Gaussian distribution of configurations. Although the work of Kirkwood and Riseman actually preceded the work of Rouse, Rouse did not include their results in his development, so it is more logical to open this section with a discussion of Rouse's work. Rouse and Zimm are not the only ones who used the bead–spring model (see Bird *et al.* (1987) for an in-depth listing), but over time their names and their treatments of hydrodynamic interaction have become associated with the model. Recently Öttinger has developed a new approach to the averaging process that is not restricted to the equilibrium distribution. Öttinger also was the first to propose a method capable of introducing fluctuations in the interactions away from their averaged values. The advantages of Stokesian dynamics over each method will be discussed.

Rouse (1956) first proposed use of the bead–spring model. He did not use this expression, but rather spoke of "submolecules" within the polymer molecule – – groups of monomers sufficiently large so that the end-to-end separation of the submolecules obeyed a Gaussian distribution function. The only interaction between the polymer and fluid occurred at the junctions of these submolecules. Rouse assumed that these junctions (which would become known as "beads") experienced drag from the surrounding fluid, but did not disturb the fluid themselves. The junctions did not interact hydrodynamically with one another, nor did they contribute any hydrodynamic stress to the solution. Thus, Rouse's model could more appropriately be called a *point*–spring model, with the points providing no disturbance in the fluid. The model had M submolecules and $M - 1$ submolecule junctions. The configuration of the model was given by the M end-to-end vectors describing each submolecule.

Rouse considered the polymer's addition to the stress in a solution undergoing an oscillatory shear. He calculated the stress by considering the change in the free energy of the system caused by the thermodynamic Brownian forces acting to move the configuration of the submolecules back to its equilibrium distribution. This argument is equivalent to saying that the submolecule acts as an entropic spring. It can be shown (Bird *et al.* 1987) that if it is assumed that the monomer units along the polymer backbone can be described by a random walk, then the force **F** between two points in the polymer chain is given by

$$\mathbf{F}(\mathbf{r}) = \frac{3kT}{(N_S - 1)l^2}\mathbf{r} \quad , \tag{2.1}$$

where k is Boltzmann's constant, T is the absolute temperature, N_S is the number of steps between the two points, l is the size of the random step, and $\mathbf{r}$ is the vector separation of the two points. This describes the two points as being connected by a Hookean spring with spring constant $K = 3kT/(N_S - 1)l^2$. This argument is valid only near equilibrium and for large N_S, and it ignores excluded-volume effects and other interactions, but it is a useful first approximation.

Using this description, and assuming a shear flow $\mathbf{u}_x = \dot{\gamma}\mathbf{y}$, Rouse's equations of motion for the submolecules in the x, y and z directions are

$$\mathbf{u}_x = \mathbf{u}_x^{\infty} - B(K\mathbf{A}) \cdot \mathbf{x}, \tag{2.2a}$$

$$\mathbf{u}_y = -B(K\mathbf{A}) \cdot \mathbf{y}, \tag{2.2b}$$

$$\mathbf{u}_z = -B(K\mathbf{A}) \cdot \mathbf{z}, \tag{2.2c}$$

where $\mathbf{u}_i$ is an M vector specifying the i velocity of each submolecule, $\dot{\gamma}$ is the rate of strain, $\mathbf{u}_x^\infty$ is an M vector of the fluid velocity at each submolecule's midpoint, B is the mobility of the ends of the submolecules (a constant, averaged over all submolecules in the solution), and $\mathbf{x}$, $\mathbf{y}$ and $\mathbf{z}$ are M vectors specifying the positions of the submolecules. $\mathbf{A}$ is an $M \times M$ tensor that computes the sum of adjacent connector vectors to bead i and sets the magnitude and direction of the resulting "spring" forces,

$$A_{ij} = \begin{cases} 2 & \text{if } |i-j| = 0; \\ -1 & \text{if } |i-j| = 1; \\ 0 & \text{otherwise.} \end{cases} \tag{2.3}$$

Rouse did a normal mode analysis, which required the introduction of a matrix transformation to normal coordinates, $\mathbf{R}$, which would decouple the spring forces,

$$\mathbf{R}^{-1} \cdot \mathbf{A} \cdot \mathbf{R} = \mathbf{\Lambda} = \lambda_p \delta_{pq}, \quad \text{(no sum on } p\text{)}, \tag{2.4}$$

where λ_p is the pth eigenvalue of the set of M eigenvalues of $\mathbf{A}$,

$$\lambda_p = 4 \sin^2 \left(\frac{p\pi}{2M} \right) \quad . \tag{2.5}$$

Rouse was thereby able to relate these eigenvalues to the spectrum of modes or relaxation times of the polymer. These results are given in §3.3.

While Rouse's theory gave good agreement for the viscoelastic functions in oscillatory shear (§3.2), it still had some obvious shortcomings. It predicted that the viscosity and normal-stress differences in steady shear would all be independent of shear rate, in conflict with experimental evidence that showed most polymer solutions exhibited shear thinning. The intrinsic viscosity of a polymer, $[\eta]_0$, is defined as

$$[\eta]_0 = \lim_{c \to 0} \frac{(\eta - \eta_s)}{c\eta_s} \quad , \tag{2.6}$$

where $[\eta]_0$ is the intrinsic viscosity at zero shear rate, c is the concentration, η is the solution viscosity and η_s is the pure-solvent viscosity. Earlier works by

Staudinger (1932), Kuhn (1932), Huggins (1939) and Kramers (1946), using models that incorporated the same physics as the Rouse model, had concluded that it should be proportional to the polymer's molecular weight,

$$[\eta]_0 = CW^q, \tag{2.7}$$

where W is the molecular weight of the polymer, C is a constant characteristic of the particular polymer-solvent pair, and the exponent q should equal one. When experiments showed that q did not equal one, instead falling in the range of 0.5 to 0.8 (Bird *et al.* 1987), the models used in the derivation of (2.6) (similar to the Rouse model) were examined more closely. This examination revealed that the models made no allowance for the effect of the presence of the molecule on the flow field. Although each junction or bead in the models experienced a drag from the fluid moving past it, the complementary effect – – the disturbance of the flow field by the bead – – was not accounted for. Since it is well known that this disturbance decays as $1/r$, this was a critical aspect to overlook, especially since many flow situations will bring the beads in the model close together. The magnitude of this omission is revealed by consideration of a set of spheres, initially in a line, falling through an unbounded, viscous fluid. With no hydrodynamic interactions, the spheres will remain in a line. With hydrodynamic interactions, the spheres near the center of the arrangement will fall more rapidly, leaving the end spheres behind (Durlofsky *et al.* 1987).

In their paper, Kirkwood and Riseman (1948) introduced a method for calculating hydrodynamic interactions within the polymer models. Kirkwood and Riseman did not use the bead–spring model, instead examining a more molecularly based bead–rod model with fixed angles between successive rods. Nonetheless, their analysis of the hydrodynamics applies equally well to the bead–spring model.

Consider a single bead from the Rouse model or the Kirkwood-and-Riseman model, translating in a Newtonian fluid because of an imposed force. If the bead were isolated, then the force $\mathbf{F}$ exerted on the bead is related to the bead's velocity, $\mathbf{u}^0$, by the Stokes drag law,

$$\mathbf{F} = 6\pi\eta_s a \Delta\mathbf{u} \quad , \tag{2.8}$$

where a is the bead radius, $\Delta\mathbf{u} = \mathbf{U}^\infty - \mathbf{u}^0$ and $\mathbf{U}^\infty$ is the undisturbed fluid velocity at infinity evaluated at the bead center. The motion of the bead disturbs the flow field, and the disturbance alters the flow field at a vector distance $\mathbf{r}$ by an amount $\mathbf{u}'$, which, to leading order in bead size, is given by

$$\mathbf{u}' = \frac{1}{8\pi\eta_s r}\left[\left(\mathbf{I} + \frac{\mathbf{rr}}{r^2}\right) + \left(\frac{a}{r}\right)^2\left(\frac{1}{3}\mathbf{I} - \frac{\mathbf{rr}}{r^2}\right)\right]\cdot\mathbf{F} \quad , \tag{2.9a}$$

$$= \mathcal{J}\cdot\mathbf{F} + O\left(\frac{1}{r^3}\right), \tag{2.9b}$$

where $\mathbf{I}$ is the unit tensor, $\mathrm{r} = |\mathbf{r}|$ and $\mathcal{J} = [\mathbf{I} + \mathbf{rr}/r^2]/(8\pi\eta_s r)$, the *Oseen tensor.* Now, if there is a second bead at $\mathbf{r}$, it will feel the velocity disturbance $\mathbf{u}'$, and the $\Delta\mathbf{u}$ in Eq.(2.8) for this second bead becomes $\Delta\mathbf{u} = \mathbf{U}^\infty - \mathbf{u}^0 + \mathbf{u}'$. Kirkwood and Riseman made the simplification that

$$\mathbf{u}' = \mathcal{J}\cdot\mathbf{F} \quad , \tag{2.10}$$

i.e., that the $O(1/r^3)$ term is negligible. This approximation is justified if the beads are widely separated, so $1/r^3$ is small. This is the same as assuming the disturbance is a point disturbance, so a in Equation (2.9a) is taken to be zero and the fact that the size of the bead is non-zero is ignored. Since in general the beads are not required to be far apart, and in fact certain flow conditions will bring them close together, the validity of this assumption is questionable, and for very close separations the Oseen tensor leads to negative diffusivities. Furthermore, Kirkwood and Riseman found it necessary to average these approximated hydrodynamic interactions in order to solve the equations of motion for their model. They "preaveraged" the interactions; i.e., they used an Oseen tensor averaged over the equilibrium distribution function, given by

$$\langle \mathcal{J} \rangle_{eq} = \int \mathcal{J} \Psi_{eq} d\mathbf{r} \quad , \tag{2.11a}$$

$$= \frac{1}{6\pi\eta_s} \langle \frac{1}{r_{jk}} \rangle, \tag{2.11b}$$

$$= \frac{1}{(6\pi^3)^{\frac{1}{2}} \eta_s b(|j-k|)^{\frac{1}{2}}} \quad , \tag{2.11c}$$

where Ψ_{eq} represents the equilibrium distribution function for the polymer model, $\langle 1/r_{jk} \rangle$ is the average separation of beads j and k, and b is the rod length. This simplification, later used by Zimm and most other researchers, sets some terms to zero that in actuality are non-zero, leading to qualitatively improper results and incorrect physics. It also ignores fluctuations of the interactions. This further reduces the ability with which this method can accurately capture the true hydrodynamic interactions of the polymer.

Zimm (1956) attempted to improve Rouse's model by introducing hydrodynamic interaction between the beads. Zimm's springs were identical to Rouse's, but instead of assuming that the beads moved with the local fluid velocity, Zimm followed Kirkwood and Riseman in assuming that the beads produced a point-force disturbance in the fluid. Like Rouse, however, Zimm used the bead–spring model rather than the bead-rod model. Zimm used a pairwise sum to calculate the disturbed fluid velocity at any point in the fluid. The disturbance u_j' at the location of bead j is given by

$$u_j' = u_j + \sum_{j \neq k} \langle \mathcal{J}_{jk} \rangle_{eq} F_k, \tag{2.12}$$

where u_j is the undisturbed fluid velocity at bead j, $\langle \mathcal{J}_{jk} \rangle_{eq}$ is the equilibrium-averaged Oseen interaction, and F_k is the point-force disturbance of the k^{th} bead. Since Zimm did not consider any hydrodynamic contributions to the stress, and his beads had no finite size, his model could more appropriately be called a *point-force*–spring model. This addition of point-force interaction leads to the equations of motion for the spring segments

$$\mathbf{u}_x = \mathbf{u}_x^\infty - B\mathbf{H}\cdot(K\mathbf{A})\cdot\mathbf{x} - D\mathbf{H}\cdot\frac{\partial}{\partial\mathbf{x}}\ln\psi, \tag{2.13a}$$

$$\mathbf{u}_y = -B\mathbf{H}\cdot(K\mathbf{A})\cdot\mathbf{y} - D\mathbf{H}\cdot\frac{\partial}{\partial\mathbf{y}}\ln\psi, \tag{2.13b}$$

$$\mathbf{u}_z = -B\mathbf{H}\cdot(K\mathbf{A})\cdot\mathbf{z} - D\mathbf{H}\cdot\frac{\partial}{\partial\mathbf{z}}\ln\psi, \tag{2.13c}$$

differing from Rouse's equations of motion, Eqs.(2.2), by the additions of the diffusivity $D = kTB$, the bead probability-distribution function ψ, and the hydrodynamic mobility matrix H,

$$H_{ij} = \begin{cases} 1 & \text{if } i = j; \\ \frac{1}{B}\langle\mathcal{J}_{ij}\rangle_{eq} & \text{if } i \neq j. \end{cases} \tag{2.14}$$

The solution of Zimm's equation of motion, Eq. (2.13), again required the solution of an eigenvalue problem, this time

$$\mathbf{R}^{-1}\cdot\mathbf{H}\cdot\mathbf{A}\cdot\mathbf{R} = \mathbf{\Lambda} = \lambda_p\delta_{pq}, \quad \text{(no sum on } p\text{)}, \tag{2.15}$$

which is considerably more complex than Rouse's eigenvalue problem, Eq.(2.4). Zimm determined that in the case of large M, the components of the eigenvectors from (2.15) may be represented by a continuous function $\alpha(r)$, and the eigenvalues λ are found by solution of the equation

$$\alpha''(r) + h\int_{-1}^{1}\alpha''(s)\left(|r-s|\right)^{-\frac{1}{2}}\,ds = \left(\frac{-M^2}{4}\right)\lambda\alpha(r), \tag{2.16}$$

subject to the boundary condition for free ends,

$$\alpha'(\pm 1) = 0. \tag{2.17}$$

The predictions of the Zimm model based on these preaveraged time constants are given in §3.3.

The quantity h in Eq.(2.16) is known as the *hydrodynamic-interaction parameter*, and is defined by

$$h = \frac{M^{\frac{1}{2}}\zeta}{(12\pi^3)^{\frac{1}{2}}\, b\eta_s} \quad , \tag{2.18}$$

where ζ is the drag coefficient of a single bead and b is the RMS extension of a single spring. Using the Kirkwood-and-Riseman ζ value of $6\pi\eta_s a$ from Eq.(2.8), this becomes

$$h = \left(\frac{3M}{\pi}\right)^{\frac{1}{2}} \frac{a}{b} \quad . \tag{2.19}$$

Assuming a Boltzmann distribution for the spring extension, $P(r) = e^{-\frac{1}{2}Kr^2}$, then $b = (3kT/K)^{1/2}$, and

$$h = \left(\frac{MK}{\pi kT}\right)^{\frac{1}{2}} a \quad ; \tag{2.20}$$

h is a ratio of the hydrodynamic forces to the spring forces. When $h = 0$, the spring forces dominate, giving back the Rouse solution. This is often called the "free-draining" case, since it assumes that the fluid moves past each bead as though that bead were alone in the fluid; no consideration is given to the restriction of flow that is due to nearby beads. As $h \to \infty$, hydrodynamic forces dominate.

The M-dependence of h often is removed by defining a new parameter

$$h^* = \frac{h}{M^{\frac{1}{2}}} = \left(\frac{K}{\pi kT}\right)^{\frac{1}{2}} a \quad ; \tag{2.21}$$

h^*, though dimensionless, is not a traditional dimensionless number. Its value ranges from 0 to ≈ 0.5, not ∞. This is seen by taking Eq.(2.19) and dividing by $M^{1/2}$, giving

$$h^* = \left(\frac{3}{\pi}\right)^{\frac{1}{2}} \frac{a}{b}, \tag{2.22a}$$

$$\approx \frac{a}{b}, \tag{2.22b}$$

which shows that h^* may be thought of as a ratio of the bead size to the bead separation. At contact $b = 2a$; thus h^* must be less than 0.5. Because this study involves relatively small numbers of segments per chain, h^* will be used in all subsequent references as the hydrodynamic-interaction parameter.

Although Zimm did consider hydrodynamics in his model, it is important to note two major limitations to his analysis. First, the beads were treated only as point forces. No consideration was given to finite size of the polymer. Second and more importantly, the hydrodynamics were examined only insofar as they affected the configuration of the model, not as to how they might affect the stress in the fluid, and then only for equilibrium or preaveraged configurations. The hydrodynamic interactions influenced the bead separations, thus changing the extensions of the spring. It was through the changes in spring extensions and the resultant changes in the magnitude of the spring contribution to the stress that the inclusion of hydrodynamics caused the Zimm results to differ from those of Rouse. The interparticle spring-force contribution was still the only polymer contribution to the stress – – no hydrodynamic, excluded-volume or direct Brownian stresses were calculated. Section 4 presents results that suggest that the hydrodynamic stress dominates the polymer rheology during high-frequency, oscillatory shear.

By basing their calculation on equilibrium configurations and interactions, both Rouse and Zimm were restricted to calculations of equilibrium and near-equilibrium properties ($Pe \approx 0$). In recent years Öttinger (1985;1986a,b;1987;1989) has done extensive work on improving the description of hydrodynamic interactions in bead–spring models to loosen this restriction. Initially, he introduced the concept of "consistently averaged" interactions, which can be described roughly as an iterative approach to the Zimm interactions. In his development, Öttinger describes the behavior of the polymer through a diffusion equation for the configurational distribution function,

$$\frac{\partial\psi}{\partial t} = f(\psi, \langle \mathcal{J} \rangle, K, \mathbf{r}, \dot{\gamma}). \tag{2.23}$$

Öttinger does not average $\mathcal{J}$ based on Ψ_{eq}. Instead, he proposes a distribution ψ' and averages $\mathcal{J}$ over ψ',

$$\langle \mathcal{J} \rangle' = \int \mathcal{J} \psi' \, d\mathbf{r}, \tag{2.24}$$

then solves (2.23) using $\langle \mathcal{J} \rangle'$. If the final ψ does not match the initial ψ', an improved estimate of ψ' is made. This iteration is continued until a suitable level of convergence is obtained, resulting in $\psi(\kappa)$ and $\langle \mathcal{J}(\kappa) \rangle$. The consistently averaged approach is not limited to low Pe; it can be used to examine high Pe behavior.

Although the concept of consistently averaged hydrodynamic interactions removed the restriction to near-equilibrium behavior, it still ignored fluctuations in hydrodynamic interactions about the mean, which are known to have an important influence on polymer rheology (Fixman 1981 ; Zylka and Öttinger, 1989). Öttinger proposed that this problem be addressed by assuming *a priori* that the polymer distribution function ψ was always Gaussian. This allowed him to solve for ψ without having to perform any averaging of $\mathcal{J}$. As with the consistently averaged method, the Gaussian approximation can be used for high Pe. Öttinger found the agreement between numerical simulation and the Gaussian-approximation predictions of the stress to be excellent. Nonetheless, it is unclear what biases may be introduced by imposing a form on ψ. With Stokesian dynamics, no *a priori* decisions about the form of the ψ need be made. The interactions of all the forces at each time step sets the polymer configuration; fluctuations in the hydrodynamic interactions occur based on the calculated forces acting on these configurations. The only restriction is that sufficient initial configurations are chosen and simulation runs are long enough that the data do indeed give an accurate representation of the actual distribution. In addition, Öttinger still does not calculate any direct hydrodynamic contributions to the stress. As in Zimm's model, the interactions between the beads alter the distribution function of the beads, thereby changing the spring contribution to the stress. This interparticle stress remains the only stress calculated.

It should be noted that there are interaction descriptions other than the Oseen tensor, which may be used in all of the models discussed above. (In fact, for numerical simulations the Oseen tensor usually *cannot* be used, because it gives negative mobilities when the separation r is less than $1.5a$.) For instance, the effect of the finite size of the bead is approximated by the *Rotne-Prager tensor*,

$$\mathcal{J} = \frac{1}{8\pi\eta_s r} \begin{cases} \left[\left(1 + \frac{2a^2}{3r^2}\right)\mathbf{I} + \left(1 - \frac{2a^2}{r^2}\right)\frac{\mathbf{rr}}{r^2}\right] & (r \geq 2a) \\ \frac{r}{2a}\left[\left(\frac{8}{3} - \frac{3r}{4a}\right)\mathbf{I} + \frac{r}{4a}\frac{\mathbf{rr}}{r^2}\right] & (r < 2a). \end{cases} \tag{2.25}$$

But the application of this tensor and others based on the Oseen tensor still have some major shortcomings. First, the implementations of these tensors have not accounted for so-called reflected disturbances. As explained above, the effect of bead i on the $\mathbf{u}^\infty$ flow field at bead j is calculated as though bead i were moving at velocity $\mathbf{u}^0$. But $\mathbf{u}^0$ will be altered by the reflected disturbance of $\mathbf{u}_j$, and so on. Previous implementations have also assumed that the disturbances are pairwise additive, simply summing up the effects of the interaction as though each pair were alone in the fluid. This can lead to aphysical behavior, such as bead-bead overlap (Durlofsky *et al.* 1987). Stokesian dynamics accounts for the reflections and also calculates many-body effects accurately -- the pairwise-additivity assumption need not be invoked. In addition, most analyses do not address excluded-volume effects. These effects, when examined, usually are treated as a change in the distribution function, expanding the polymer. While this gives more realistic values for the end-to-end distance and radius of gyration, it does nothing to describe the physical problems involved in trying to move one portion of the polymer past another portion. Stokesian dynamics automatically accounts for excluded volume, preventing bead-bead overlap, and also accounts for the frictional hindrances through lubrication forces. Finally, the Oseen-like tensors become mathematically much more difficult if the beads are not of equal size. When the a_i are not equal, then 1) terms of the form M/ζ must be expanded as $1/\zeta_1 + 1/\zeta_2 + ... + 1/\zeta_M$, and 2) terms of the form $1/\zeta_i - 1/\zeta_j$ no longer cancel, and must be carried through while solving the problem. Although this study involves beads of equal size, this is not a restriction of the method. The extension of Stokesian dynamics to unequal bead sizes is straightforward, requiring only minor changes.

Many improvements on the description of the interparticle force as a Hookean spring are also possible, the most common being the Finitely Extensible Non-linear Elastic (FENE) spring force,

$$\mathbf{F}(\mathbf{r}) = \frac{K}{\left[1 - \left(r/r_0\right)^2\right]}\mathbf{r}, \tag{2.26}$$

($r = |\mathbf{r}|$), which is Hookean for small r but has a maximum extension of r_0. Stokesian dynamics is easily adaptable to this or to other spring potentials. Nonetheless, the Hookean spring is the most popular choice for interparticle potentials in polymer modeling because of its mathematical simplicity, and it is the potential used for this study.

Most previous work in polymer modeling has been based on the number of segments in the model, M. Since Stokesian dynamics was originally developed for the analysis of the rheology of suspensions of rigid particles, it is more convenient for this study to consider the number of beads in the model, $N = M + 1$. All subsequent formulae will be in terms of N.

2.2 Stokesian Dynamics Model

This section summarizes Stokesian dynamics, a method that is able to assess accurately the full hydrodynamics in the bead-spring model. The microstructural mechanics of the method will be discussed, explaining how the hydrodynamics is accounted for, and then the calculation of the macroscopic stress is explained. A more in-depth discussion may be found in Brady and Bossis (1988).

2.2.1 Microstructural mechanics

Consider N rigid particles suspended in an incompressible, Newtonian fluid of viscosity, η_s, and density, ρ. The motion of the fluid is governed by the Navier-Stokes equations, and the particle motion is described by the coupled N-body Langevin equation, which can be written

$$\mathbf{m} \cdot \frac{d\mathbf{U}}{dt} = \mathbf{F}^{IP} + \mathbf{F}^{H} + \mathbf{F}^{B}. \tag{2.27}$$

where $\mathbf{m}$ is a generalized mass/moment of inertia matrix of dimension $6N \times 6N$, $\mathbf{U}$ is the particle translational/rotational velocity vector of dimension $6N$, and the $6N$ force/torque vectors, $\mathbf{F}$, represent: 1) the deterministic non-hydrodynamic forces, $\mathbf{F}^{IP}$, which may be interparticle and/or external; 2) the hydrodynamic forces, $\mathbf{F}^{H}$, exerted on the particles because of their motion relative to the fluid; and 3) the stochastic forces, $\mathbf{F}^{B}$, that give rise to Brownian motion. This simply states that the time rate-of-change of the momentum equals the sum of the forces.

The Reynolds number for this system undergoing shear is

$$\mathrm{Re} = \frac{\rho \dot{\gamma} a^2}{\eta_s} \quad , \tag{2.28}$$

where $\dot{\gamma}$ is the magnitude of the shear rate and a is the characteristic size of the particles. If Re → 0, then the left side of (2.27) drops out, leaving the sum of the forces equal to zero.

For polymer models $\mathbf{F}^{IP}$ represents the force that is due to the connectors between the beads, excluded-volume forces, and any external force, such as gravity. The hydrodynamic force/torque exerted on the particles in a solution undergoing a bulk linear shear flow is

$$\mathbf{F}^{H} = -\mathbf{R}_{FU} \cdot (\mathbf{U} - \mathbf{U}^{\infty}) + \mathbf{R}_{FE} : \mathbf{E}^{\infty} \tag{2.29}$$

(see Brenner and O'Neill 1972; Kim and Mifflin 1985; Bossis and Brady 1984). $\mathbf{U}^{\infty}$ is the imposed flow at infinity evaluated at the particle centers; i.e., $\mathbf{U}^{\infty}_{\alpha} = \boldsymbol{\Omega}^{\infty}$ for rotation and $\mathbf{U}^{\infty}_{\alpha} = \mathbf{E}^{\infty} \cdot \mathbf{x}_{\alpha}$ for translation, where $\mathbf{x}_{\alpha}$ is the position vector of the α^{th} particle. $\mathbf{E}^{\infty}$ and $\boldsymbol{\Omega}^{\infty}$ are the symmetric (and traceless from continuity) and antisymmetric parts of the the velocity-gradient tensor, respectively. Both are constants in space, but may be arbitrary functions of time. $\mathbf{R}_{FU}(\mathbf{x})$ and $\mathbf{R}_{FE}(\mathbf{x})$ are resistance matrices that give the hydrodynamic force/torque on the particles that is due to their motion relative to the fluid ($\mathbf{R}_{FU}(\mathbf{x})$) and due to the imposed shear flow ($\mathbf{R}_{FE}(\mathbf{x})$). These matrices depend only upon the configuration of the particles when the Reynolds number is vanishingly small. The $6N$ vector $\mathbf{x}$ represents the generalized configuration vector specifying the location *and* orientation of all N particles, and $\mathbf{U}$ is the particles' translational/rotational velocity vector. Note that the subscripts on the matrices indicate the coupling between the kinematic and dynamic quantities. The stochastic or Brownian force arises from the thermal fluctuations in the fluid and is characterized by

$$\langle \mathbf{F}^{B} \rangle = \mathbf{0} \qquad \textit{and} \qquad \langle \mathbf{F}^{B}(0)\mathbf{F}^{B}(t) \rangle = 2kT\mathbf{R}_{FU}\delta(t), \tag{2.30}$$

where $\delta(t)$ is the delta function, and the angle brackets denote an ensemble average. The amplitude of the correlation between the Brownian forces at time 0 and time t results from the fluctuation-dissipation theorem for the N-body system. The fluctuating forces can be considered instantaneous for the time scales of interest to us, which are much longer than the molecular time scale ($\sim 10^{-13}s$). The

Langevin equation, which includes this formulation of the Brownian forces, is valid provided the configuration of the particles does not change significantly during the time required for the particle's momentum to relax after a Brownian impulse. This condition is generally satisfied, and indeed, dynamic light-scattering experiments detect only motion that occurs over times large compared to this relaxation time. (The reader is referred to discussions by Hinch 1975; Batchelor 1976; Ermak and McCammon 1978; Russel 1981; and Rallison and Hinch 1986, for further discussion of the stochastic problem.)

The evolution equation for the particles is obtained by following Ermak and McCammon (1978) and integrating the Langevin equation over a time step Δt that is large compared with the Brownian relaxation time, but small compared with the time over which the configuration changes. A second integration in time produces the evolution equation for the particle positions and orientations with an error of $O(\Delta t^2)$:

$$\begin{aligned}\Delta \mathbf{x} =& Pe\{\mathbf{U}^\infty + \mathbf{R}_{FU}^{-1} \cdot [\mathbf{R}_{FE} : \mathbf{E}^\infty + (\dot\gamma^*)^{-1}\mathbf{F}^{IP}]\}\Delta t \\ &+ \nabla \cdot \mathbf{R}_{FU}^{-1}\Delta t + \mathbf{X}(\Delta t),\end{aligned} \tag{2.31a}$$

where

$$\langle \mathbf{X} \rangle = \mathbf{0} \qquad \text{and} \qquad \langle \mathbf{X}(\Delta t)\, \mathbf{X}(\Delta t) \rangle = 2\mathbf{R}_{FU}^{-1}\Delta t. \tag{2.31b}$$

$\Delta\mathbf{x}$ is the vector representing the change in position and orientation of every particle during the time step Δt. $\mathbf{X}(\Delta t)$ is the random displacement that is due to Brownian motion, which has a zero mean and a covariance given by the inverse of the resistance matrix. The vector $\mathbf{x}$ has been non-dimensionalized by the particle size a, the time by the diffusive time scale a^2/D_0 ($D_0 = kT/6\pi\eta_s a$ is the diffusion coefficient of a single, isolated Brownian particle), the shear force by $6\pi\eta_s\dot\gamma$ ($\dot\gamma = |\mathbf{E}^\infty|$ is the magnitude of the shear rate), and the interparticle and/or external forces by $|\mathbf{F}^{IP}|$. $\dot\gamma^* = 6\pi\eta_s a^2\dot\gamma/|\mathbf{F}^{IP}|$ is the non-dimensional shear rate that gives the relative importance of the shear flow and the imposed interparticle and/or external forces. For problems where the shear flow is more important than the imposed forces, $Pe = \dot{\gamma}a/D_0$ $(= 6\pi\eta_s a^3\dot{\gamma}/kT)$ is the relevant Péclet number, which measures the relative importance of the shear flow and Brownian motion.

For this study, the relevant interparticle forces $\mathbf{F}^{IP}$ are the spring forces connecting the beads. From §2.1,

$$\begin{aligned} h^* &= \left(\frac{a^2K}{\pi kT}\right)^{\frac{1}{2}} \\ &= \left(\frac{K^*}{\pi}\right)^{\frac{1}{2}}, \end{aligned} \tag{2.32}$$

where K has been made non-dimensional by kT/a^2. Hence, h^* is varied in this study by changing K^*. This non-dimensionalization is appropriate because the Hookean description of the interparticle springs was developed based upon the Brownian motion of the monomers joining two points in the real polymer (Bird *et al.* 1987). Since $\mathbf{F}^{IP} = K\mathbf{r}$,

$$\begin{aligned} |\mathbf{F}^{IP}| &= Ka, && (K \text{ dimensional}) \\ &= \frac{K^*kT}{a}, && (K^* \text{ non} - \text{dimensional}) \end{aligned} \tag{2.33}$$

and it follows that

$$\begin{aligned} \dot{\gamma}^* &= 6\pi\eta_s a^2\dot{\gamma}/\left(\frac{K^*kT}{a}\right) \\ &= 6\pi\eta_s a^3\dot{\gamma}/kT/K^*, \\ &= \frac{Pe}{K^*}. \end{aligned} \tag{2.34}$$

Therefore, given the above choice of non-dimensionalization for K, the interparticle spring forces and the Brownian forces should be scaled identically. This is appropriate for low Pe, where the spring forces balance the Brownian forces. For high Pe, where shear forces dominate, the spring forces balance the hydrodynamic forces. This has the effect of dividing $\dot{\gamma}^*$ by Pe.

2.2.2 Hydrodynamic interactions

Consider the problem of determining the motion of particles subject to a constant body force, such as the buoyancy force. The motion of the particles in Stokes flow can be calculated from

$$\mathbf{U} - \mathbf{U}^{\infty} = \mathbf{M} \cdot \mathbf{F}, \qquad (2.35)$$

where $\mathbf{U}$ is the translational-angular velocity vector, $\mathbf{F}$ is the total force-torque vector ($\mathbf{F}^{IP} + \mathbf{F}^{H} + \mathbf{F}^{B}$), both of which are dimensioned $6N$, and $\mathbf{M}$ is the $6N \times 6N$ mobility matrix. The mobility matrix depends on the instantaneous configuration of the particles only, not on their velocities. The mobility matrix is symmetric, as can be shown from the reciprocal theorem, and positive-definite, because of the dissipative nature of the system. Since there is no general solution to the N-body Stokes equation, an approximation for $\mathbf{M}$ must be developed. Durlofsky *et al.* (1987) developed an excellent approximation to the true mobility matrix, which preserves the dominant multibody interactions and lubrication forces among an arbitrary number of spheres. This section is a brief description of how the Stokesian dynamics simulation approximates the exact mobility matrix for a finite number of spheres.

The goal is to generate an approximate N-particle mobility matrix, $\mathbf{M}$, that relates the particles' translational and rotational velocities to the forces and torques imposed on them. The development begins with the exact integral representation of the velocity field in Stokes flow, in conjunction with Faxén's laws; the force density on the surface of each particle is expanded in a series of moments about the center of each particle. The monopole, or zeroth moment of the force density, corresponds to the total force on the particle, $\mathbf{F}_t$. The dipole, or first moment of the force density, has both symmetric and antisymmetric parts: the antisymmetric part is the total torque, $\mathbf{L}$, and the symmetric part is known as the stresslet,

S. The multipole expansion can be truncated at any order, depending on the level of accuracy desired, but to include the effects of lubrication, all moments are necessary. Since the effects of lubrication will be included in the resistance formulation, the expansion is truncated after the first moment, except for two higher-order, multipole contributions that result from the finite size of the particles. A more complete derivation that explicitly considers the quadrupole contribution to the mobility matrix can be found in Brady *et al.* (1987). Recall that the Oseen tensor considers only point forces. The Rotne-Prager description is identical to using only the zeroth moment in Stokesian dynamics.

The accuracy of the mobility matrix can be increased by including the stresslet interactions. This is necessary for problems where there is an imposed linear shear field. The grand mobility matrix, $\mathcal{M}$, which includes the stresslet interactions, is formed as follows:

$$\begin{pmatrix} \mathbf{U} - \mathbf{U}^{\infty} \\ -\mathbf{E}^{\infty} \end{pmatrix} = \mathcal{M} \cdot \begin{pmatrix} \mathbf{F} \\ \mathbf{S} \end{pmatrix}, \tag{2.36}$$

with $\mathcal{M}$ partitioned as

$$\mathcal{M} = \begin{pmatrix} \mathbf{M}_{UF} & \mathbf{M}_{US} \\ \mathbf{M}_{EF} & \mathbf{M}_{ES} \end{pmatrix}. \tag{2.37}$$

The grand mobility matrix, $\mathcal{M}$, is written as an $11N \times 11N$ matrix. The $6N \times 5N$ matrix $\mathbf{M}_{US}$ relates the velocities and the stresslets, the $5N \times 6N$ matrix $\mathbf{M}_{EF}$ relates the rate of strain and forces, and the $5N \times 5N$ matrix $\mathbf{M}_{ES}$ relates the rate of strain and the stresslets. In addition, $\mathbf{E}^{\infty}$ and $\mathbf{S}$ are written in a compact form, which takes advantage of the fact the stresslets are traceless and symmetric. This is done so that $\mathcal{M}$ is not singular and therefore may be inverted (see below). To include higher-order multipole moments, extend the vector on the right-hand side of Equation (2.36) by including the irreducible (quadrupole, octopole, etc.) moments, and extend the kinematical vector on the left-hand side with zeros, since all higher-order velocity gradients must be zero. As constructed, $\mathcal{M}$, $\mathbf{M}_{UF}$ and

$\mathbf{M}_{ES}$ are all symmetric and positive-definite like $\mathbf{M}$. Details of the construction of these matrices can be found in Durlofsky *et al.* 1987.

In Stokesian dynamics, these matrices are far-field approximations to the pairwise hydrodynamic interactions between spherical particles. Consider the small (as opposed to grand) mobility matrix, $\mathbf{M}_{UF}$, and neglect the stresslets for a moment. Solving Equation (2.35) for the sphere velocities would sum only the pairwise interactions between spheres. If the spheres are moved, given these velocities, the spheres would overlap since the far-field approximations to the sphere interactions do not include the strong lubrication interactions that would prevent this overlap. To include these lubrication interactions, first invert $\mathbf{M}_{UF}$. The invert, $\mathbf{M}_{UF}^{-1}$, is the far-field approximation to the resistance matrix $\mathbf{R}$ defined by the inverse of Equation (2.35),

$$\mathbf{F} = \mathbf{R} \cdot (\mathbf{U} - \mathbf{U}^{\infty}). \tag{2.38}$$

More importantly, this invert is a true many-body approximation of $\mathbf{R}$. Upon inversion, the reflections among all elements – – point force, finite-size effects, stresslet interactions, etc. – – and between all spheres are summed. The proof of this is in Durlofsky *et al.* 1987.

The invert, $\mathbf{M}_{UF}^{-1}$, is still only a far-field approximation to the true resistance matrix. Lubrication effects would occur only if all multipole moments were included in the mobility matrix. These important near-field interactions are added to the resistance formulation in a pairwise fashion. To each element of the $\mathbf{M}_{UF}^{-1}$ the exact two-sphere resistance interactions are added. This additional two-body resistance matrix is known as $\mathbf{R}_{2b}$. However, $\mathbf{M}_{UF}^{-1}$ already contains the far-field part of the two-sphere interactions. These far-field interactions, denoted by $\mathbf{R}_{2b}^{\infty}$, must be subtracted from $\mathbf{R}_{2b}$. The approximation to the exact resistance matrix is then

$$\mathbf{R} \approx \mathbf{M}_{UF}^{-1} + \mathbf{R}_{2b} - \mathbf{R}_{2b}^{\infty}. \tag{2.39}$$

In an actual simulation, the equation set in Equation (2.38) is solved for the translational and rotational velocities of the spheres. This calculation of $\mathbf{R}$ using only the $\mathbf{M}_{UF}$ portion of the mobility matrix (i.e., only the forces and torques) is known as the FT method.

When there is no imposed linear shear flow, Durlofsky *et al.* (1987) have shown that the FT method gives accurate results. The accuracy of the results can be improved by including the effect of induced stresslets when forming the grand mobility matrix, $\mathcal{M}$. The invert of the grand mobility matrix is the grand resistance matrix $\mathcal{R}$:

$$\begin{pmatrix} \mathbf{F} \\ \mathbf{S} \end{pmatrix} = \mathcal{R} \cdot \begin{pmatrix} \mathbf{U} - \mathbf{U}^{\infty} \\ -\mathbf{E}^{\infty} \end{pmatrix}, \tag{2.40}$$

where $\mathcal{R}$ is partitioned as

$$\mathcal{R} = \begin{pmatrix} \mathbf{R}_{FU} & \mathbf{R}_{FE} \\ \mathbf{R}_{SU} & \mathbf{R}_{SE} \end{pmatrix}. \tag{2.41}$$

The effect of the induced stresslets is obvious when one realizes that $\mathbf{R}_{FU} \neq \mathbf{M}_{UF}^{-1}$. The approximation for the true resistance matrix is now

$$\mathbf{R} \approx \mathbf{R}_{FU} + \mathbf{R}_{2b} - \mathbf{R}_{2b}^{\infty}. \tag{2.42}$$

This is the FTS formulation. Note that inverting the larger grand mobility matrix is approximately 6.25 $\left[(\frac{11}{6})^3\right]$ times slower than inverting the small mobility matrix.

The results of these methods, when applied to several known cases involving the interactions among a finite number of spheres, compare excellently with reported results (cf. Durlofsky *et al.* 1987). The procedure reproduces both the proper near-field lubrication forces and the dominant, many-body interactions that occur among a finite number of spheres subject to imposed forces.

2.2.3 Viscosity calculation

This section considers calculation of the bulk viscosity of a polymer solution, which can be determined from the corresponding averaged expressions of the microscale results. Most of the general formulae for the viscosity (and other macroscopic properties) have been derived by Batchelor (1970,1972,1976,1977). Except for the spring contribution to the stress, all involve averages of the hydrodynamic-interaction tensors.

For rheology, the symmetric part of the bulk deviatoric stress, known as the bulk stress, $\langle \mathbf{\Sigma} \rangle$, is required. This is defined as

$$\langle \mathbf{\Sigma} \rangle = \mathrm{I.T.} + 2\eta_s \mathbf{E}^\infty + \frac{N}{V}\{\langle \mathbf{S}^{IP} \rangle + \langle \mathbf{S}^{H} \rangle + \langle \mathbf{S}^{B} \rangle\}. \tag{2.43}$$

I.T. stands for an isotropic term, which is of no interest since the fluid is incompressible. $2\eta_s \mathbf{E}^\infty$ is the contribution to the stress from the Newtonian solvent. This leaves three contributions from the polymer molecule, corresponding exactly to the forces in (2.27): 1) an "elastic" stress that is due to the interparticle forces, $\langle \mathbf{S}^{IP} \rangle$; 2) a mechanical or contact stress transmitted by the fluid that is due to the shear flow and the motions induced by $\mathbf{F}^{IP}$, $\langle \mathbf{S}^{H} \rangle$; and 3) a direct contribution from the Brownian motion, $\langle \mathbf{S}^{B} \rangle$. The particle contributions to the bulk stress are given by

$$\langle \mathbf{S}^{IP} \rangle = -\langle \mathbf{x} \mathbf{F}^{IP} \rangle, \tag{2.44a}$$

$$\langle \mathbf{S}^{H} \rangle = -\langle \mathbf{R}_{SU} \cdot (\mathbf{U} - \mathbf{U}^\infty) \; - \; \mathbf{R}_{SE} : \mathbf{E}^\infty \rangle, \tag{2.44b}$$

$$\langle \mathbf{S}^{B} \rangle = -kT \langle \nabla \cdot (\mathbf{R}_{SU} \cdot \mathbf{R}_{FU}^{-1}) \rangle. \tag{2.44c}$$

$\mathbf{R}_{SU}(\mathbf{x})$ and $\mathbf{R}_{SE}(\mathbf{x})$ are configuration-dependent, resistance matrices, similar to $\mathbf{R}_{FU}$ and $\mathbf{R}_{FE}$, relating the particle "stresslet," $\mathbf{S}$, to the particle velocities ($\mathbf{R}_{SU}$) and to the imposed rate of strain ($\mathbf{R}_{SE}$). The particle velocities to be used in Equation (2.44*b*) are those coming from the deterministic displacements in Equation (2.31*a*); i.e., $\mathbf{U} - \mathbf{U}^\infty = \mathbf{R}_{FU}^{-1} \cdot [\dot{\gamma}^* \mathbf{R}_{FE} : \mathbf{E}^\infty + \mathbf{F}^{IP}] \Delta t$.

To understand the way in which the configuration of the dumbbell affects $\mathbf{S}^{IP}$, consider two dumbbells in a shear flow, as shown in Figure (2.1). The second dumbbell has the same angular orientation as the first, but with a greater extension. From Equation (2.44a), the S_{xy}^{IP} term, for example, is given by

$$S_{xy}^{IP} = -xF_y^{IP}. \tag{2.45}$$

Since both x and F_y^{IP} are greater for the second dumbbell than for the first, the greater extension of the second dumbbell results in a larger contribution to the stress. The same analysis holds for any two polymer configurations and for any element of $\mathbf{S}^{IP}$.

The physical, rather than mathematical, origins of the three different stresses are as follows: $\langle \mathbf{S}^{IP} \rangle$ – The springs connecting the beads have elastic energy, which manifests itself as tension along the length of the polymer. At equilibrium, the polymer has an isotropic distribution, so this tension does not contribute to the deviatoric stress in the fluid. It influences only the isotropic pressure in the fluid, the osmotic pressure. A macroscopic flow can induce anisotropy in the polymer distribution, in which case the tension along the polymer increases the measurable (deviatoric) stress in the fluid. $\langle \mathbf{S}^{H} \rangle$ – The polymer molecule is dynamically different from the fluid surrounding it. When subjected to a local strain, the polymer does not deform as a fluid element would; the fluid must expend extra energy to move past the polymer, which increases the stress in the fluid. $\langle \mathbf{S}^{B} \rangle$ – At equilibrium, the Brownian forces act on the polymer in a balanced manner (on average), so the net effect is zero. When the polymer moves away from equilibrium, the Brownian forces act to move it back to its equilibrium distribution. The imposed flow must do extra work against this tendency toward equilibrium, and this extra work increases the stress in the fluid.

The Stokesian dynamics results for $\langle \mathbf{S}^{IP} \rangle, \langle \mathbf{S}^{H} \rangle$, and $\langle \mathbf{S}^{B} \rangle$ are compared to the Rouse and Zimm results for $\langle \mathbf{S}^{IP} \rangle$ in §4.

2.3 Zimm Model

This section gives a short description of the development of the Zimm model. It follows exactly the development of the Stokesian dynamics model, so that differences between the two models can be easily seen. The same forces are present, and Re is still assumed to be small, so the governing equation remains

$$\mathbf{F}^{IP} + \mathbf{F}^{H} + \mathbf{F}^{B} = 0. \tag{2.46}$$

Unlike the Stokesian dynamics model, $\mathbf{F}^{IP}$, $\mathbf{F}^{H}$ and $\mathbf{F}^{B}$ are $3N$ vectors, not $6N$. This is because the Zimm beads are points, so that there are no rotational degrees of freedom. While $\mathbf{F}^{IP}$ is otherwise identical to the Stokesian dynamics description, $\mathbf{F}^{H}$ and $\mathbf{F}^{B}$ are much simpler:

$$\mathbf{F}^{H} = -\mathbf{R}_{FU} \cdot (\mathbf{U} - \mathbf{U}^{\infty}), \tag{2.47}$$

and

$$\langle \mathbf{F}^{B} \rangle = \mathbf{0} \qquad \textit{and} \qquad \langle \mathbf{F}^{B}(0)\mathbf{F}^{B}(t) \rangle = 2kT\mathbf{R}_{FU}\delta(t). \tag{2.48}$$

The primary simplification in (2.47) and (2.48) is that $\mathbf{R}_{FU} = \mathbf{M}_{UF}^{-1}$ exactly, where $\mathbf{M}_{UF}$ is simply the far-field mobility matrix formed from the two-body interaction description of the Rotne-Prager tensor, Eq. (2.25). There are no torques, no stresslets, no many-body effects and no lubrication forces. This results in an evolution equation for the particle positions

$$\Delta \mathbf{x} = Pe\{\mathbf{U}^{\infty} + \mathbf{M}_{UF} \cdot (\dot{\gamma}^{*})^{-1}\mathbf{F}^{IP}\}\Delta t + \mathbf{X}(\Delta t), \tag{2.49a}$$

where

$$\langle \mathbf{X} \rangle = \mathbf{0} \qquad \text{and} \qquad \langle \mathbf{X}(\Delta t)\ \mathbf{X}(\Delta t) \rangle = 2\mathbf{M}_{UF}\Delta t. \tag{2.49b}$$

Note that $\nabla \cdot \mathbf{R}_{FU}^{-1} = \nabla \cdot \mathbf{M}_{UF}$ is zero for the Zimm model using the Rotne-Prager hydrodynamic interaction.

$\mathbf{S}^{IP}$ for the Zimm model is calculated the same as in the Stokesian dynamics model, Eq. (2.44a). $\mathbf{S}^{H}$ and $\mathbf{S}^{B}$ are not present in the Zimm model. This is because $\mathbf{S}^{H}$ and $\mathbf{S}^{B}$ are finite-size, $O(a^3)$ effects. Since the Zimm beads have no finite size, $\mathbf{S}^{H}$ and $\mathbf{S}^{B}$ are zero.

The primary computational savings with the Zimm model result from using $3N$ vectors and matrices instead of the $6N$ and $11N$ vectors and matrices required by the Stokesian dynamics model. These simplifications result from (1) discarding rotational degrees of freedom, and (2) neglecting any rate-of-strain effects (the imposed shear flow appears only in the $\mathbf{U}^{\infty}$ contribution). Although $\mathbf{R}_{FU}^{-1} = \mathbf{M}_{UF}$ so that no matrix inversion is required in the Zimm simulations, the square root of $\mathbf{M}_{UF}$ still must be calculated for the Brownian-displacement term, and this is computationally just as costly as a matrix inversion.

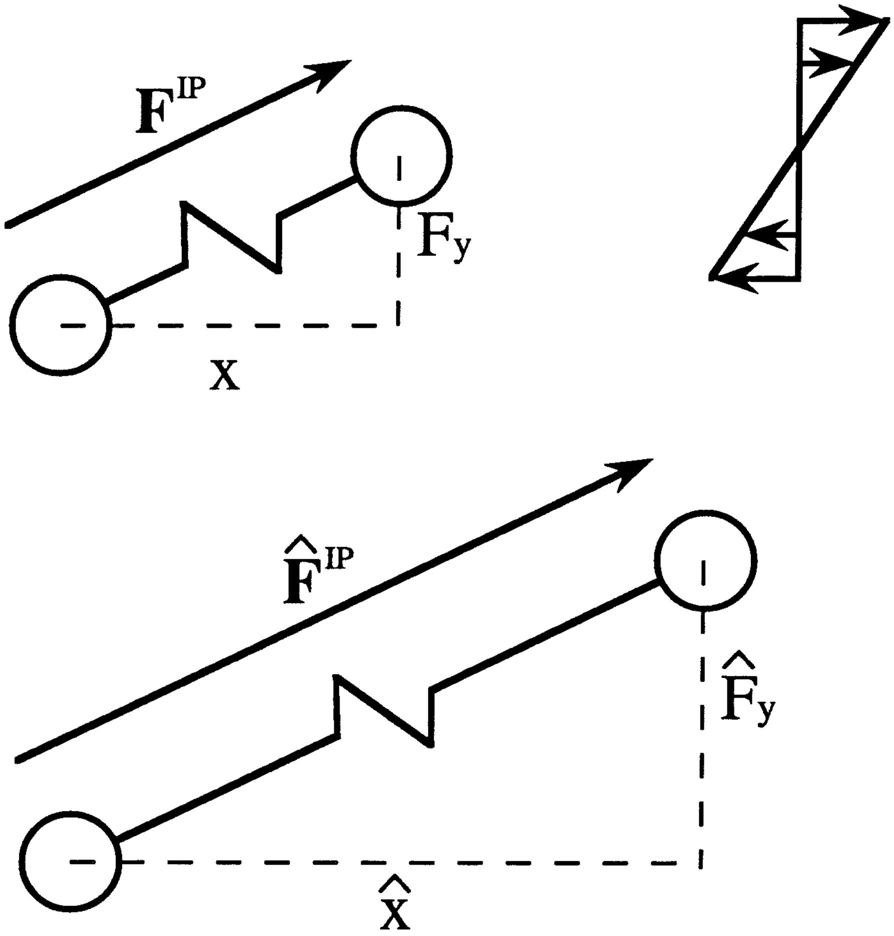

$$\boxed{\hat{S}^{IP}_{xy} = \hat{x}\hat{F}_y \quad > \quad S^{IP}_{xy} = xF_y}$$

Figure (2.1)

Two dumbbells in a shear flow with the same angular orientation but different extensions. The dumbbell with the larger extension makes a greater contribution to the stress.

3. FLOWS STUDIED

3.1 Equilibrium

Before one can interpret the behavior of the models under flow, the equilibrium states must be well understood. The equilibrium state means that the Péclet number goes to zero, so the hydrodynamic forces play no role. For the 2–bead dumbbell model, the starting point is the standard conservation equation for particle pairs,

$$\frac{\partial P_2}{\partial t} + \nabla \cdot \mathbf{U}_2 P_2 - \nabla \cdot \mathbf{M}_2 \cdot [\nabla V_2 + kT \nabla \ln P_2] P_2 = 0. \tag{3.1}$$

In (3.1), P_2 is the pair-distribution function, $P_2 = P_0 e^{-V(1,2)/kT}$, where V is the 2-body, interparticle potential and P_0 is the normalization constant. $\mathbf{U}_2$ is the relative velocity of two particles coming from an imposed flow, and $\mathbf{M}_2$ is the hydrodynamic-mobility tensor for the relative motion of two particles (i.e., $\mathbf{M}_{UF}$ for two particles). For the bead-spring model, $\nabla V_2 = -\mathbf{F}^{IP}$, where $\mathbf{F}^{IP}$ is the interparticle force (including both spring and hard-sphere forces). For the Rouse and Zimm models, the "beads" have no excluded volume, so the Hookean spring connecting the beads gives

$$\mathbf{F}^{IP} = -K\mathbf{r} \tag{3.2}$$

for all $\mathbf{r}$, where K is the Hookean spring constant. This results in a distribution function

$$P_2^0(\mathbf{r}) = P_0 e^{-\frac{1}{2}Kr^2}. \tag{3.3}$$

Hence the Rouse model and the Zimm model are identical at equilibrium; the inclusion of hydrodynamic interaction has no significance at zero Pe.

For the Stokesian dynamics model, the beads are actual hard spheres of radius a. When connected by Hookean springs, this produces an interparticle force of

$$\mathbf{F}^{IP} = \begin{cases} K\mathbf{r} & (r > 2a); \\ \infty & (r \leq 2a). \end{cases} \tag{3.4}$$

This description of the interparticle force results in a distribution function identical in form to the Rouse and Zimm distributions, but with a different normalization constant P_0, since the Stokesian dynamics model has a probability density equal to zero for $r < 2$. Graphs of Eq. (3.5) for the Rouse/Zimm (simple spring) potential and for the Stokesian dynamics (hard-sphere/spring) potential are shown in Figure (3.1) for $K = 0.19635$ (this K will give an $h^* = 0.25$ in flow). Figure (3.2) shows the same potentials angularly averaged over all space; i.e., they show $Q_2^0(r)$, where

$$Q_2^0(r) = 4\pi r^2 P_2^0(r). \tag{3.5}$$

Note that the Stokesian dynamics $Q_2^0(r)$ is zero up to $r = 2$, and then immediately jumps to a non-zero value. Although each model is most likely to be found at its shortest extension ($r = 0$ for Rouse and Zimm), when this is integrated over all space, the probability of finding the Rouse and Zimm models at contact is zero. Since the Stokesian dynamics beads have finite size, the probability of their actually touching one another is non-zero.

The $Q_2^0(r)$ representation will be used in all subsequent discussions, since it shows the actual distribution of extensions r in three dimensions, which is useful in the analysis of the **xF** contributions to the stress. When the polymer is subjected to a flow, the distribution P_2 is no longer isotropic, and the more general form for the angularly averaged radial distribution is

$$Q_2(r) = r^2 \int_0^{2\pi} \int_0^{\pi} P_2(r, \phi, \theta) \sin\theta d\theta d\phi. \tag{3.6}$$

Although not used in this study, the application of other spring potentials is straightforward. A general rule is that non-linear potentials are trivial for use in simulations, but difficult in preaveraging or other direct, analytical solution methods.

3.2 Steady Simple Shear

The behaviors of the Rouse, Zimm and Stokesian dynamics models were compared for steady, simple shear flow, $u_x = \dot{\gamma} y$, as shown in Figure (3.3). The models were examined for differences in their orientational distributions and their shear viscosities as a function of Pe. While no analytical solutions exist for the Zimm or Stokesian dynamics models, the distribution function for the Rouse dumbbell is known exactly for arbitrary, time-dependent flow. This distribution function, P_2^R, is given by (Bird et al. 1987):

$$P_2^R(\mathbf{r},t) = \frac{\left(\frac{K}{2\pi kT}\right)^{3/2}}{(\det\boldsymbol{\alpha})^{1/2}} exp\left(-\frac{K}{2kT}(\boldsymbol{\alpha}^{-1} : \mathbf{rr})\right), \tag{3.7}$$

where

$$\boldsymbol{\alpha}(t) = \boldsymbol{\delta} - \frac{1}{\lambda_K}\int_{-\infty}^{t} exp(-(t-t')/\lambda_K)\,\boldsymbol{\gamma}_{[0]}(t,t')dt', \tag{3.8}$$

$$\boldsymbol{\gamma}_{[0]} = \boldsymbol{\delta} - \mathbf{B}, \tag{3.9}$$

and $\mathbf{B}$ is the *Finger strain tensor.* For steady, simple shear flow, Eq.(3.7) becomes

$$P_2^R(\mathbf{r}; Pe, K) = \frac{1}{a^3}\left(\frac{K^3}{8\pi^3}\right)^{1/2} \times$$

$$exp\left[-\frac{1}{2}Kr^2\left(1 - \frac{1}{2}\frac{Pe}{K}r_x r_y + \frac{1}{16}\left(\frac{Pe}{K}\right)^2 r_y r_y\right)\right]. \tag{3.10}$$

Thus, for a given Pe and K, the orientational distribution of the Rouse dumbbell is known exactly. From this the mean stress predicted by the model $\langle \mathbf{S}^{IP}\rangle$ can be calculated by

$$\langle \mathbf{S}^{IP}(Pe,K)\rangle = \int_0^\infty \mathbf{S}^{IP}(\mathbf{r})P_2^R(\mathbf{r}; Pe, K)d\mathbf{r}. \tag{3.11}$$

Recall that the Rouse model generates only $\mathbf{S}^{IP}$; $\mathbf{S}^H$ and $\mathbf{S}^B$ are both zero. The results for the Rouse model are compared to the Zimm and Stokesian dynamics model results in §4.2 .

3.3 Oscillatory Simple Shear

If a polymer solution is subjected to an oscillatory strain,

$$\gamma(t) = \gamma^0 \sin \omega t, \tag{3.12}$$

where $\gamma(t)$ is the strain, γ^0 is the maximum amplitude of the strain and ω is the frequency of the oscillation, then the stress will also oscillate. If γ^0 is small enough so that the viscoelastic response is linear, then the stress will oscillate with the same period as the imposed strain, but will be out of phase with it, as shown in Figure (3.4). In this regime of linear, viscoelastic behavior, the measured shear stress S_{xy} may be decomposed into two parts, one part in phase with the imposed strain and one part out of phase,

$$S_{xy} = \gamma^0 (G^{'} \sin \omega t + G^{''} \cos \omega t). \tag{3.13}$$

The coefficient of the term in phase with the strain, $G^{'}$, represents the elastic nature and is called the storage modulus, while the coefficient of the out-of-phase term, $G^{''}$, describes the dissipative nature and is called the loss modulus. Together, these two terms form the complex modulus G^*,

$$G^* = G^{'} - iG^{''}. \tag{3.14}$$

For a pure, Newtonian fluid of viscosity μ, $G^{'} = 0$, and $G^{''} = \omega\mu$. In the limit of infinite dilution, the quantities of interest are the intrinsic storage and loss moduli,

$$[G^{'}] = \lim_{c \to 0} \frac{G^{'}}{c} \quad , \tag{3.15a}$$

$$[G^{''}] = \lim_{c \to 0} \frac{(G^{''} - \omega\eta_s)}{c} \quad . \tag{3.15b}$$

(For experimental data, these quantities are reduced by temperature and molecular weight M to give

$$[G^{'}]_R = \frac{[G^{'}]M}{RT} \quad , \tag{3.16a}$$

$$[G^{''}]_R = \frac{[G^{''}]M}{RT} \quad , \tag{3.16b}$$

where R is the universal gas constant.)

For an infinitely dilute solution of a polymer, monodisperse in molecular weight, the Rouse theory predicts (Ferry 1980)

$$[G']_R = \sum_{p=1}^{N-1} \frac{\omega^2 \tau_p^2}{1+\omega^2\tau_p^2} \quad , \tag{3.17a}$$

$$[G'']_R = \sum_{p=1}^{N-1} \frac{\omega \tau_p}{1+\omega^2\tau_p^2} \quad , \tag{3.17b}$$

where the τ_p are the time constants for the model,

$$\tau_p = \frac{b^2 \zeta}{24kT \sin^2 [p\pi/2N]} \quad , \tag{3.18}$$

where b is the RMS extension of the springs and ζ is the drag coefficient for a single bead. As noted in §2.1, the preaveraged Zimm model does not result in a closed-form equation for the τ_p. However, the spectrum of τ_p for large N was calculated by Zimm, and these results are shown in Figure (3.5) along with the Rouse predictions. The plots show that there are three frequency regimes for the models. At low frequencies both models show G' proportional to ω^2 and G'' proportional to ω. At high frequencies the slopes of G' and G'' become identical, but because of the inclusion of hydrodynamic interaction, the limiting slope is different in each model: 1/2 for Rouse and 2/3 for Zimm. Lastly, there is a transition region between the low-frequency and high-frequency limits.

These equations are strictly valid only for large N. If $\tau_{p=N-1}$ makes a non-negligible contribution to the total sum, then N is too small and the results will describe unrealistic behavior because of the artificially low number of segments in the model -- the model does not have sufficient degrees of freedom to react to high-frequency disturbances. As expected, the theory breaks down at progressively lower values of ω as N is reduced. This effect is shown in Figure (3.6), where (3.17*a*,*b*) are plotted for the Rouse model for $N = 100, 10$ and 2. Obviously, the dumbbell model is inadequate to describe the high-frequency behavior of dilute polymer solutions. Nonetheless, a comparison between the predictions of the models can provide insight into fundamental differences between them, as shown in §4.3 .

Examining the viscoelastic behavior from an analysis of the modulus involves relating the stress to the strain. This analysis is based on the elastic or solidlike nature of the solution. From a fluid-mechanics point of view, favoring the fluidlike nature, the response can be expressed as a dynamic viscosity, η^*, which relates the stress to the rate of strain $\dot{\gamma}(t)$. Differentiation of (3.11) gives

$$\dot{\gamma}(t) = \omega\gamma^0 \cos\omega t, \tag{3.19a}$$

$$= \dot{\gamma}^0 \cos\omega t. \tag{3.19b}$$

Again, if $\dot{\gamma}^0$ is small enough so that the viscoelastic response is linear, the measured stress may be decomposed into

$$S_{xy} = \dot{\gamma}^0 \left(\eta^{'} \cos\omega t + \eta^{''} \sin\omega t\right). \tag{3.20}$$

The coefficient of the term in-phase with the strain rate, $\eta^{'}$, is the loss or dissipative portion, while the coefficient of the out-of-phase term, $\eta^{''}$, is the storage or elastic portion. Together, these two terms form the complex viscosity η^*,

$$\eta^* = \eta^{'} - i\eta^{''}. \tag{3.21}$$

For a pure Newtonian fluid $\eta^{''} = 0$ and $\eta^{'}$ is simply the Newtonian viscosity μ. Comparisons of (3.13) and (3.20) show

$$\eta^{'} = \frac{G^{''}}{\omega} \quad , \tag{3.22a}$$

$$\eta^{''} = \frac{G^{'}}{\omega} \quad , \tag{3.22b}$$

so

$$\eta^* = -\frac{i}{\omega}G^* \quad . \tag{3.23}$$

Thus η^* and G^* are related by a phase change and a factor of ω. There are also intrinsic viscosity components corresponding to the intrinsic moduli:

$$[\eta'] = \lim_{c\to 0} \frac{(\eta' - \eta_s)}{\eta_s c} \quad , \tag{3.24a}$$

$$[\eta''] = \lim_{c\to 0} \frac{\eta''}{\eta_s c} \quad . \tag{3.24b}$$

Since most experimental data are reported in terms of G' and G'', most of the simulation data in §4.3 are in terms of these quantities. η' and η'' are used during the discussion of the high-frequency viscosity and for comparing the magnitudes of different contributions to the stress, where the fact that η^* is always $O(1)$ makes comparisons over a range of frequency easier.

3.4 Data Collection

Data for the Stokesian dynamics model and the Zimm model were collected from simulation runs on two computer systems: a SUN Microsystems SPARC 4/360, with a speed of 2 MFLOPS, and an IBM RISC/6000 model 530, with a speed of 20 MFLOPS. In all cases, the quantities of interest were the configurational distribution function of the dumbbell $Q_2(r,\phi,\theta)$ (defined in §3.1) and the stress contributions $\langle \mathbf{S}^{IP}\rangle$,$\langle \mathbf{S}^{H}\rangle$, and $\langle \mathbf{S}^{B}\rangle$, from §2.2.3 (Eqs. (2.42 *a,b,c*)). The configuration distribution of the end-to-end vector $\mathbf{r}$ was stored as a histogram in r, ϕ, and θ, as noted in §3.1 . The definition of these coordinates relative to the imposed shear flow is shown in Figure (3.7). For $r < 10$, where the probability density is the highest, the grid size is 0.1 . For $r > 10$, the grid size is 0.5 . The grid size was $2\pi/100$ for both ϕ and θ. As shown in Fig. (3.7), a ϕ value in the range $\pi \le \phi < 2\pi$ is indistinguishable from ϕ in the range $0 \le \phi < \pi$; the only change is the direction of the vector $\mathbf{r}$. Hence, it is necessary to store configuration data only for $0 \leq \phi < \pi$. Similarly, only data for $0 \leq \theta \leq \pi/2$ were stored by the simulations.

Equilibrium runs were performed for two reasons. First, the equilibrium state is the only state for which the behavior of all of the models is known analytically. The angular distribution is isotropic, and the extensional distribution is a Boltzmann distribution as seen in Eq.(3.5). The models may be compared to the analytical predictions to provide a check on the accuracy of the simulations. Second, because of this analytic comparison, it is possible to determine the order of magnitude of data required for good statistics from the models. The objective is to find the minimum number of data that still give good predictions of the orientation and the stress for the models. Section 4.1 shows that $O(10^6)$ data are required for suitably accurate results. The data requirements for the Zimm model are similar.

To obtain data for the Stokesian dynamics model in steady shear, the simulations were run for 4,400,000 time steps, discarding the initial 400,000 steps. Data for the configurational distribution and the stress were collected at each time step. From the stress data the material functions for shear flow were calculated. These material functions are: the shear viscosity $\eta(\dot{\gamma})$; the first normal-stress coefficient $\Psi_1(\dot{\gamma})$; and the second normal-stress coefficient $\Psi_2(\dot{\gamma})$. These quantities are defined as

$$\eta(\dot{\gamma}) = \frac{\langle S_{xy} \rangle}{\dot{\gamma}}, \tag{3.25}$$

$$\Psi_1(\dot{\gamma}) = \frac{\langle S_{xx} - S_{yy} \rangle}{\dot{\gamma}^2}, \tag{3.26}$$

$$\Psi_2(\dot{\gamma}) = \frac{\langle S_{yy} - S_{zz} \rangle}{\dot{\gamma}^2}. \tag{3.27}$$

S_{xy}, S_{xx}, etc., are the appropriate elements of either $\mathbf{S}^{IP}$, $\mathbf{S}^{H}$, $\mathbf{S}^{B}$, or any combination of the three. The results were normalized so that plotting them versus Pe is identical to plotting them versus $\dot{\gamma}$. Since it was determined that 10^6 data points were required for a good estimation of the configuration and thereby the stress contributions, the stress data were broken down into four samples, each representing an average over 1,000,000 time steps. These four samples were used to generate the mean and standard deviation for each run. Data collection for the behavior in steady shear of the Zimm model was identical, except for the length of the runs. The duration of each Zimm run was 22,000,000 time steps, with the initial 2,000,000 being discarded. These data provided 20 sample averages of the stress predicted by the model.

For oscillatory shear flow, the stress in the fluid is given in §3.3 as

$$S_{xy} = \dot{\gamma}^0 \left(\eta^{'} \cos\omega t + \eta^{''} \sin\omega t\right), \tag{3.28}$$

where again S_{xy} may be the xy element of $\mathbf{S}^{IP}$, $\mathbf{S}^{H}$, $\mathbf{S}^{B}$, or any combination. The components of the complex viscosity, $\eta^{'}$ and $\eta^{''}$, may be separated by orthogonal integration over a cycle of the imposed, oscillating shear flow. For $\eta^{'}$, integration with the cosine function gives:

$$\begin{aligned}\int_0^{\frac{2\pi}{\omega}} S_{xy} \cos\omega t dt &= \int_0^{\frac{2\pi}{\omega}} \dot{\gamma}^0 \left(\eta^{'} \cos\omega t + \eta^{''} \sin\omega t\right) \cos\omega t dt \\ &= \frac{\dot{\gamma}^0 \eta^{'} \pi}{\omega},\end{aligned} \tag{3.29}$$

so

$$\eta^{'} = \frac{\omega}{\dot{\gamma}^0 \pi} \int_0^{\frac{2\pi}{\omega}} S_{xy} \cos\omega t dt. \tag{3.30}$$

Similarly, $\eta^{''}$ is given by

$$\eta^{''} = \frac{\omega}{\dot{\gamma}^0 \pi} \int_0^{\frac{2\pi}{\omega}} S_{xy} \sin\omega t dt. \tag{3.31}$$

The simulations were run for several cycles of the oscillation. To obtain the components of the complex viscosity for an integral multiple of the cycle period, $N(2\pi/\omega)$, the appropriate integrals are

$$\eta' = \frac{\omega}{N\dot{\gamma}^0\pi}\int_0^{\frac{2N\pi}{\omega}} S_{xy}\cos\omega t dt, \tag{3.32}$$

and

$$\eta'' = \frac{\omega}{N\dot{\gamma}^0\pi}\int_0^{\frac{2N\pi}{\omega}} S_{xy}\sin\omega t dt. \tag{3.33}$$

For the simulations of dumbbells, the Stokesian dynamics simulations were run for 180 cycles, discarding the first 20 cycles. This was repeated for 10 different initial conditions, resulting in 1,000,000 data points for the orientation and the stresses. The Zimm simulations were run for 1100 cycles, discarding the initial 100 cycles, producing 6,000,000 data points. For the more time-consuming 10-bead simulations, the Stokesian dynamics data were collected over three cycles, the Zimm data over ten cycles. 10 sets of initial conditions were examined in each case.

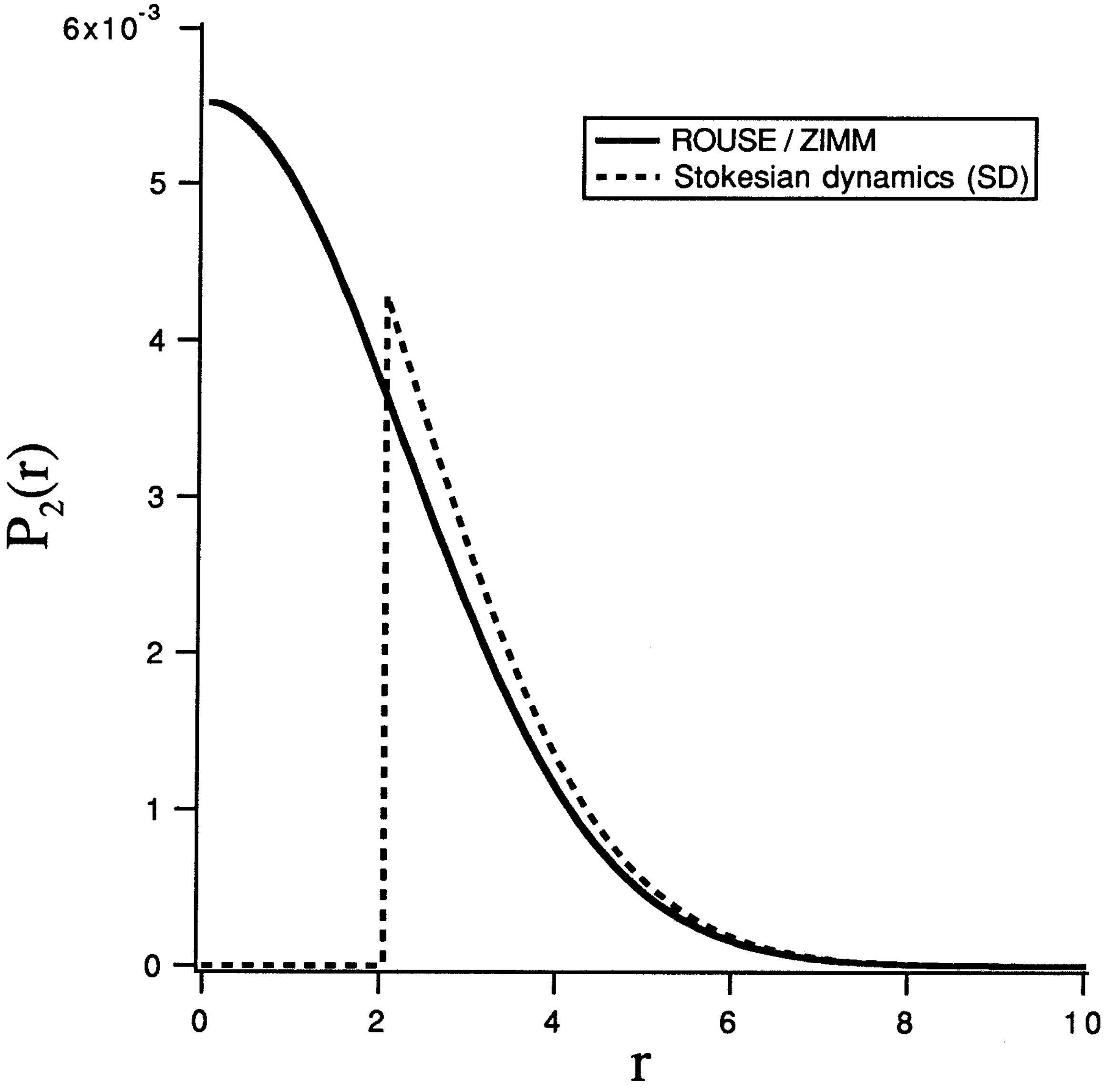

Figure (3.1)

Comparison of equilibrium radial distribution functions for dumbbell end-to-end vectors of Rouse/Zimm model (no excluded volume) and Stokesian dynamics model (with excluded volume). The spring constant K=0.19635 .

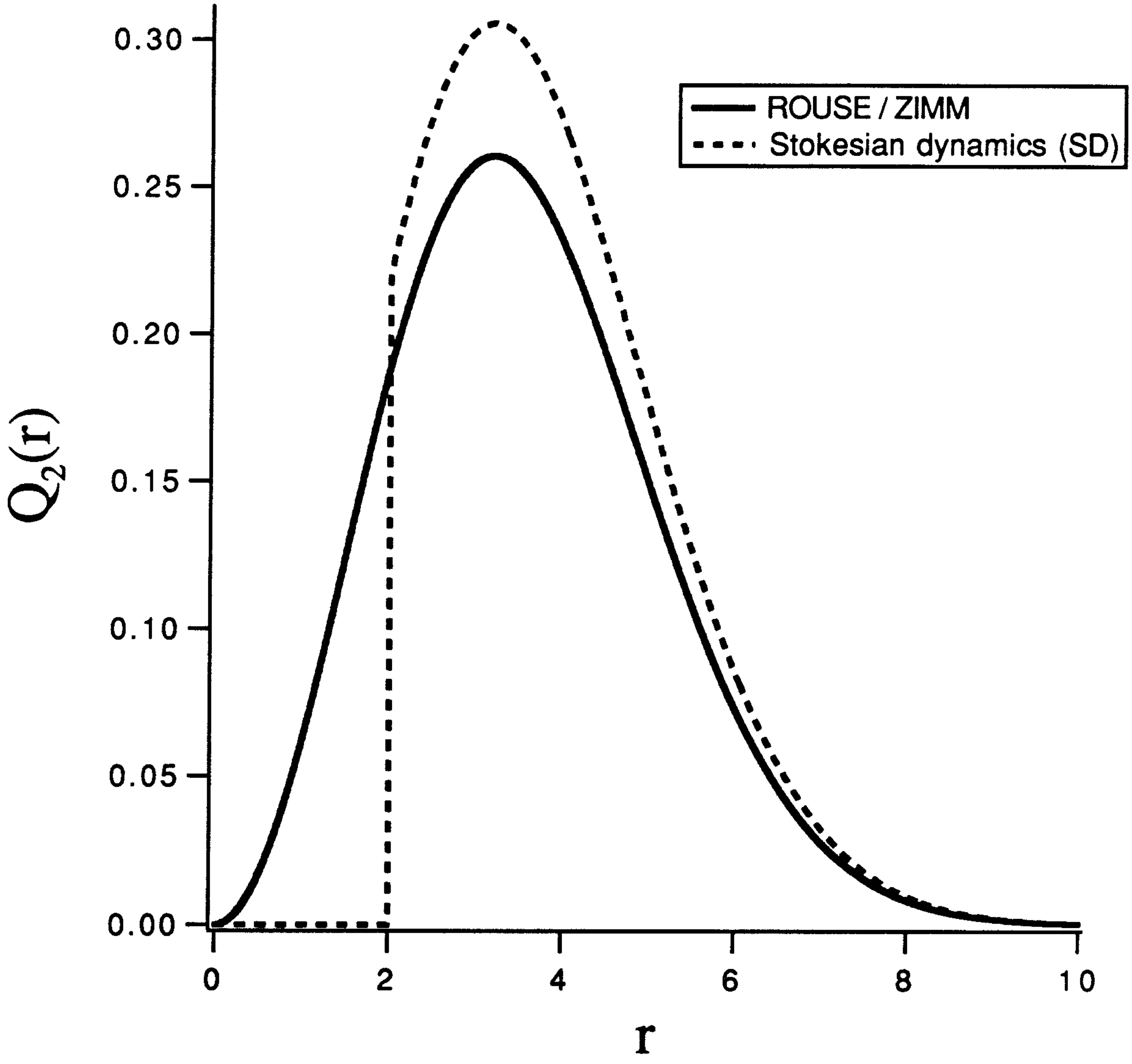

Figure (3.2)

Comparison of angularly averaged equilibrium radial distribution functions for dumbbell end-to-end vectors of Rouse/Zimm model (no excluded volume) and Stokesian dynamics model (with excluded volume). The spring constant K=0.19635 .

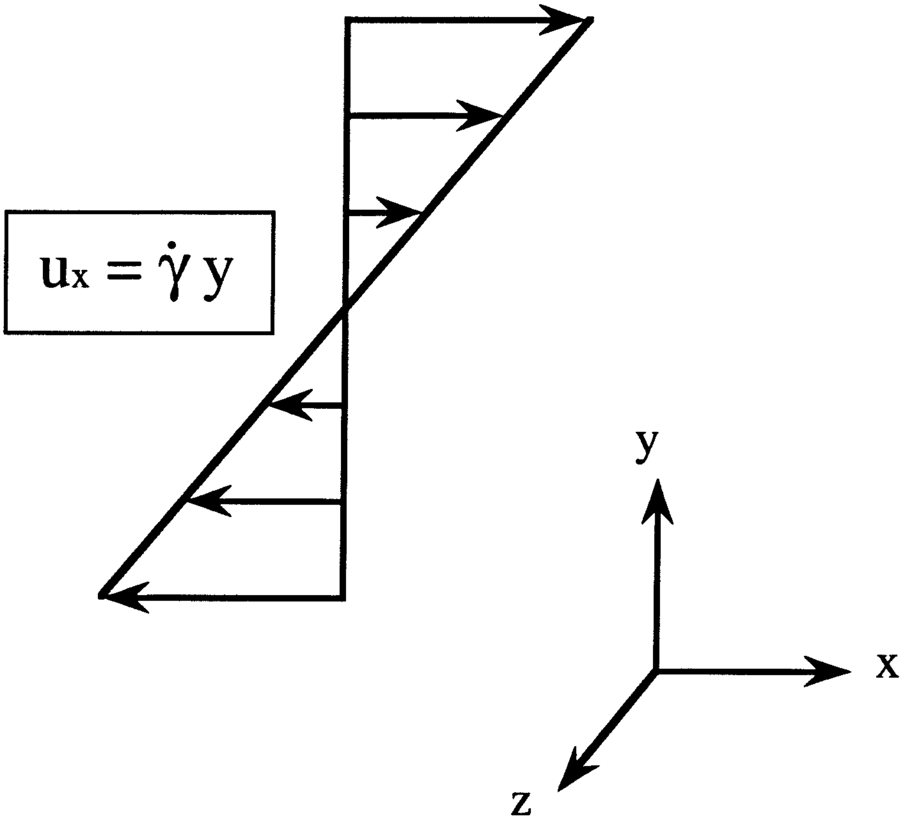

Figure (3.3)

Coordinates for steady shear flow.
$\dot{\gamma}$ is the imposed rate of strain.

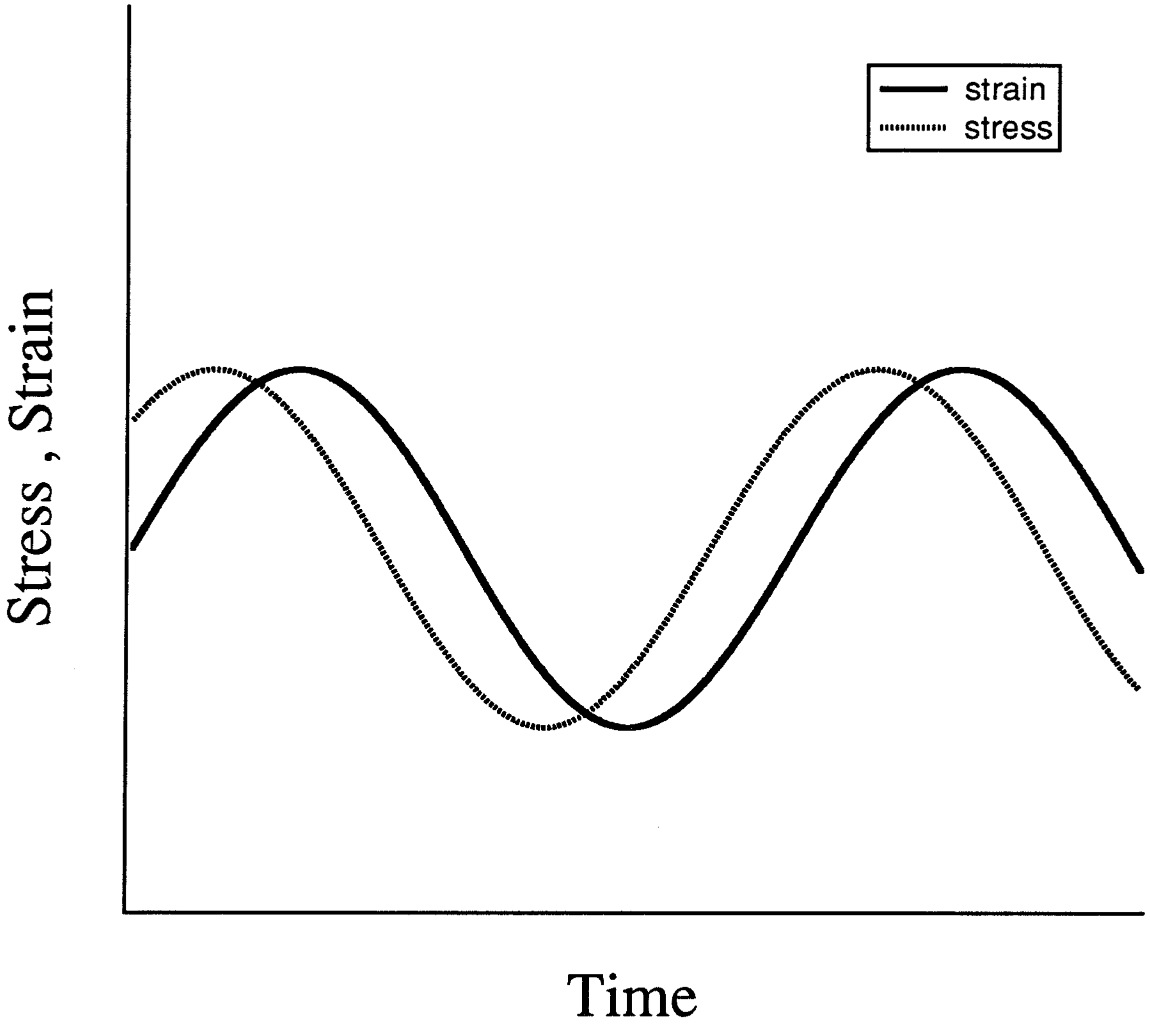

Figure (3.4)

Phase relationship between stress and strain for a dilute polymer solution undergoing low-amplitude oscillatory shear flow.

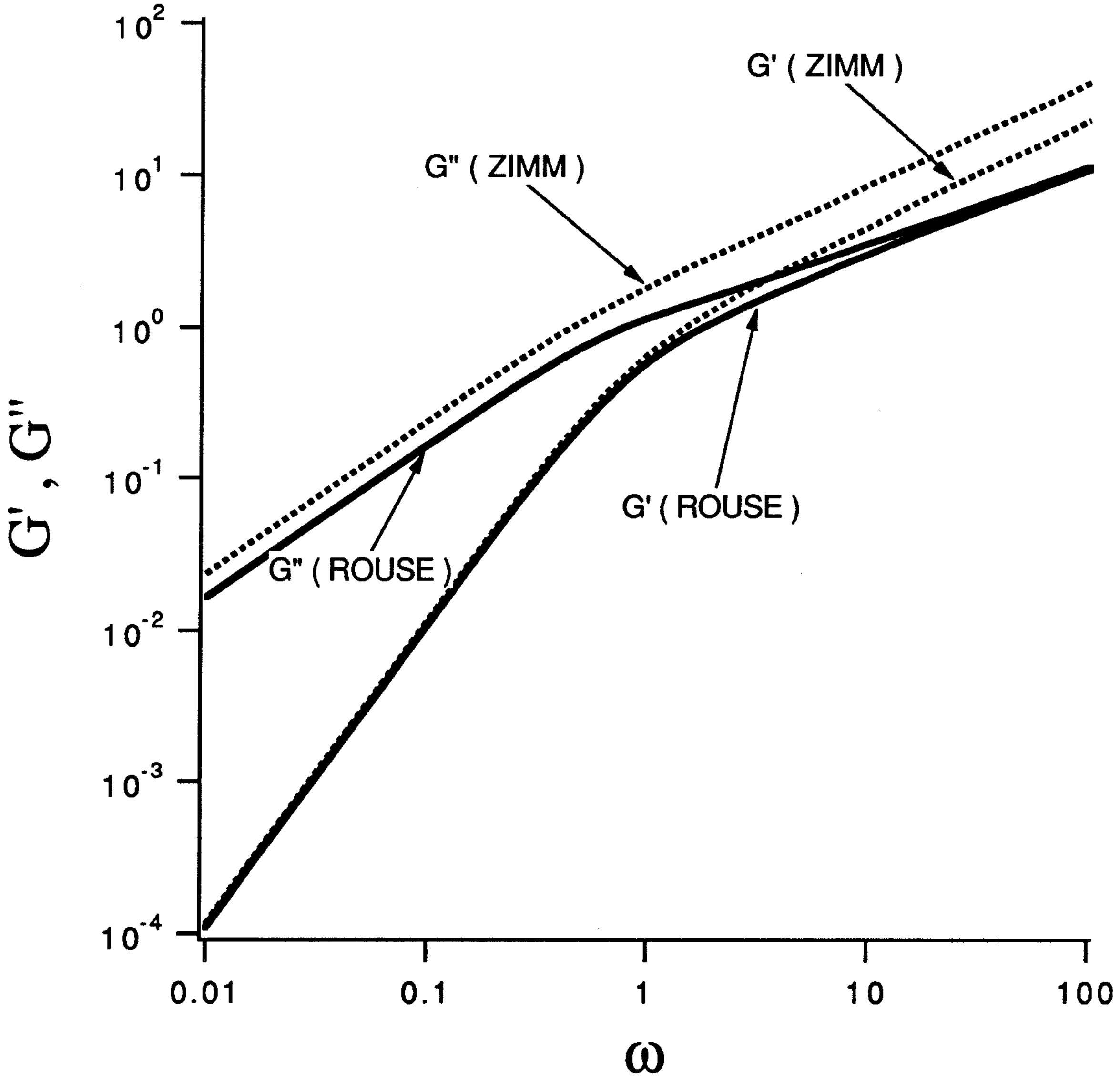

Figure (3.5)

Components of the complex modulus
for the Rouse model and the preaveraged
Zimm model, for large N.

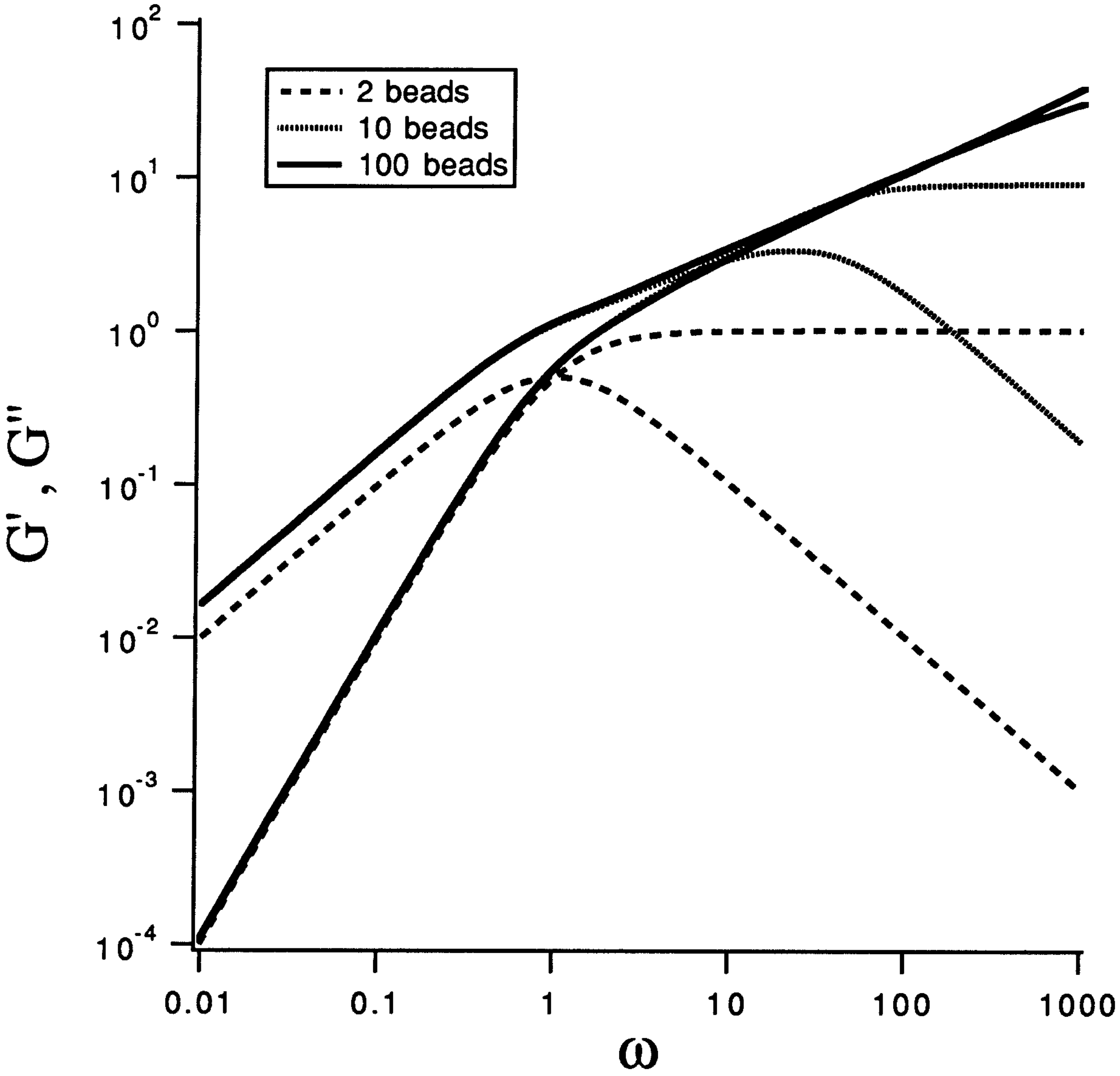

Figure (3.6)

Components of the complex modulus of the Rouse model as a function of number of beads N.

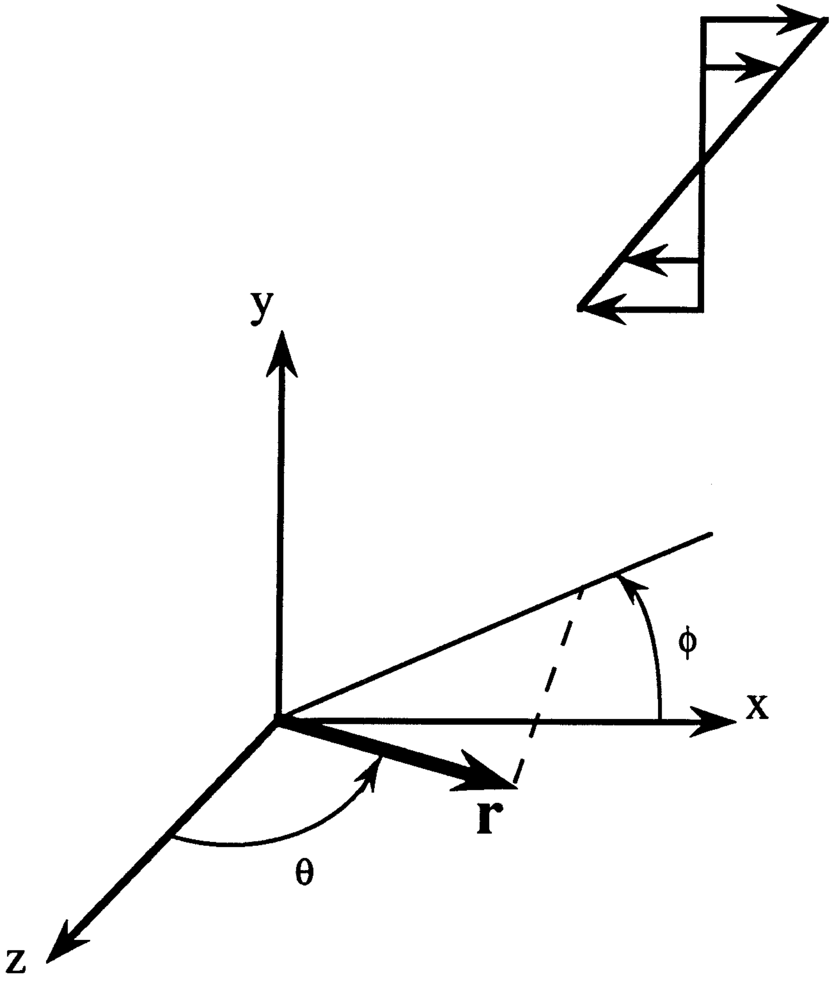

Figure (3.7)

Coordinate system for storing configurational distribution of dumbbell end-to-end vector **r**.

4. INFINITE DILUTION RESULTS

4.1 Equilibrium

An analysis of data from simulations of the Zimm and Stokesian dynamics models at equilibrium reveals the amount of data required in order to generate good statistics. There must be sufficient data to determine both the distribution of extensions, $Q_2(r)$, and also the angular distribution at a given r. Although no meaningful stress measurements can be made at equilibrium, that does not mean that the accuracy of the stress cannot be estimated. The stress predicted by each model is completely dependent upon the the distribution of configurations. If the configurational distribution is accurate, the stress calculations based on that configuration must also be accurate.

Figure (4.1) presents $Q_2^0(r)$ for the Stokesian dynamics model vs. the analytic prediction of Eq.(3.7) for 10^5 and 10^6 time steps. While 10^5 data points produce a poor description of the radial distribution, $Q_2^0(r)$ is well described with 10^6 data points. At equilibrium, there is no angular dependence, so for any extension r the distribution in ϕ and θ should be a spherical shell. The ϕ dependence of the distribution at $\theta = \pi/2$ is shown for $r = 3$ (Figure (4.2)) and $r = 6$ (Figure (4.3)) for 10^5 and 10^6 data points. Both distributions should be circular. Similar results were obtained for the Zimm Model. These plots show that 10^5 data are inadequate to give reasonable estimates of the models' behavior. From this analysis it was determined that $O(10^6)$ time steps were the minimum required to obtain reliable predictions of the orientation, and hence the stress, from the Stokesian dynamics and Zimm models. An increased amount of data would, of course, further improve the models' predictions, but computer-speed limitations made longer analyses unreasonable considering the wide range of flow parameters that were to be examined.

An additional equilibrium result arises from the inclusion of excluded volume. This is of interest in the analysis of oscillatory-shear data, where it presents some important considerations when comparing results for different values of N. As noted in §2.1, h^* may be thought of as a ratio of the size of the beads to the bead separation, as well as a ratio of hydrodynamic forces to spring forces. Previous studies have used the RMS spring-extension b as given by the Gaussian-distribution value,

$$b_{Gauss} = \left(\frac{3kT}{K}\right)^{\frac{1}{2}}. \tag{4.1}$$

While this is appropriate in a θ solvent, where by definition excluded-volume effects are not present, non-θ solvents demand that the effect of excluded volume on the value of b be considered. Table (4.1) lists b for various spring constants K for both Gaussian dumbbells and excluded-volume dumbbells. Although shown only for $N = 2$, this has implications for larger values of N. The differences between the two methods can be as great as 25%. This is an important consideration when trying to compare results for different values of N. Plotting results for a spectrum of N requires some type of renormalization, and these renormalizations usually involve the mean spring-extension b. Changing the magnitude of b changes the frequency at which the chain no longer experiences intrachain motion, and this is the transition frequency for G' and G''. Thus, if the Gaussian predictions of b are used for chains with excluded volume, the data will be normalized improperly. This could lead to spurious peaks or dips in the moduli curves, which in turn would lead to invalid conclusions. Appendix A shows the effect of excluded volume on the complex moduli predicted by the dumbbell model, using preaveraged hydrodynamic interaction.

4.2 Steady Simple Shear

One important aspect of the behavior of dilute polymer solutions is that they generally exhibit shear thinning. As noted in §2.1, the Rouse model does not predict shear thinning, in fact giving a constant viscosity no matter what the shear rate. The preaveraged Zimm model also gives a shear-rate independent viscosity. However, when the Zimm model is evaluated without preaveraging of the hydrodynamic interactions, it does exhibit shear thinning, as does the Stokesian dynamics model. This behavior is shown in Figures (4.4) and (4.5) for $h^* = 0.15$ and $h^* = 0.25$, respectively. Since the preaveraged Zimm model does not shear thin, while the non-preaveraged Zimm model does, the decrease in viscosity must be a function of the variation in hydrodynamic interaction at different shear rates. This is noted in Öttinger (1989). While this conclusion is obvious, since the variation in hydrodynamic interaction is the only difference between the preaveraged and non-preaveraged Zimm models, the mechanism by which these variations cause that change has not been addressed. The results presented below reveal how the hydrodynamic interactions modify the microstructure of the polymer in solution, and how this change causes the shear thinning.

To observe the nature of this change in the microstructure, it is convenient to examine the orientational distribution of the models in two ways: first, by examining their angularly averaged spring extensions $Q_2(r)$; second, by selecting fixed values of r and examining the angular-probability distributions at these extensions. These two analyses reveal the mechanism by which hydrodynamic interactions cause shear thinning.

Figures (4.6) - (4.8) show $Q_2(r)$ for the Rouse, Zimm and Stokesian dynamics models for $Pe = 0.1, 1$ and 10, respectively. The hydrodynamic-interaction parameter $h^* = 0.25$. Both the Zimm and the Stokesian dynamics models show a slightly greater extension than the Rouse model for all values of Pe, resulting in higher viscosities in each case (cf. Fig. (4.5)). Unlike the equilibrium plot, the Stokesian dynamics model shows an additional peak right at $r = 2$. This is an excluded-volume effect. The beads in each model are pushed together along the compressional axis of the shear flow. The Rouse and Zimm models allow the bead separation to become arbitrarily small. The Stokesian dynamics beads, however, come into contact at $r = 2$ and can come no closer. The touching beads continue to rotate until they reach the extensional portion of the flow, and this extra time in contact provides the peak in the distribution at $r = 2$.

While the Rouse distribution remains peaked at approximately $r = 3$, the Zimm and Stokesian dynamics distributions move toward larger r as Pe increases beyond 0.1 . This indicates an increase in the mean tension in the spring as the shear rate increases, which would seem to indicate shear *thickening* in the Zimm and Stokesian dynamics models (because of an increased $\mathbf{xF}$ stress contribution), not shear thinning. The resolution to this apparent contradiction lies in the accompanying change in the angular-distribution function as Pe increases.

Figures (4.9) - (4.17) show cross sections of the the angular distributions of the Rouse, Zimm and Stokesian dynamics models in the x-y plane ($\theta = \pi/2$ in spherical coordinates.) Graphs for r values from 2 to 10, and Pe from 0.01 to 10, are presented. $h^* = 0.25$. For $Pe = 0.01$, the distribution cross sections are essentially identical, and only slightly disturbed from the circular cross section indicative of the equilibrium distribution. At $Pe = 0.1$, the distributions show an increased relative density along the extensional axis of the shear flow at larger r, but the distributions are still similar for the three models, consistent with the steady viscosities predicted by each model up to $Pe = 0.1$.

The microstructural origin of shear thinning in the Zimm and Stokesian dynamics models becomes apparent from the relative distributions at $Pe = 1$. While similar in shape, the Zimm and Stokesian dynamics distributions differ from the

Rouse in that they are tilted more toward the x-axis. Recall that the particular element of the **xF** matrix that is relevant to a shearing measurement is the xF_y component, as was shown in Figure (2.1). Although the mean value of x increases as Pe increases, the accompanying tilt toward the x-axis means that the F_y component of force is reduced, and this reduction is sufficient to produce a net *decrease* in the product xF_y; hence, the measured viscosity decreases. The graphs for $Pe = 10$ show a continuation of this trend. At higher Pe the behavior is similar, but since even the Rouse distribution approaches the x-axis as Pe increases, the effect becomes progressively smaller. As $Pe \to \infty$, the Zimm model predictions approach the Rouse value. At large Pe the model is highly extended most of the time, so the assumption that the two beads do not interact hydrodynamically is valid, and the viscosity predictions reach the non-interacting limit. Although the reported results for the Zimm model actually go below the Rouse prediction, the Rouse limit is still within the statistical error of the simulation runs. In addition, the reported results are the actual results for the simulations using a dimensionless time step $\Delta t = 0.01$. It is known that the use of a finite step size can introduce a bias into the simulation results (Zylka and Öttinger 1989). Repeating the simulation results for a few other size Δt's and extrapolating the results to $\Delta t = 0$ should bring the numerical values up to the Rouse limit. This has not been done because the focus of this analysis has been to determine the relative magnitudes of the stress predictions of the models and the effect of the microstructure on the stress, not to obtain "exact" numerical values for their predictions. In any event, the reported results for the Zimm model are within 3% of the expected high Pe limit.

The Stokesian dynamics model also approaches the high Pe Rouse limit, but always predicts a slightly higher viscosity than the Zimm or the Rouse models. This appears to be a result of the finite bead size, as shown in Figure (4.15) for $r = 2$ and $Pe = 10$. When the beads are brought close together along the compressional axis of the flow, the Rouse and Zimm models allow arbitrarily small spring extensions, and therefore $\mathbf{S}^{IP} = 0$. The Stokesian dynamics model has a minimum spring extension of $r = 2$, so it still predicts a non-zero $\mathbf{S}^{IP}$. A particularly striking effect of the excluded volume is that for larger Pe, the angular distribution of the Stokesian dynamics model for $r = 2$ is greatest along the *compressional* axis of flow. The beads are forced together and stay together along the compressional side. As soon as the dumbbell rotates to the extensional side of flow, the beads are quickly pulled apart, resulting in a lower probability density on that side of the distribution. The Rouse and Zimm models quickly move past $r = 2$ on the compressional side, so their distributions favor the extensional region.

The way that hydrodynamic interaction causes the distribution to shift toward the x-axis can be seen most easily by considering just the Rouse model and the Stokesian dynamics model. Figures (4.18) and (4.19) display the relative trajectories of two force-free particles (i.e., no connecting spring) in simple shear flow based on the Rouse interaction and the Stokesian dynamics interaction, respectively. Figure (4.19) is part of the family of curves for two interacting spheres first shown in Lin *et al.* (1970) and Batchelor and Green (1972), and is reproduced exactly by Stokesian dynamics.

The trajectories are shown as "snapshots" of the center of particle 2 relative to a coordinate system fixed at the center of particle 1. These trajectories are shown for $Pe = \infty$, but they have implications for finite Pe as well. The Rouse model has no interaction or excluded volume, so the two "point particles" simply move as fluid elements. If the difference in the initial y components is small, the particles move past one another more slowly, but the trajectories remain undisturbed, straight lines.

The trajectories for the Stokesian dynamics interaction are quite different. The hydrodynamics actually produces a series of *closed* trajectories; no interparticle spring force is required – – the hydrodynamic interaction between the two spheres is sufficient to keep the two spheres rotating around one another. The time-interval plotting of particle 2's center shows that most of the time on these closed curves is spent close to the x-axis. Although the introduction of Brownian motion and interparticle forces alters these trajectories, the strength of the hydrodynamics is still sufficient to shift the angular distributions of the dumbbell models towards the x-axis. Furthermore, these closed trajectories extend along the x-axis to infinity, reflecting the extremely long-ranged nature of hydrodynamic interaction. These hydrodynamic forces effectively "pull" the Zimm and Stokesian dynamics distributions toward the x-axis, reducing their viscosity contributions. The magnitude of this "pull" grows with Pe.

Although the shear-flow example is a useful demonstration for Stokesian dynamics, it fails for the Zimm model. This is a consequence of using the Rotne-Prager approximation. Unlike the Stokesian dynamics description, which introduces a velocity disturbance that is due to the finite size of the particle in any flow with straining character, the Rotne-Prager tensor describes a velocity disturbance resulting from a point force in the fluid. The "finite-size" effect it gives is only a change in the velocity disturbance at small separations. If there is no force acting on the particle, there is no disturbance, so the trajectories in simple shear flow of two particles interacting by Rotne-Prager are the same as no interaction – – straight lines. Nonetheless, when Brownian forces and spring forces are included, the beads in the Zimm model will be experiencing constant velocity disturbances, the Rotne-Prager approximation will react to these disturbances, and the long-range nature of the hydrodynamic interaction will still move the model toward the axis of shear.

The discussion up to this point has considered only the $\mathbf{S}^{IP}$ contribution to the viscosity, ignoring the $\mathbf{S}^{B}$ and $\mathbf{S}^{H}$ contributions provided by Stokesian dynamics. This is because these contributions are essentially constant for all values of Pe and h^* examined. Figures (4.20) and (4.21) show the Brownian-stress contribution $\mathbf{S}^{B}$

and the spring contribution $\mathbf{S}^{IP}$ for $h^* = 0.15$ and $h^* = 0.25$, respectively. These plots show that $\mathbf{S}^B$ is completely negligible except at $Pe < 0.1$, and even then it is very small. It seems unusual that $\mathbf{S}^B$ never makes a substantial contribution to the stress because $\mathbf{S}^B$ is the sole contributor to the stress in the theory of rod-like polymers. Like the traditional flexible-polymer theory, the rigid-polymer theory does not consider hydrodynamic stresses. Rigid-polymer models have no interparticle forces, so $\mathbf{S}^{IP} = 0$. The only contribution to the stress in rodlike polymers arises from the change in entropy of the rod orientation. Since the dumbbells in this study show a definite bias toward the x-axis in their orientation, it seems that the Stokesian dynamics model should reflect this in the Brownian-stress contribution. The absence of $\mathbf{S}^B$ seems to be due to the way the Stokesian dynamics model calculates this stress. It is based only on the beads in the model – – no consideration is given to the connection between the beads. Since most of the time spent near the x-axis is in an extended state, the beads are far apart, and the Brownian-stress contribution from the beads is small. This is true even at $Pe = 1$, where the hydrodynamic forces are not yet dominant over the Brownian forces. Note that this is not a weakness in the Stokesian dynamics model, but is a result of the original formulation of the bead-spring model. To improve upon this, all flexible-polymer models, including the Stokesian dynamics model, could include a term for the Brownian stress of the end-to-end vector. This term would be similar in form to the $\mathbf{S}^B$ term for rigid-polymer models.

Figures (4.22) and (4.23) display the hydrodynamic contribution to the stress, $\mathbf{S}^H$, along with $\mathbf{S}^{IP}$ for the two h^*'s examined. The value of $\mathbf{S}^H$ is nearly constant for both h^*'s and the entire range of Pe. This hydrodynamic-stress contribution is due entirely to the far-field hydrodynamics. The near-field lubrication effects, while having a major impact on the orientational distribution of the Stokesian dynamics model through the excluded-volume effect, provide stresses two to three orders of magnitude smaller than the far-field stresses. Furthermore, this far-field contribution is insensitive to the separation between the two beads. It is well described by the so-called Einstein viscosity or Einstein stress, S^E. This is the stress contributed to a fluid by a single, isolated, rigid sphere, and is given by

$$S^E = \frac{20}{3}\pi\eta_s a^3. \tag{4.2}$$

For each polymer chain, the total Einstein-stress contribution to the viscosity, $\mathbf{S}^E$, is the sum of the Einstein stress on each bead,

$$\begin{aligned}\mathbf{S}^E &= \sum_{i=1}^{N} S^E\mathbf{I} \\ &= NS^E\mathbf{I},\end{aligned} \tag{4.3}$$

since the beads are identical. The Einstein-stress prediction and the $\mathbf{S}^H$ predicted by the Stokesian dynamics models are shown as a function of Pe in Figure (4.24), for the case $h^* = 0.25$. The differences between the two are negligible. While this might seem to indicate that the amount of time the particles spend near contact (where lubrication forces will be dominant) is a negligible portion of the total time, the true cause is probably more subtle. The lubrication stresses are generated not just because two beads are near contact, but because they are *in relative motion* near contact. For the infinitely dilute dumbbell, when the two beads are near contact, it is more favorable for them to rotate as a unit than to move relative to one another. This motion would produce no lubrication stress, just the Einstein viscosity contribution. A bead-spring model of more than two beads, where many-body effects would be important, would likely restrict the rotation of connecting beads as a unit, forcing relative motion and thus producing lubrication stresses. Hence the dumbbell model, which is generally regarded as being an adequate model for steady-shear analysis, may be inadequate as far as hydrodynamic-stress contributions are concerned. This explanation for the negligible lubrication stresses is supported in the oscillatory-shear results, where the stress at high frequencies exceeds the Einstein prediction. It is also supported by the non-dilute results, where high concentration causes stress growth. Another way of considering the onset of the additional hydrodynamic stress (i.e., above $\mathbf{S}^E$) is to think in terms of a "local" concentration of beads. In the dumbbell case, where the local concentration is always small, $\mathbf{S}^E$ is an adequate description. In multibead chains and concentrated solutions, the local concentration is often high, and the full hydrodynamics must be examined.

A second aspect of shear rate dependence in polymer rheology involves the first normal-stress difference, defined in Eq. (3.26). Once again, the Rouse model predicts that the first normal-stress difference will be independent of shear rate. Experimental results show that the stress difference will decrease with increasing shear rate. As with the viscosity, this shear-thinning behavior is not captured by the preaveraged Zimm model, but it is reproduced by Öttinger's consistently averaged and Gaussian-approximation models (1989) as well as by the dynamical Zimm and Stokesian dynamics models. This behavior is shown in Figures (4.25) and (4.26) for $h^* = 0.15$ and 0.25, respectively, for the Rouse, Zimm and Stokesian dynamics models. As with the viscosity, the thinning of each model displays the same general curve shape, but the excluded volume in the Stokesian dynamics model always keeps the magnitude slightly above the Zimm prediction. Unlike the viscosity, however, the total contribution to the Stokesian dynamics normal-stress difference is almost entirely due to the $\mathbf{S}^{IP}$ contribution. The hydrodynamic stress makes a contribution only at very low shear rates, and then only a small amount. While the finite size of the Stokesian dynamics beads induced a shear-stress contribution when subjected to a straining flow, there is no corresponding normal-stress contribution. This may not be the case in a multibead chain or in a concentrated solution, where many-body effects become significant. The Brownian-stress contribution is negligible over the entire range of plotted shear rates. (At very small Pe – – less than 0.1 – – the Brownian stress makes a non-negligible contribution, but the fluctuations are so large at low Pe that it is not possible to get good predictions of the stress difference.)

The cause of this shear thinning of the normal-stress difference is identical to that of the viscosity. At low shear rates, the greater extensions of the models cause the normal-stress to be larger than in the non-interacting Rouse case. As the shear rate increases, the configurations approach the Rouse predictions, so at high Pe all of the models are similar.

Experimental evidence, as well as Öttinger's Gaussian approximation, predicts that the second normal-stress difference, Eq.(3.27), should be small and negative. The amount of data collected for this study was insufficient to make this determination, but a larger amount of data would certainly find this prediction to be true. Again, the origin would be found to be in a change in the orientational distribution. As noted above, the hydrodynamics causes a shift in the distribution toward the x-axis, and thus a reduction both in the y component of the end-to-end vector and in the F_y component of the interparticle force. Since this would cause $\mathbf{S}_{yy} = yF_y$ to be reduced, the net effect on $\mathbf{S}_{yy} - \mathbf{S}_{zz}$ (and thus Ψ_2) would be to drive it to be negative.

For the Stokesian dynamics model in low-Pe, steady, simple shear flow, an ordinary differential equation may be solved for the exact departure from equilibrium of the distribution function. Unfortunately, the resolution of the present simulation for low-Pe flows was not sufficient to detect the predicted disturbance to the distribution function. The development and solution of this differential equation are presented in Appendix A.

4.3 Oscillatory Simple Shear

The standard comparison for oscillatory shear is with the preaveraged Zimm model. Prior studies usually have compared with Zimm's original preaveraged results for the Oseen tensor, regardless of the actual interaction tensor used, assuming that the differences would be small. This is unnecessary, since it is simple actually to calculate the preaveraged time constants for a chain of N beads interacting via an arbitrary hydrodynamic-interaction tensor, so long as N is "not too large." All that is required is to solve for the eigenvalues of an $N \times N$ matrix, for which there are available several efficient, computer software packages. Furthermore, there is no reason not to find the eigenvalues for the actual interaction – – particularly when a simulation is being used that requires finding the square root of a $3N \times 3N$ matrix at every time step. The eigenvalue solution for the preaveraged time constants need be done only once. The solution for these time constants, however, shows that the supposed similarity between the Oseen and the Rotne-Prager time constants is justified. Nonetheless, it may not be true for all hydrodynamic-interaction representations, and certainly is not true where excluded volume is concerned. The details of the solution for the time constants involving an arbitrary interaction tensor are presented in Appendix B.

The Rouse and Zimm theories for oscillatory shear flow both were developed for the case of $Pe \to 0$. Unfortunately, the simulation results become increasingly poor at small Pe, since the increased strength of the Brownian forces requires unreasonably long simulation runs to obtain reliable predictions of the moduli. $Pe = 0.1$ was selected as a reasonable compromise between the two considerations. Some results are also presented for $Pe = 0.63$.

Unlike the steady-shear case, observations of $Q_2(r)$ or the angular distributions are not helpful for the analysis of the polymer behavior in oscillatory flow. Again, this is due to the difficulty in observing the small departures from equilibrium at low Pe. All of the $Q_2(r)$ data are nearly identical to the equilibrium $Q_2^0(r)$, and the angular-distribution plots are all essentially circular.

Figures (4.27) and (4.28) show G' and G'', respectively, for the Zimm, Stokesian dynamics, and the preaveraged-Zimm dumbbells with Rotne-Prager interaction, for $Pe = 0.1$ and $h^* = 0.25$. The simulation results lie slightly above the preaveraged results. In the Stokesian dynamics model this is because the excluded volume increases $\mathbf{S}^{IP}$, as shown in Figure (4.29), for $Pe = 0.63$ at a frequency of 0.063. This is a direct result of the excluded volume forcing the RMS spring-extension b to increase from the Gaussian value, hence increasing the average tension in the spring. As suggested in the equilibrium state, this increase in b is small for small values of h^* but increases as h^* increases. The Zimm model has no excluded volume, but the description of the hydrodynamic interaction changes when $r < 2$. The dumbbell spends more time in this range of extension than in the steady shear case, so the "excluded-volume" effect of the Rotne-Prager description becomes apparent. The preaveraging apparently does not fully reflect the impact of this near-contact region. Figures (4.30) and (4.31) show the moduli for chains of 10 beads with $h^* = 0.15$ and $Pe = 0.63$. The increase in the moduli above the preaveraged predictions is even greater than in the dumbbell case, again because of the excluded volume effects.

Although the increases in the moduli are due to the increased spring extensions, from another point of view this implies that the frequencies these data are plotted against should be normalized differently. As noted in §4.1, care must be taken when plotting data from models that include excluded volume. All non-dimensionalizations of ω to this point have been done using the diffusive time a^2/D_o, regardless of b. Taking the Stokesian dynamics dumbbell data and adjusting the frequencies by the $b_{ex.vol.}/b_{Gauss}$ ratio for $h^* = 0.25$ from Table (4.1) shift the data toward the preaveraged-Zimm results. However, as shown in Figure (4.32) for G'', the change does not account for the full difference, proving that the higher moduli predicted by Stokesian dynamics is not due simply to a difference in normalization.

For $Pe = 0.63$, the Brownian contribution is found to be about two orders of magnitude smaller than the interparticle or the hydrodynamic contributions to the stress, as shown in Figures (4.33) and (4.34) for a 10-bead chain. Even at very high values of h^*, the Brownian stress is negligible (Figure (4.35)). Obviously, as Pe decreases, the relative magnitude of the Brownian contribution must increase. This is shown in Figure (4.36) for $Pe = 0.1$. The Brownian stress now appears to be closer to perhaps 5 – 10 % of the total stress for large h^* – – larger, but probably still not worth the extra computational effort. While this small $\mathbf{S}^B$ is in part due to the fact that this analysis does not use $Pe \to 0$, it must also be due to the neglected entropic contribution from the orientational distribution of the end-to-end vector. As was discussed in the steady-shear results, some allowance should be made for the entropy that is due to the orientation of this vector, as is done in the theory of rigid polymers.

The remaining stress contribution arises from the hydrodynamic interaction between the beads and the solvent. As shown in Figures (4.29) and (4.32), the $\mathbf{S}^{IP}$ contribution to G'' decays to zero, while the addition of $\mathbf{S}^H$ causes it to grow with a slope of 1. This corresponds to a complex viscosity η^*, which has a non-zero, limiting value at high frequency. Figure (4.37) plots η',the viscous or dissipative portion of the viscosity, for the Rouse model and the preaveraged Zimm model for large N. Both of them predict that η' will decay to zero as $\omega \to \infty$. This is equivalent to saying that at high frequency a dilute polymer solution will have the same viscosity as the pure solvent. Experimentally this is known to be false; at high frequency the polymer gives a constant, non-zero addition to the solvent viscosity. Figure (4.38) presents the Stokesian dynamics results for η', both with and without the hydrodynamic-stress contribution. It shows clearly not only that η' is going to a constant value greater than zero, but also that this high-frequency contribution is due entirely to the hydrodynamic stress. This is the reason that Rouse, Zimm and other prior modeling of flexible polymers have not been able to capture the proper high-frequency behavior. None have included the hydrodynamic *stress* in their analyses, and the Stokesian dynamics model shows that this is the sole cause of the high-frequency behavior.

As in the steady-shear case, the hydrodynamic-stress contribution is well described by the Einstein viscosity. It can be seen from Figure (4.39) that for a chain of 10 beads connected by a weak spring ($h^* = 0.15$), $\mathbf{S}^E$ is almost identical to the total hydrodynamic viscosity calculated by Stokesian dynamics. This is expected, since a weak spring means the average spacing between adjacent beads is large, and thus lubrication and other finite-size effects are not as important. For a stronger spring ($h^* = 0.25$, Figure (4.40)), the total hydrodynamic stress in the 10-bead chain is still well described by $\mathbf{S}^E$ for low frequencies, but for ω equal to unity and larger, the full viscosity is 5 – 10 % larger than $\mathbf{S}^E$; the stronger spring is pulling the beads closer together, so finite-size effects are beginning to have a greater influence. The deviation from $\mathbf{S}^E$ at higher frequencies appears because the rapid variation in the velocity gradient makes relative motion at close separations more likely. As discussed in §4.2, it is this relative motion that is the primary source of the hydrodynamic stress. In a chain of 10 beads, adjacent beads cannot simply rotate as though they were dumbbells. The "local" bead concentration is high enough to contribute additional hydrodynamic stress. Figure (4.41) shows that the dumbbell, even at very high frequencies, does not predict $\mathbf{S}^H$ to be significantly larger than $\mathbf{S}^E$. As with steady shear, more beads in the model, or a non-dilute concentration, would make relative motions among the beads more prevalent, further increasing $\mathbf{S}^H$. Forcing the beads closer together will eventually generate lubrication-stress contributions, even for the infinitely dilute dumbbell. Figure (4.42) shows the changes in the stress calculated with Stokesian dynamics as h^* increases for the dumbbell model ($\mathbf{S}^E$ is, of course, invariant with respect to h^*). Even for the low frequency of $\omega = 0.0628$ shown, strong springs cause a 5 – 10 % increase above $\mathbf{S}^E$. Higher frequencies will result in an even greater enhancement of $\mathbf{S}^H$.

Spring constant H	Gaussian Extension b	Interaction Parameter h*	Excluded Volume b	Ratio of b's
0.071	6.51	0.15	6.63	0.99
0.196	3.91	0.25	4.19	0.93
0.385	2.79	0.35	3.24	0.86
0.750	2.00	0.49	2.68	0.75

Table (4.1)

Comparison of RMS spring extensions of dumbbells connected by Hookean springs with and without excluded volume.

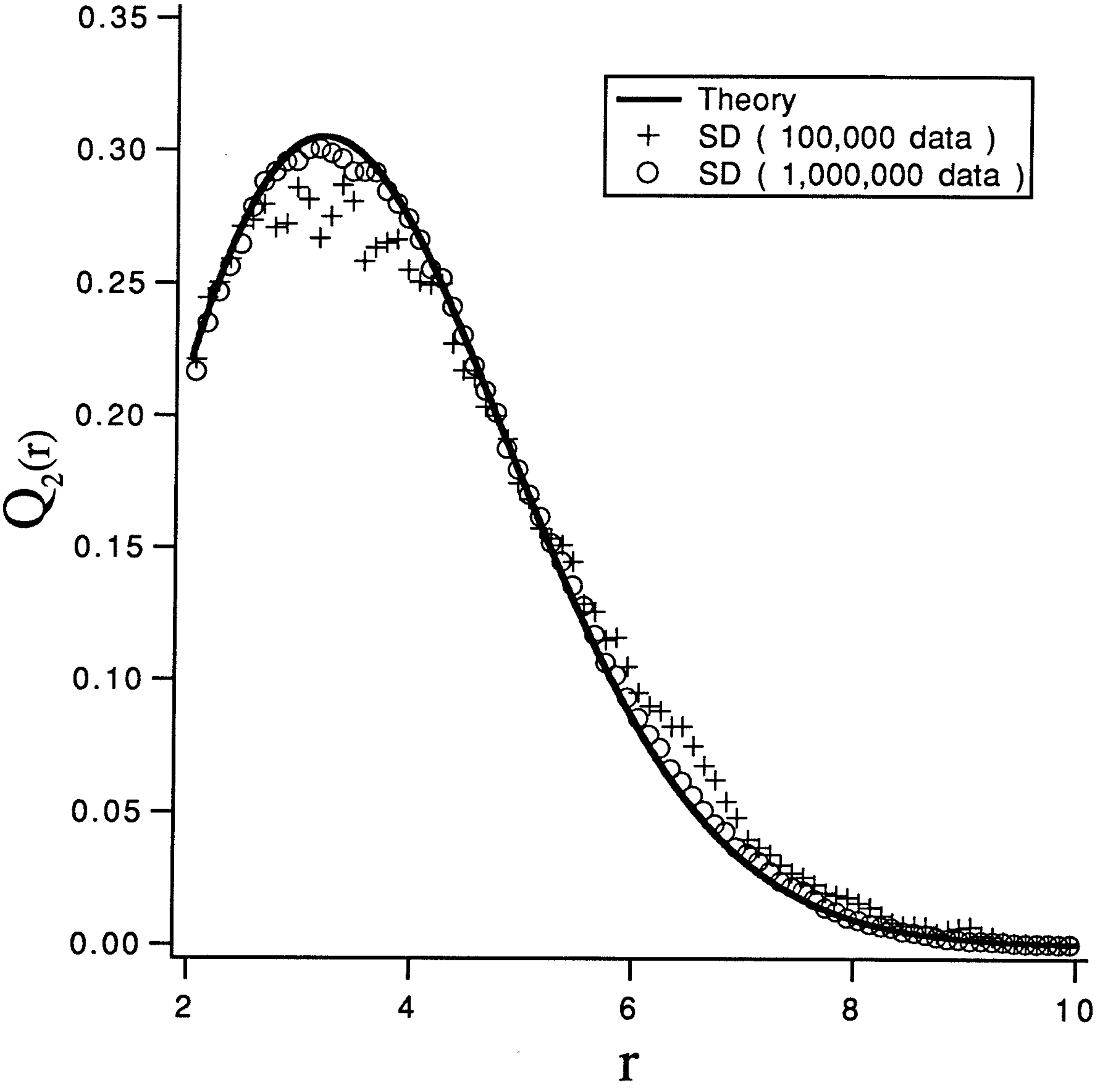

Figure (4.1)

Comparison between simulation and theory for angularly averaged equilibrium radial distribution function of Stokesian dynamics dumbbell end-to-end vector. The spring constant K=0.19635 .

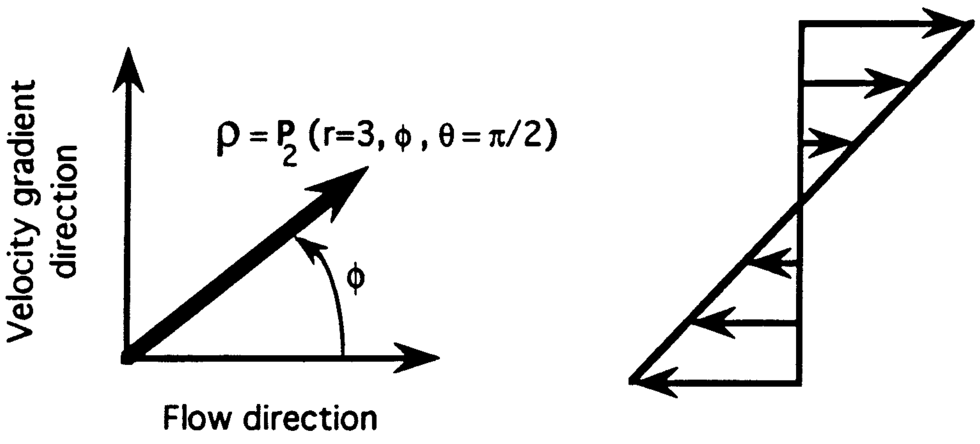

(a)

(b)

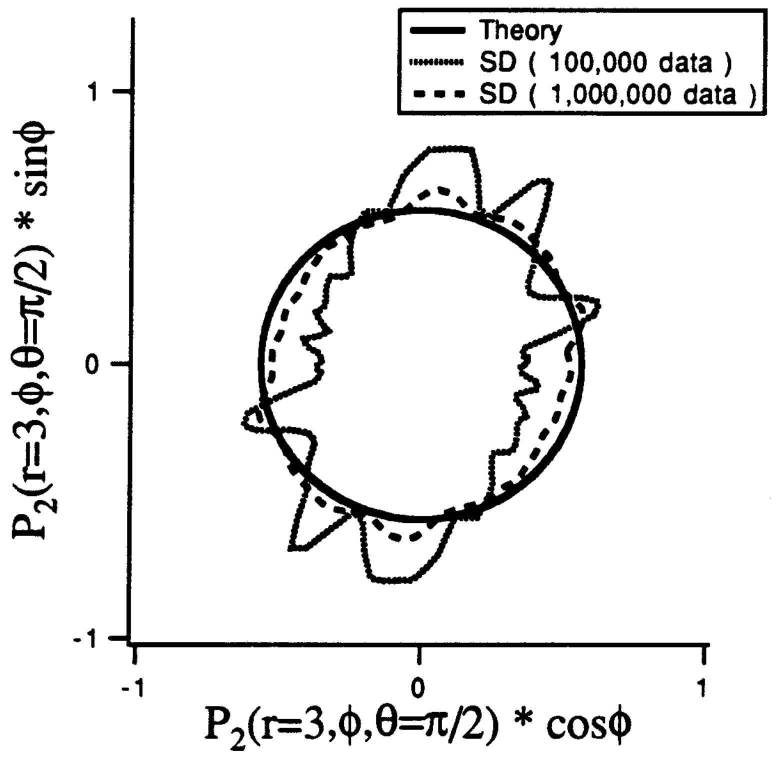

Figure (4.2)

Comparison between simulation and theory for angular distribution of dumbbell end-to-end vector at equilibrium for an extension of r=3 and h*=0.25 . Figure (a) shows the coordinate system for P_2 relative to the imposed shear flow in Figure (b).

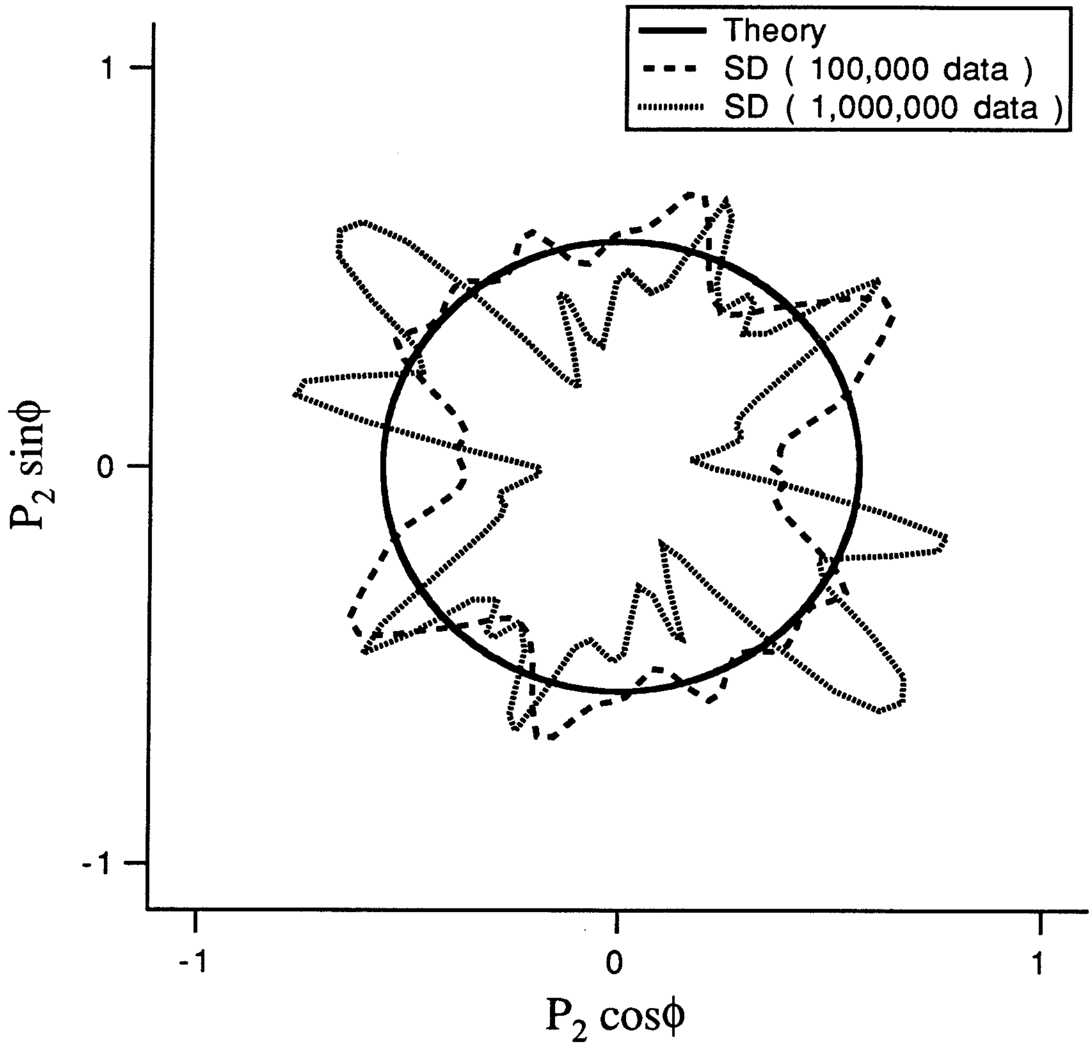

Figure (4.3)

Comparison between simulation and theory for angular distribution of dumbbell end-to-end vector at equilibrium for an extension of r=6. (h*=0.25)

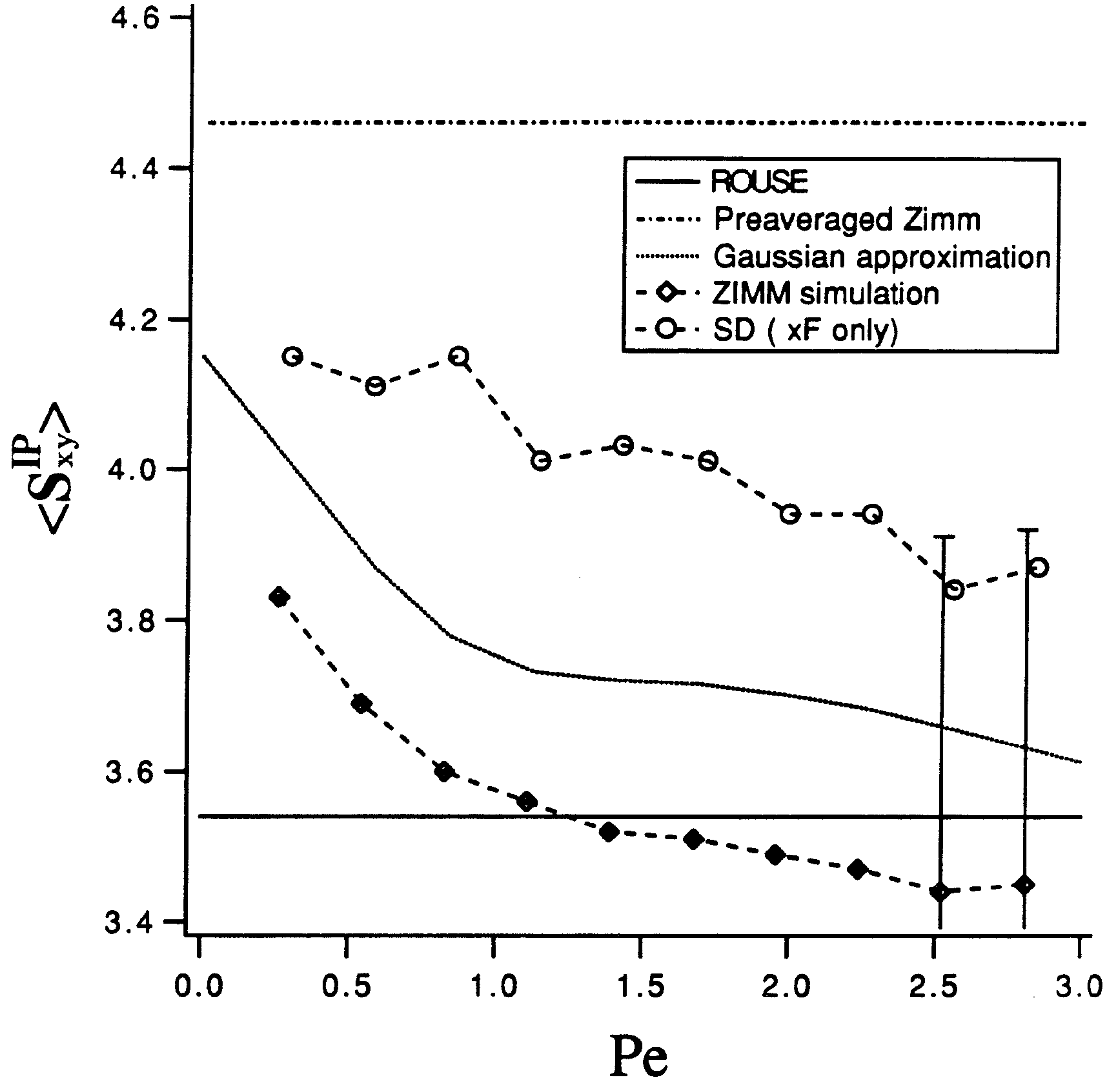

Figure (4.4)

Comparison between simulation results and various approximate analytical solutions for the shear-rate dependence of the interparticle-force contribution to the viscosity. (N=2 ; h*=0.15)

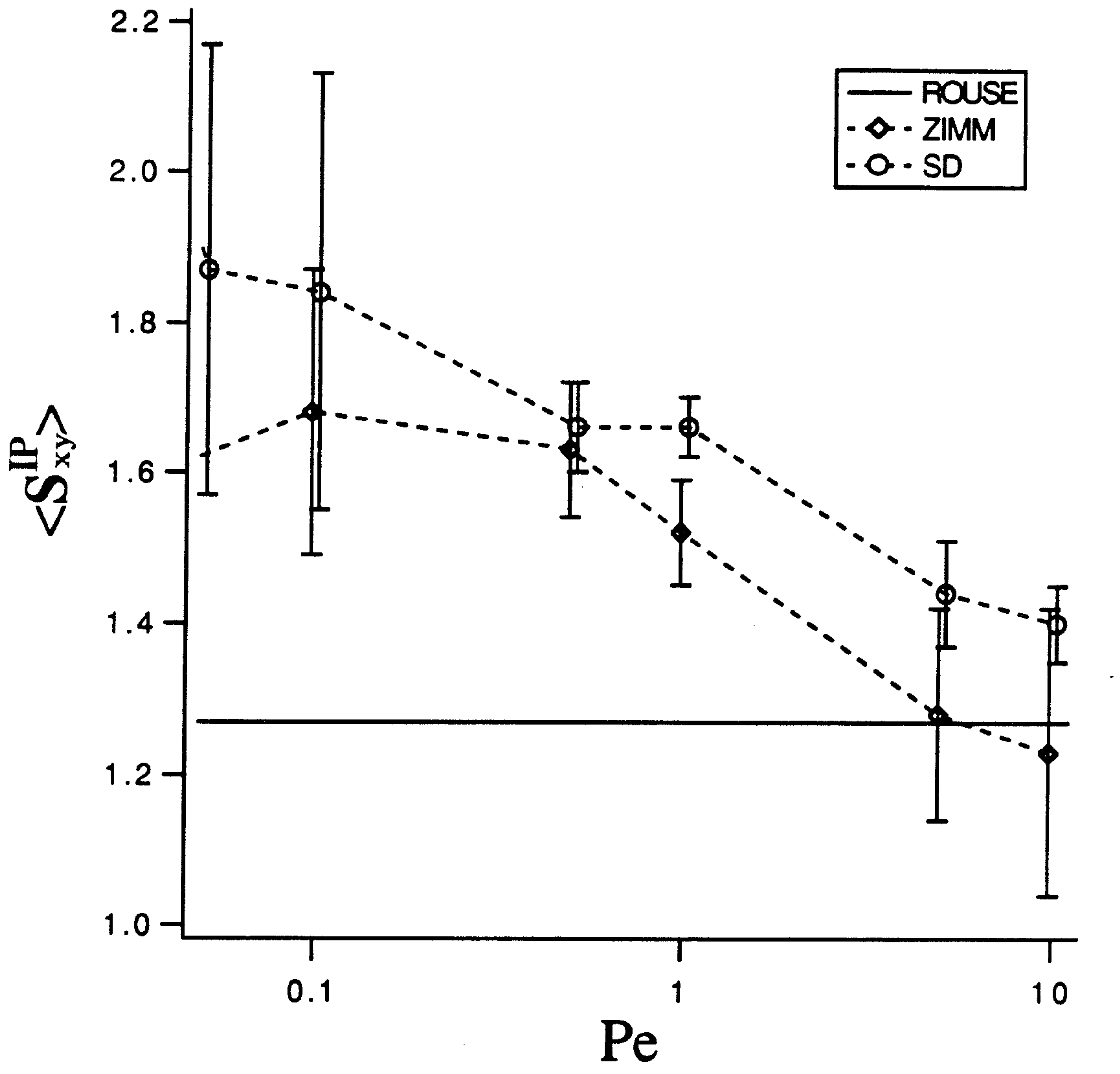

Figure (4.5)

Comparison between simulation
and Rouse model for shear-rate
dependence of viscosity.
(N=2 ; h*=0.25)

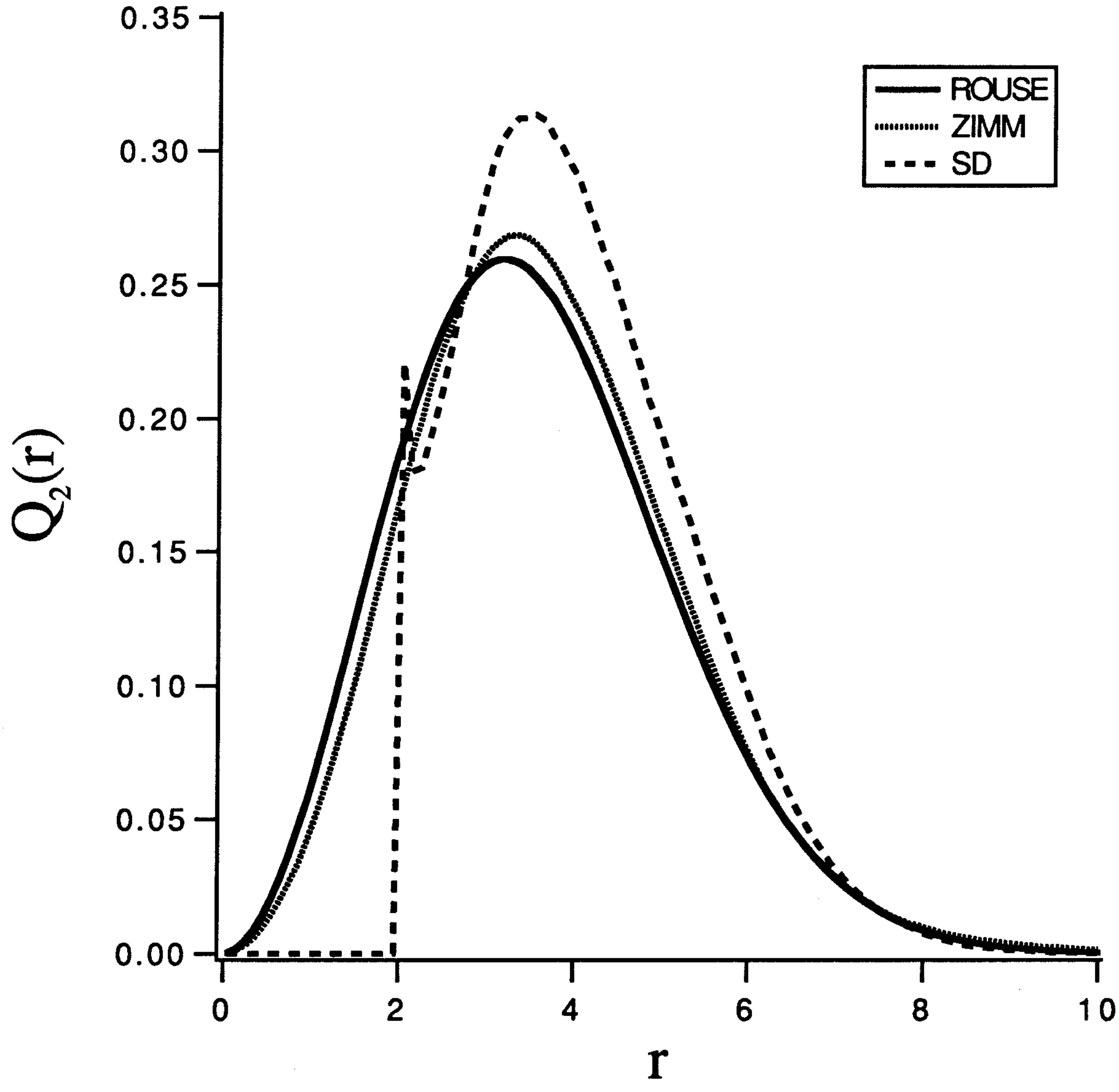

Figure (4.6)

Angularly averaged radial distribution functions of Rouse, Zimm and Stokesian dynamics dumbbells for Pe=0.1 and h*=0.25 .

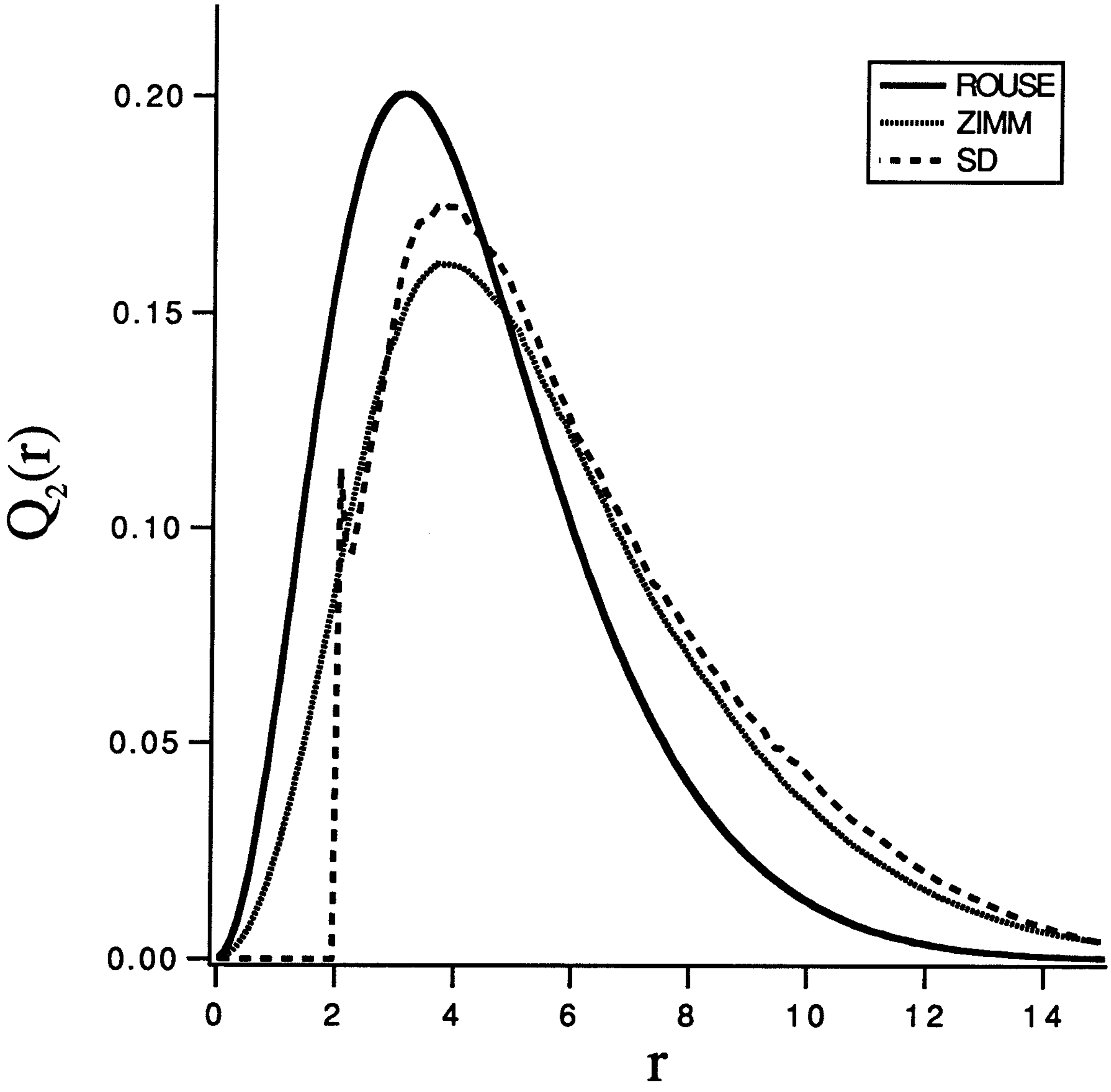

Figure (4.7)

Angularly averaged radial distribution functions of Rouse, Zimm and Stokesian dynamics dumbbells for Pe=1 and h*=0.25 .

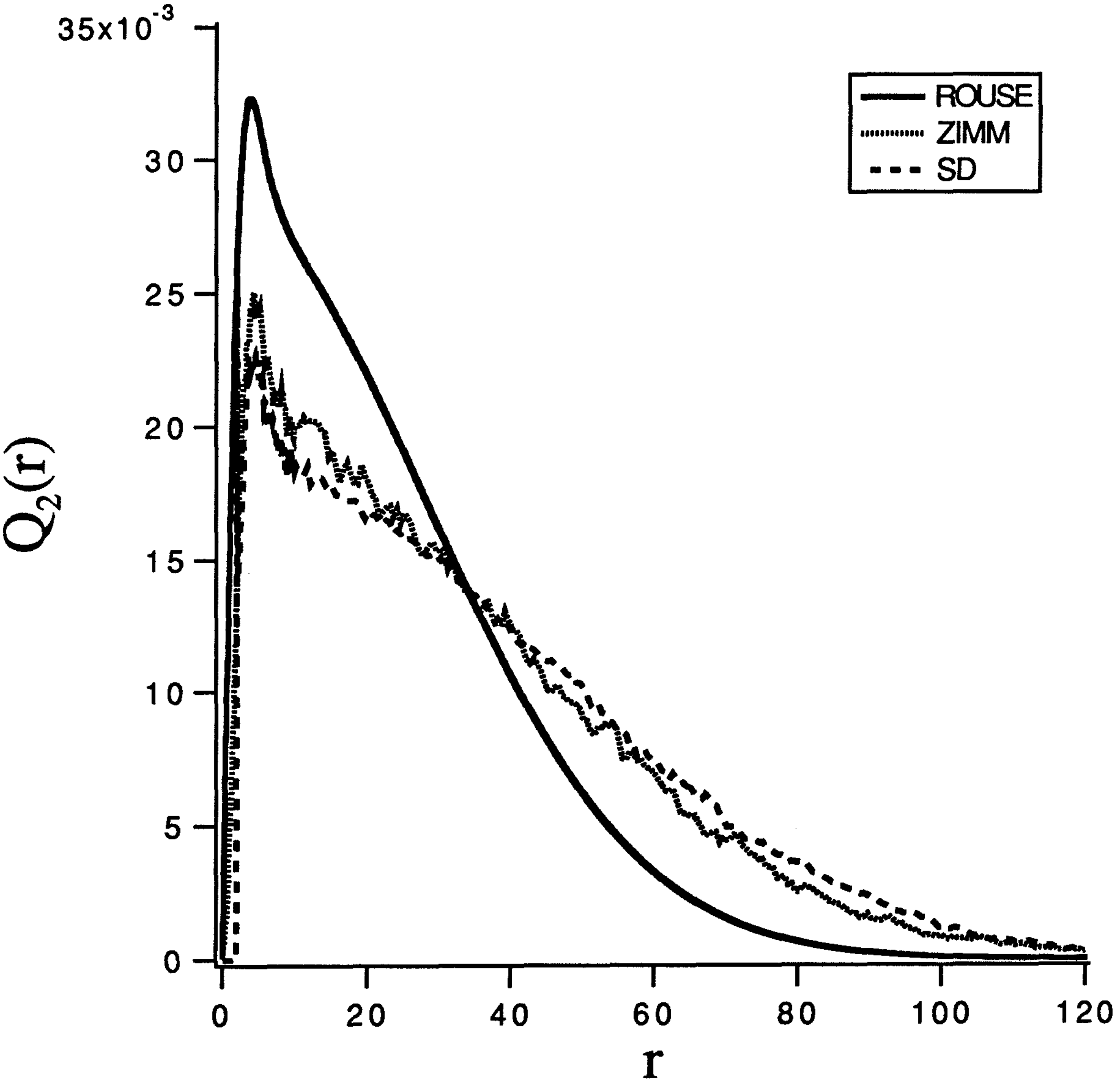

Figure (4.8)

Angularly averaged radial distribution functions of Rouse, Zimm and Stokesian dynamics dumbbells for Pe=10 and h*=0.25 .

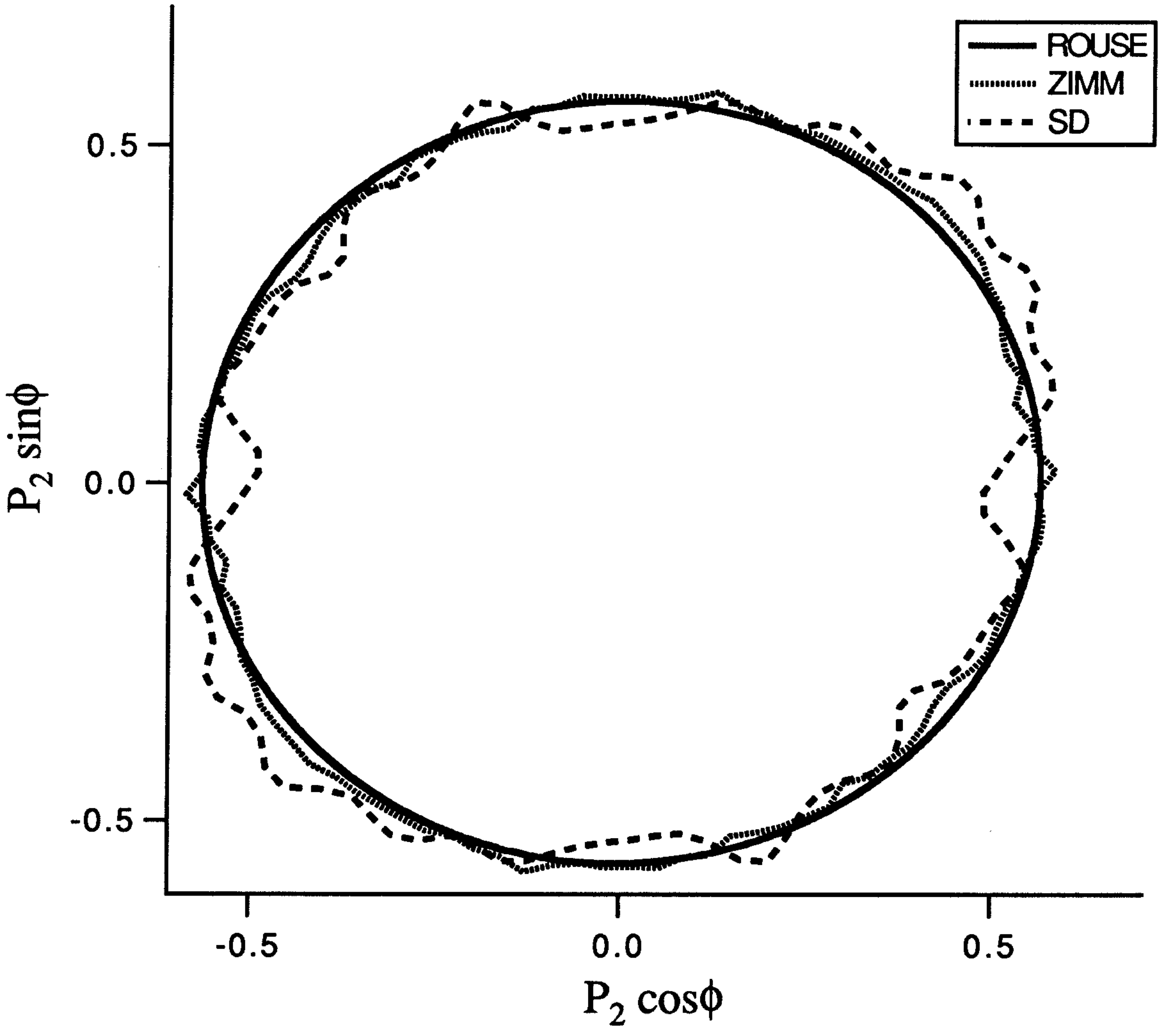

Figure (4.9)

Angular distribution functions of Rouse, Zimm and Stokesian dynamics dumbbells at an extension of r=2. Pe=0.01 and h*=0.25 .

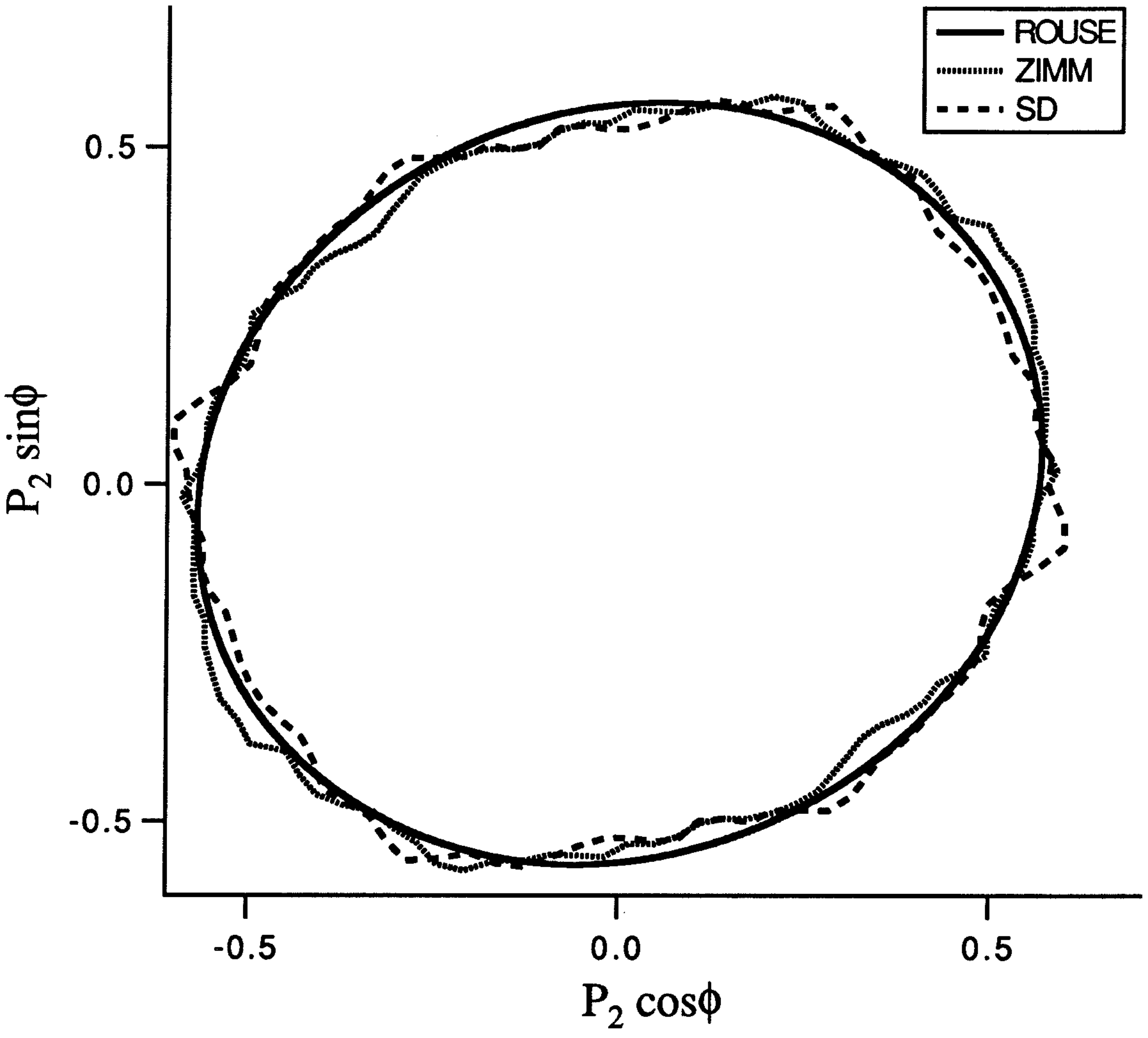

Figure (4.10)

Angular distribution functions of Rouse, Zimm and Stokesian dynamics dumbbells at an extension of r=2. Pe=0.1 and h*=0.25 .

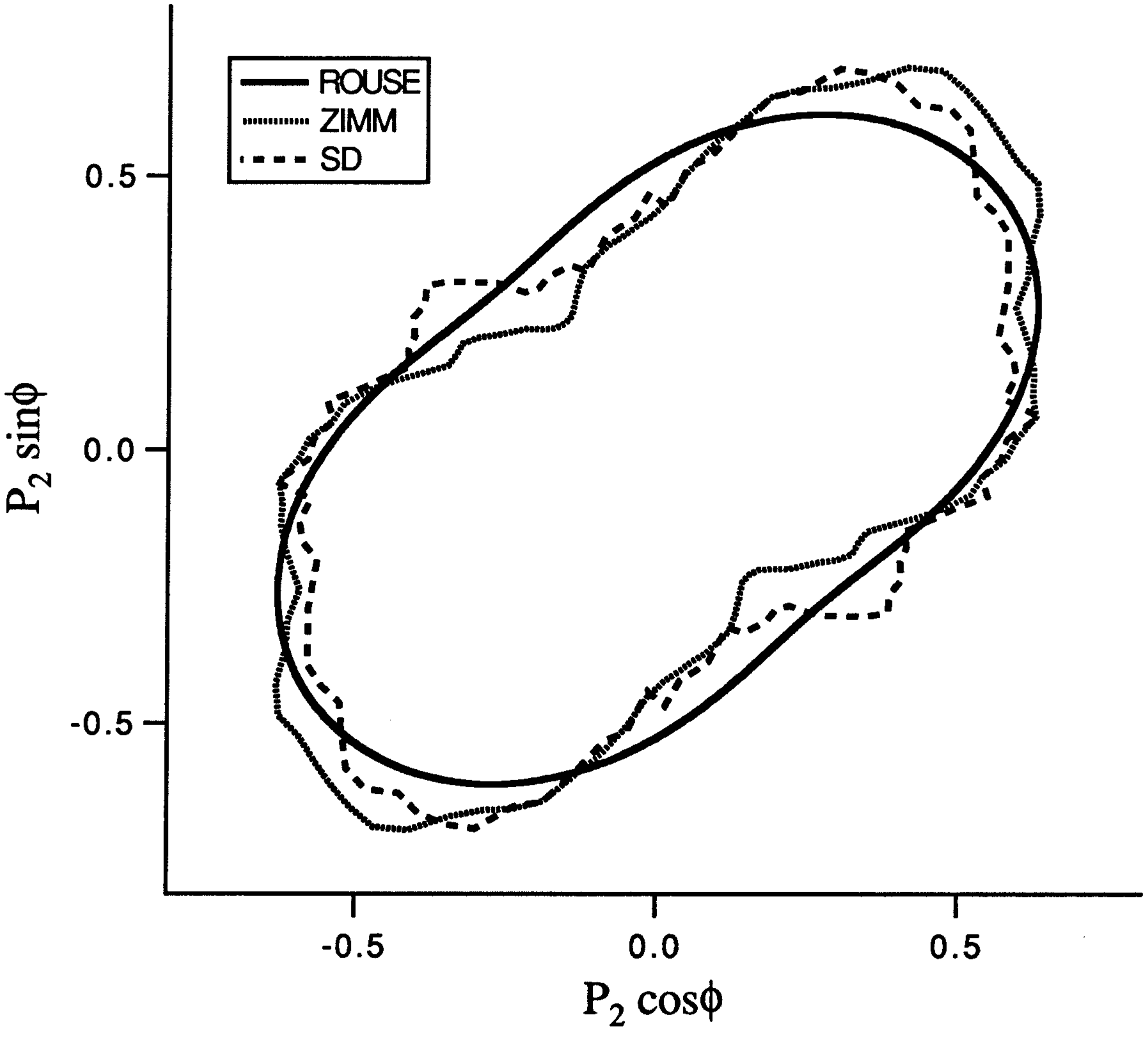

Figure (4.11)

Angular distribution functions of Rouse, Zimm and Stokesian dynamics dumbbells at an extension of r=5. Pe=0.1 and h*=0.25 .

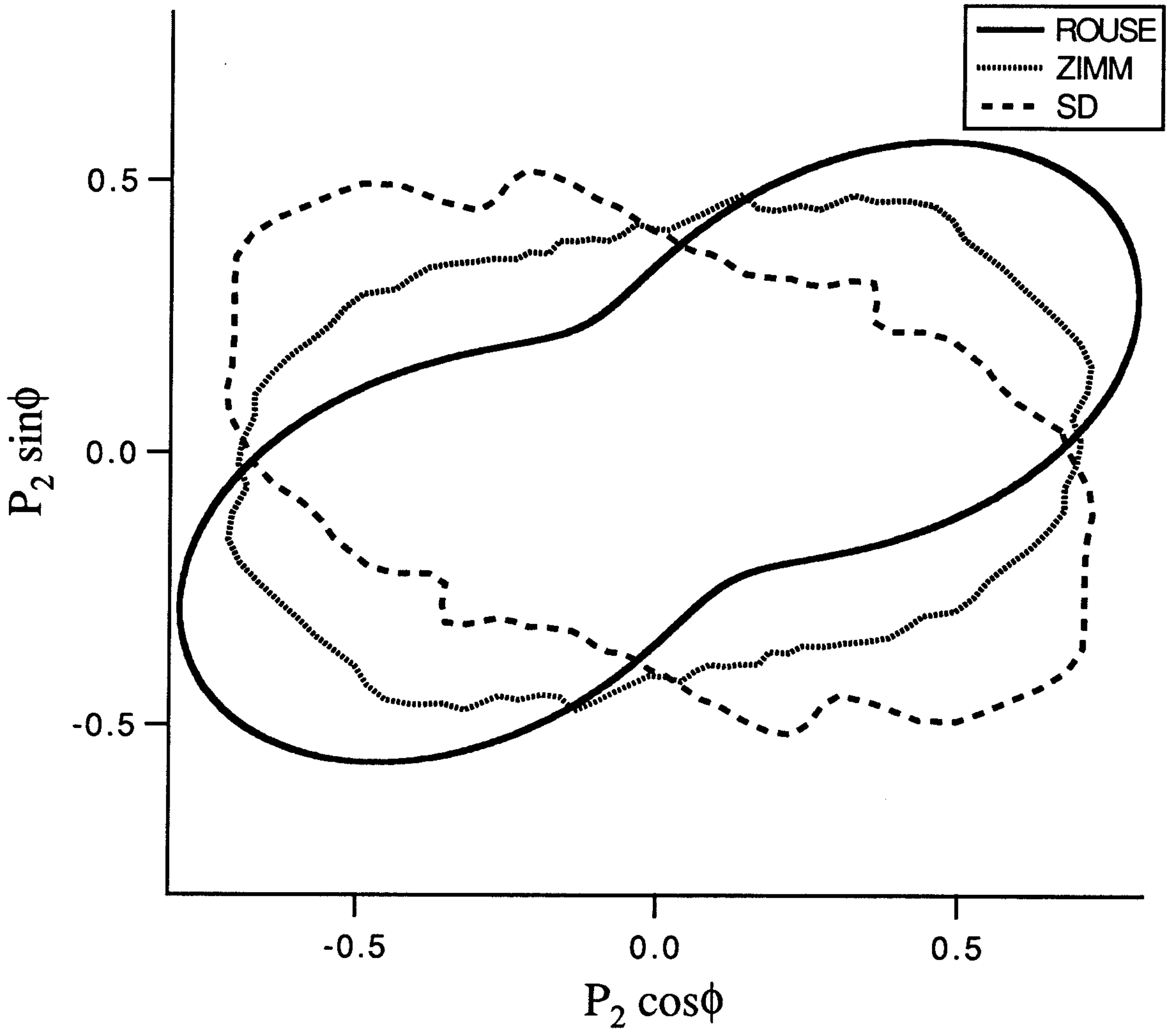

Figure (4.12)

Angular distribution functions of Rouse, Zimm and Stokesian dynamics dumbbells at an extension of r=2. Pe=1 and h*=0.25 .

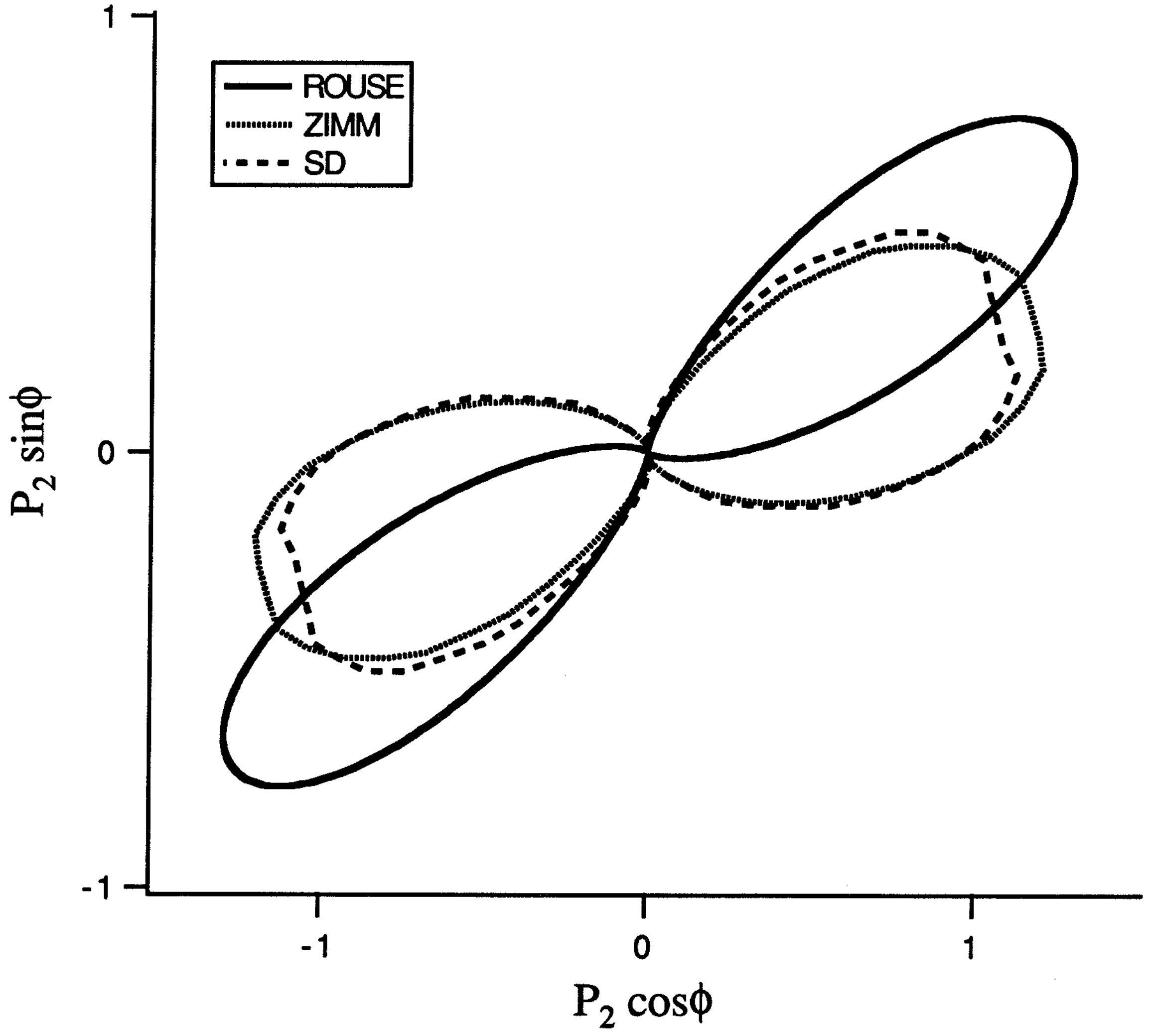

Figure (4.13)

Angular distribution functions of Rouse, Zimm and Stokesian dynamics dumbbells at an extension of r=5. Pe=1 and h*=0.25 .

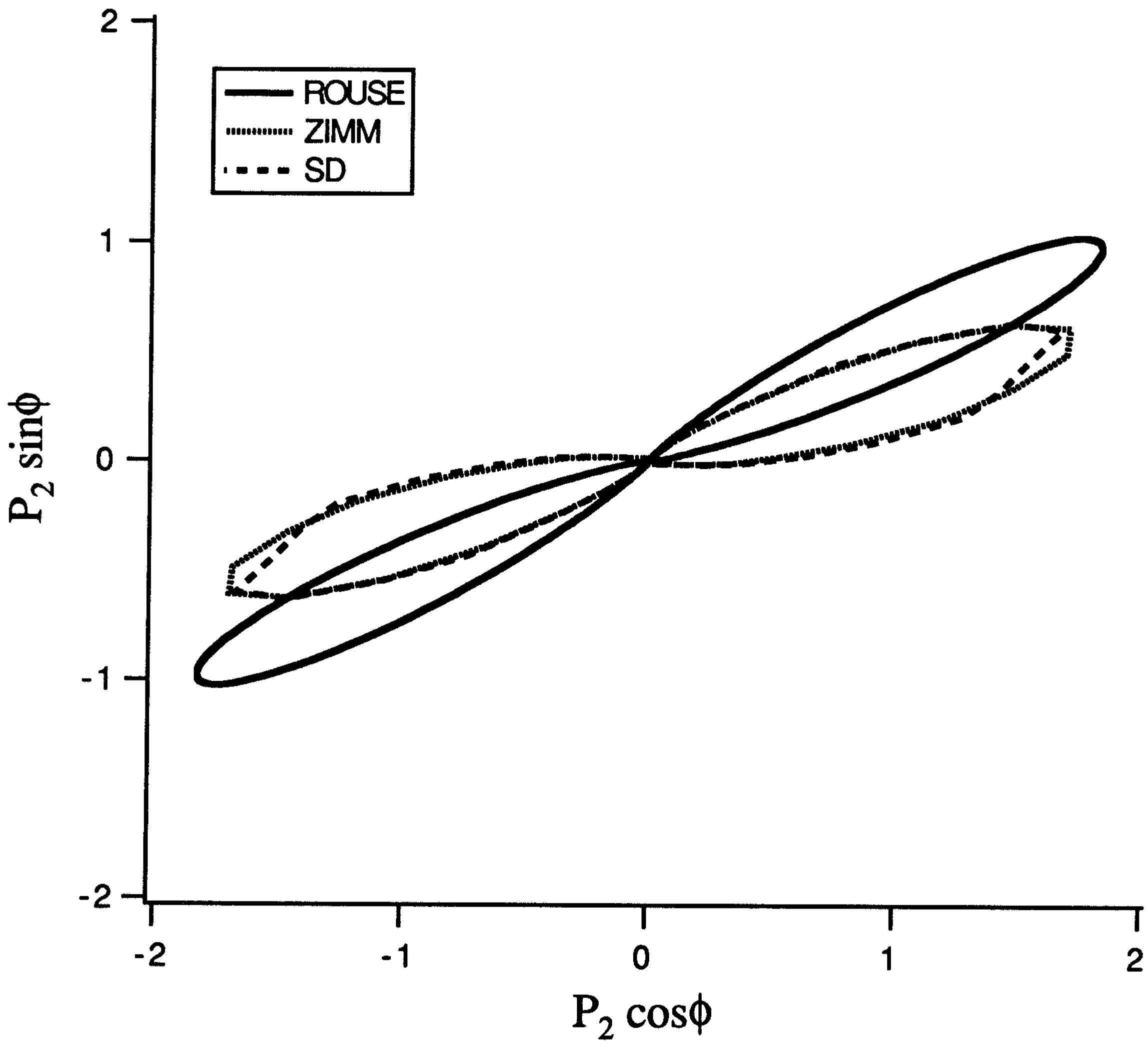

Figure (4.14)

Angular distribution functions of Rouse, Zimm and Stokesian dynamics dumbbells at an extension of r=10. Pe=1 and h*=0.25 .

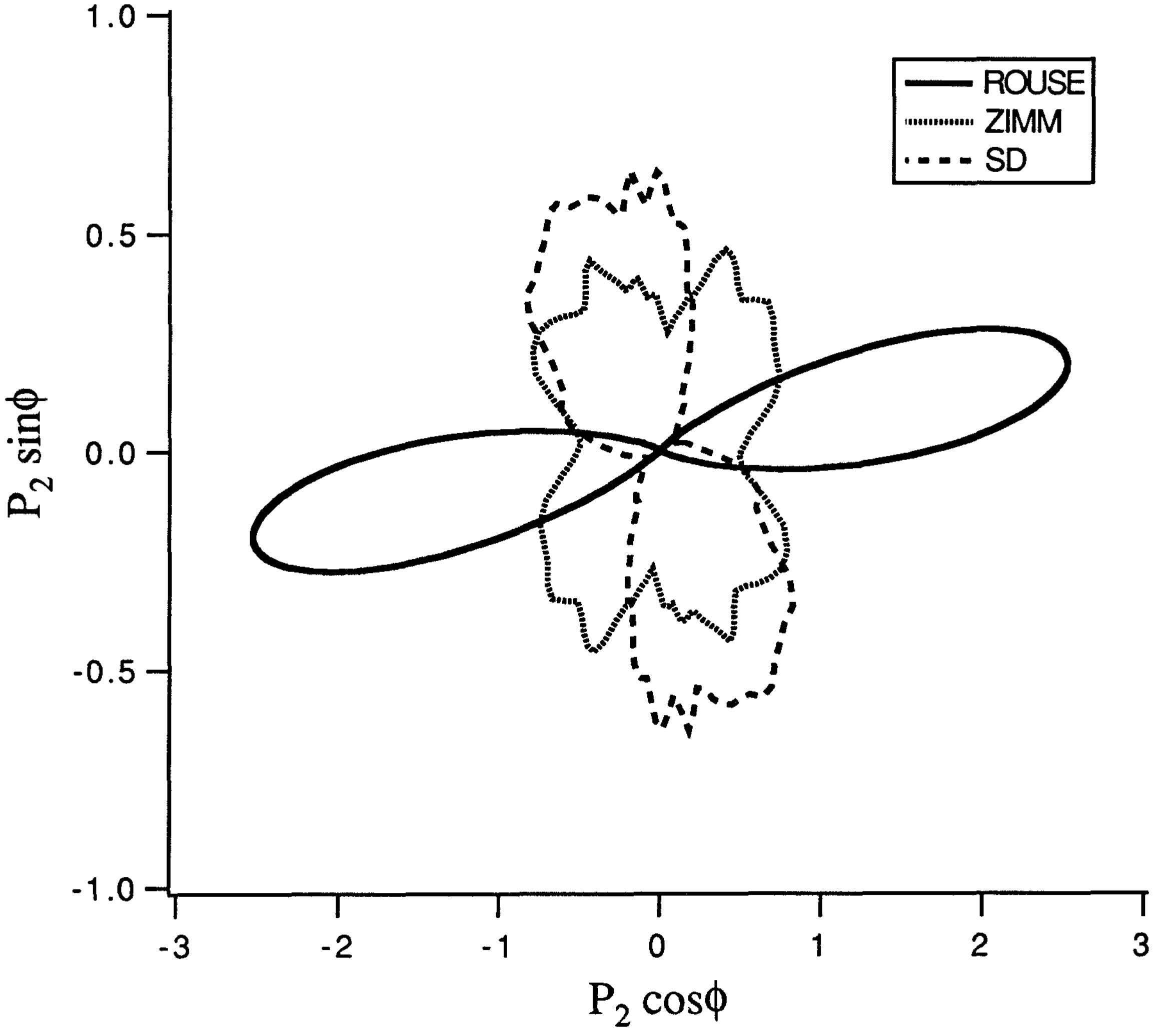

Figure (4.15)

Angular distribution functions of Rouse, Zimm and Stokesian dynamics dumbbells at an extension of r=2. Pe=10 and h*=0.25 .

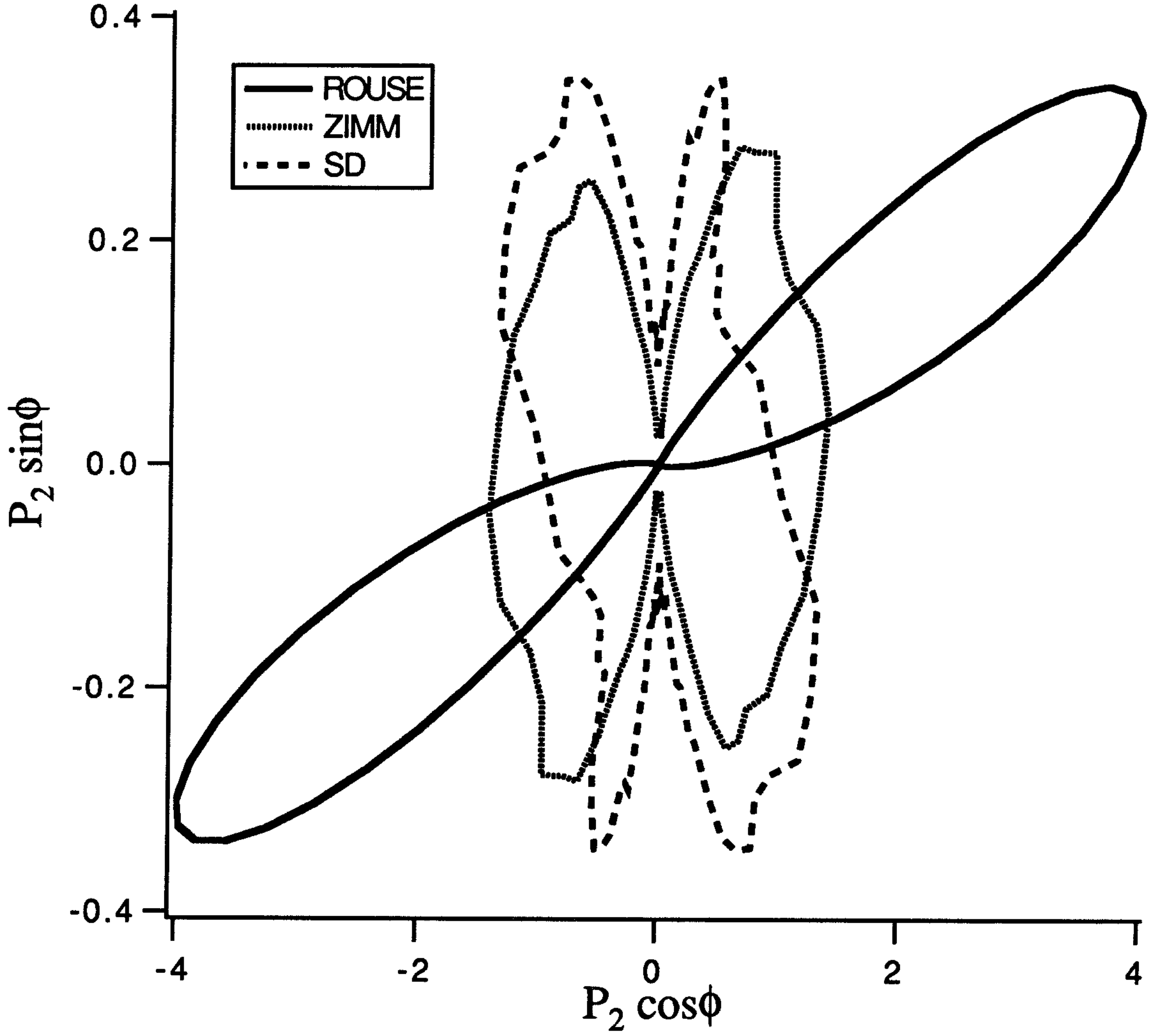

Figure (4.16)

Angular distribution functions of Rouse, Zimm and Stokesian dynamics dumbbells at an extension of r=5. Pe=10 and h*=0.25.

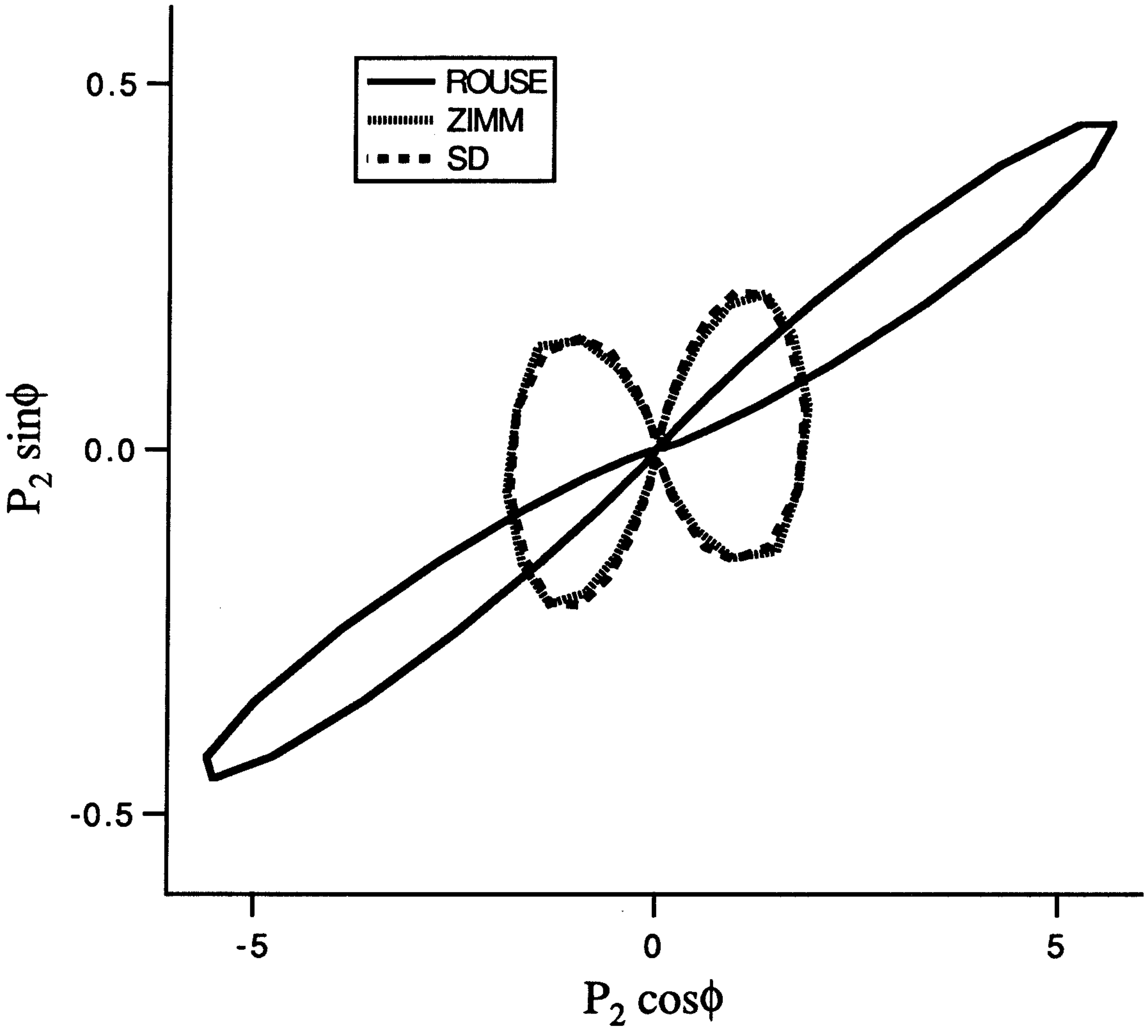

Figure (4.17)

Angular distribution functions of Rouse, Zimm and Stokesian dynamics dumbbells at an extension of r=10. Pe=10 and h*=0.25 .

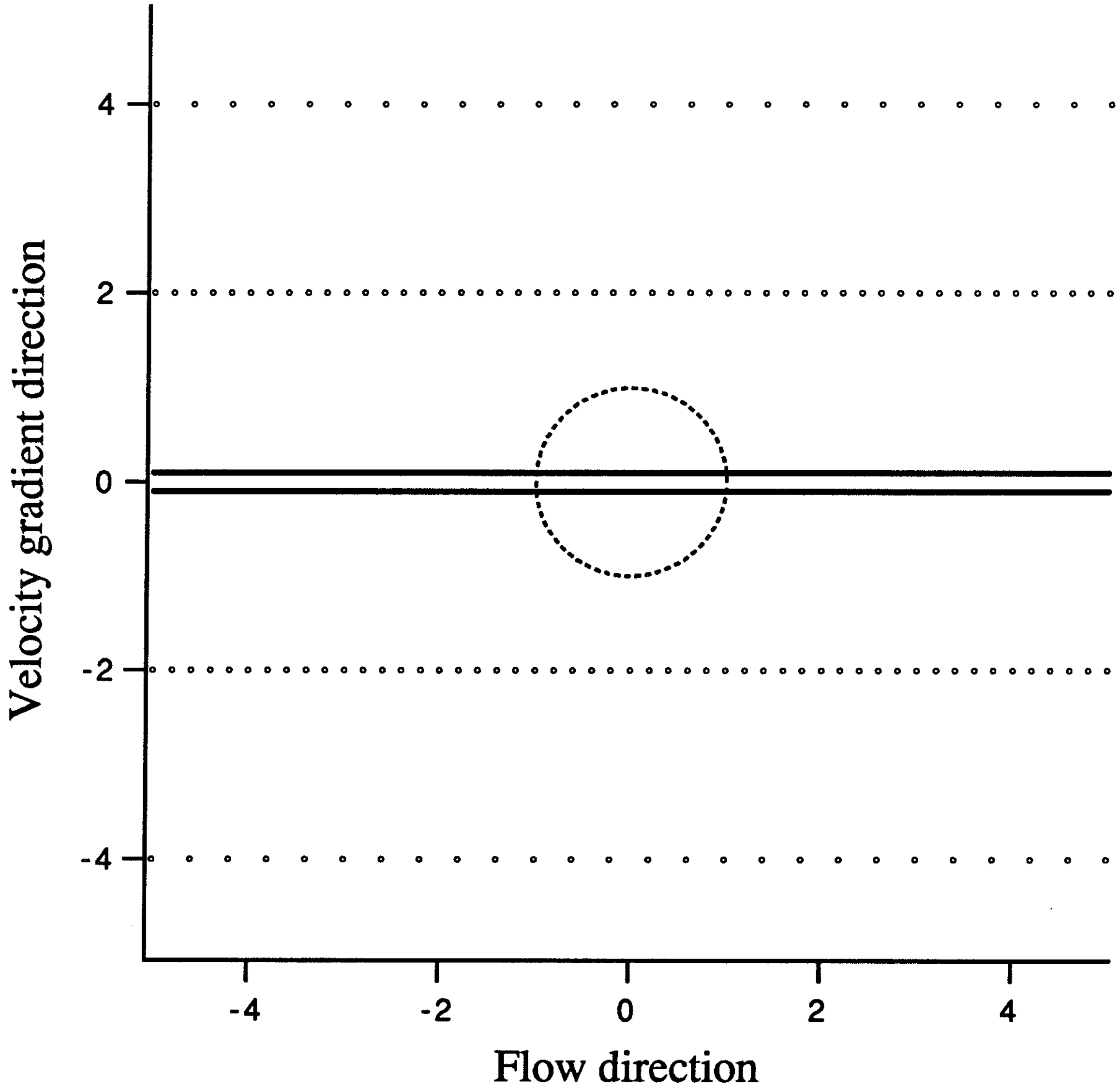

Figure (4.18)

Relative trajectories for
two "spheres" in shear flow with
no hydrodynamic interaction.

(Pe = ∞)

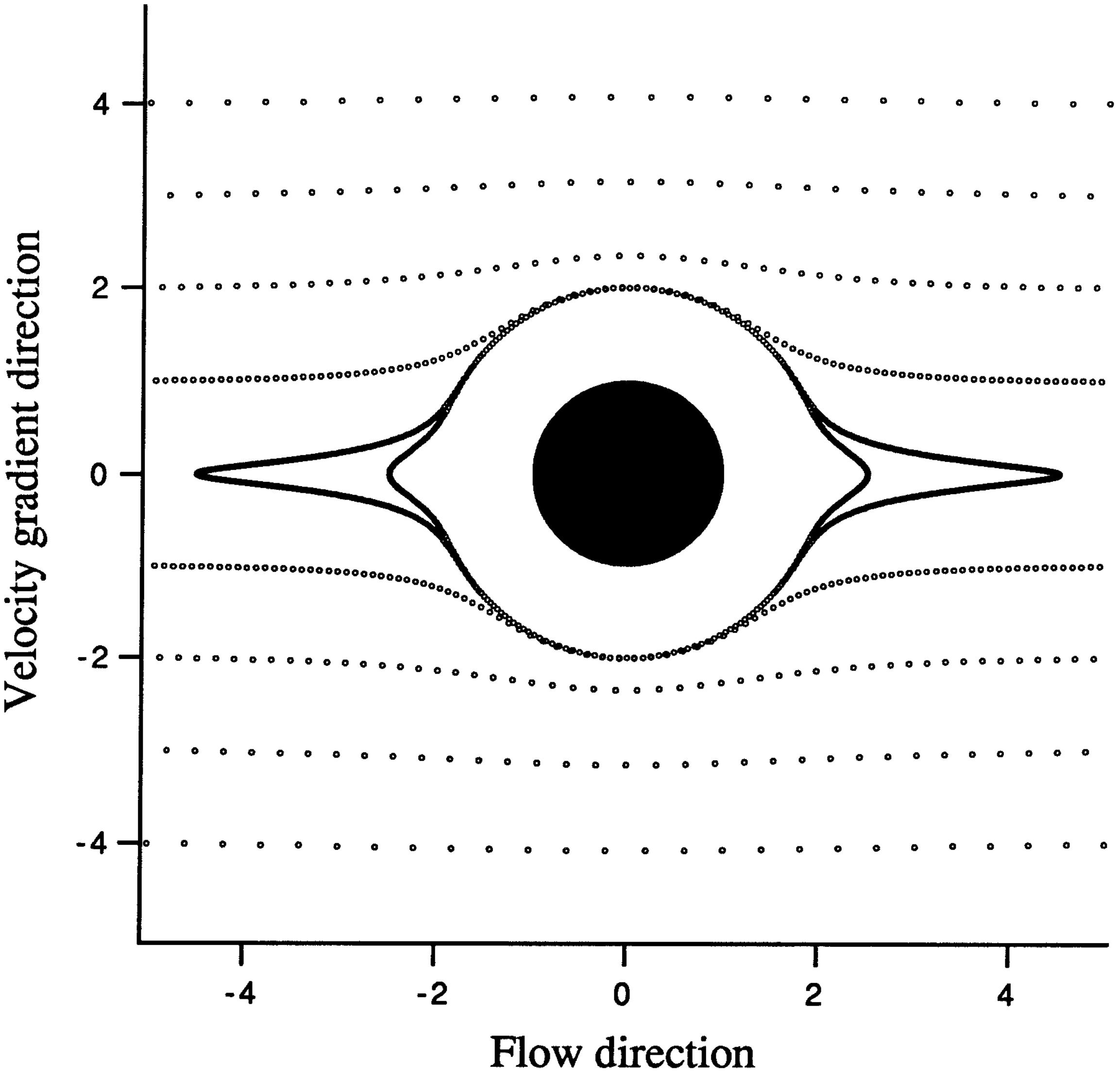

Figure (4.19)

Relative trajectories of
two spheres in shear flow with
complete hydrodynamic interaction.

(Pe = ∞)

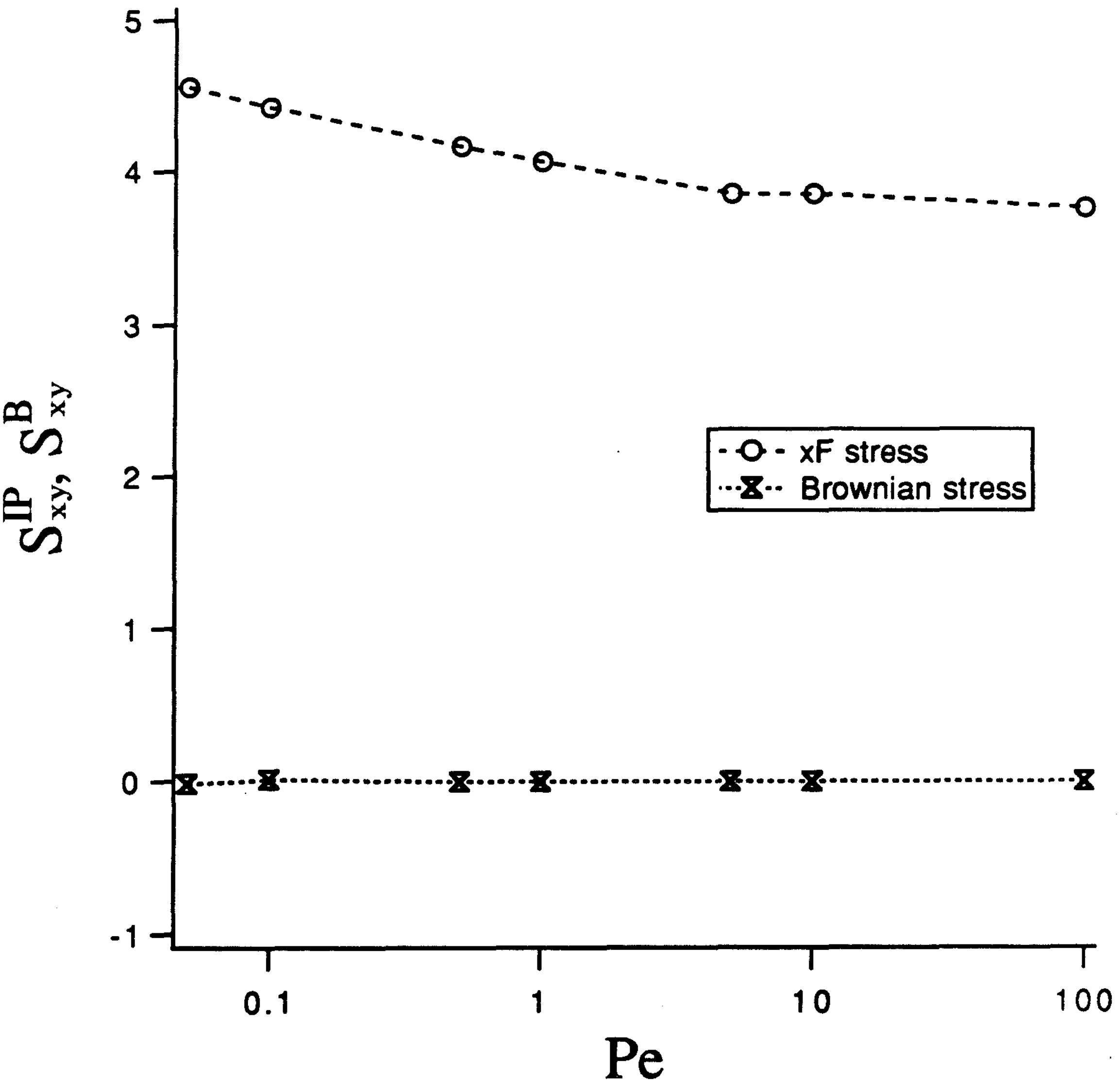

Figure (4.20)

Relative magnitudes of the interparticle-force contribution to the stress and the Brownian-force contribution to the stress as a function of Pe for h*=0.15 .

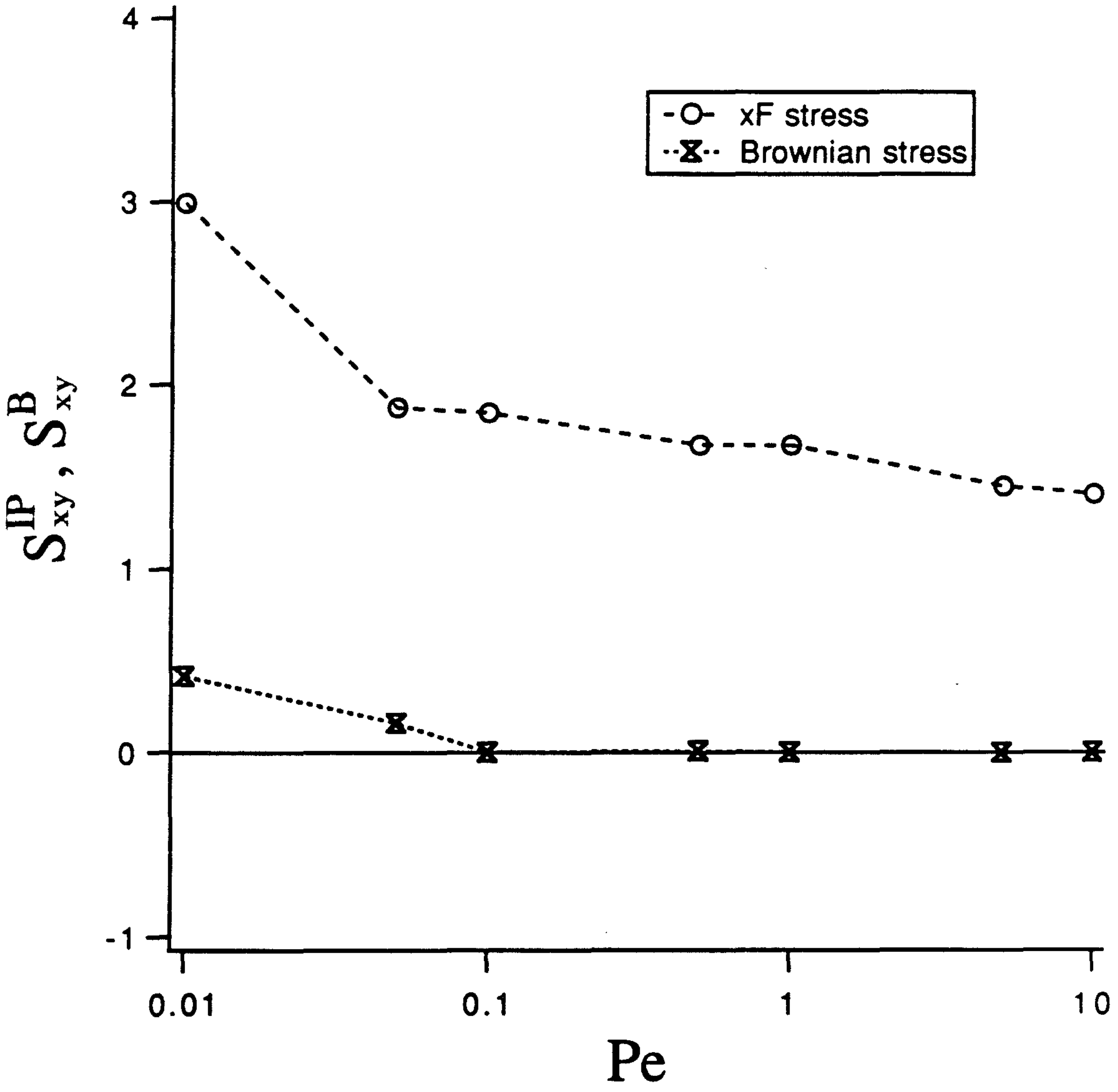

Figure (4.21)

Relative magnitudes of the interparticle-force contribution to the stress and the Brownian-force contribution to the stress as a function of Pe for h*=0.25 .

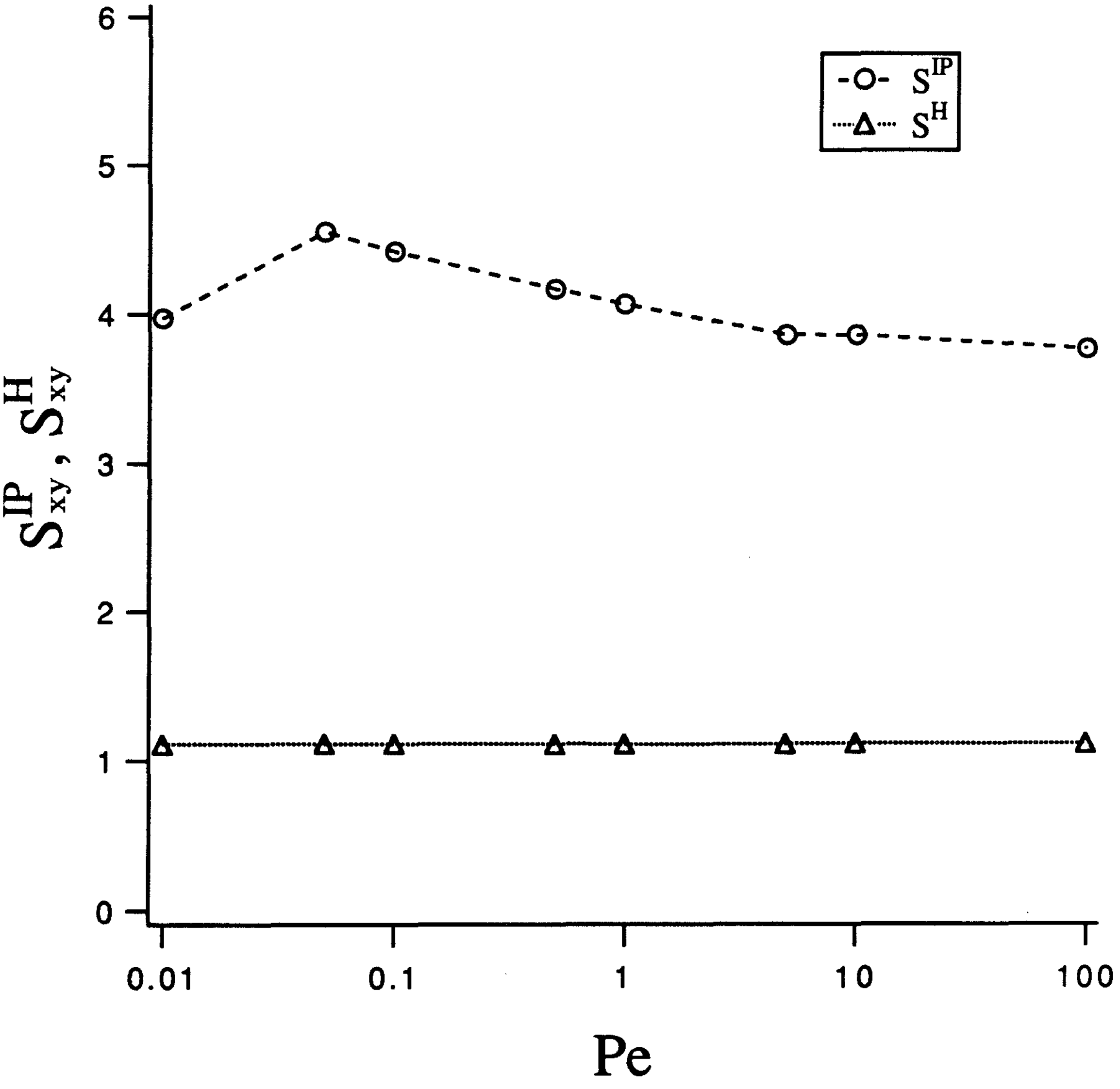

Figure (4.22)

Comparison of hydrodynamic and interparticle contributions to the stress for the Stokesian dynamics dumbbell. $h^*=0.15$

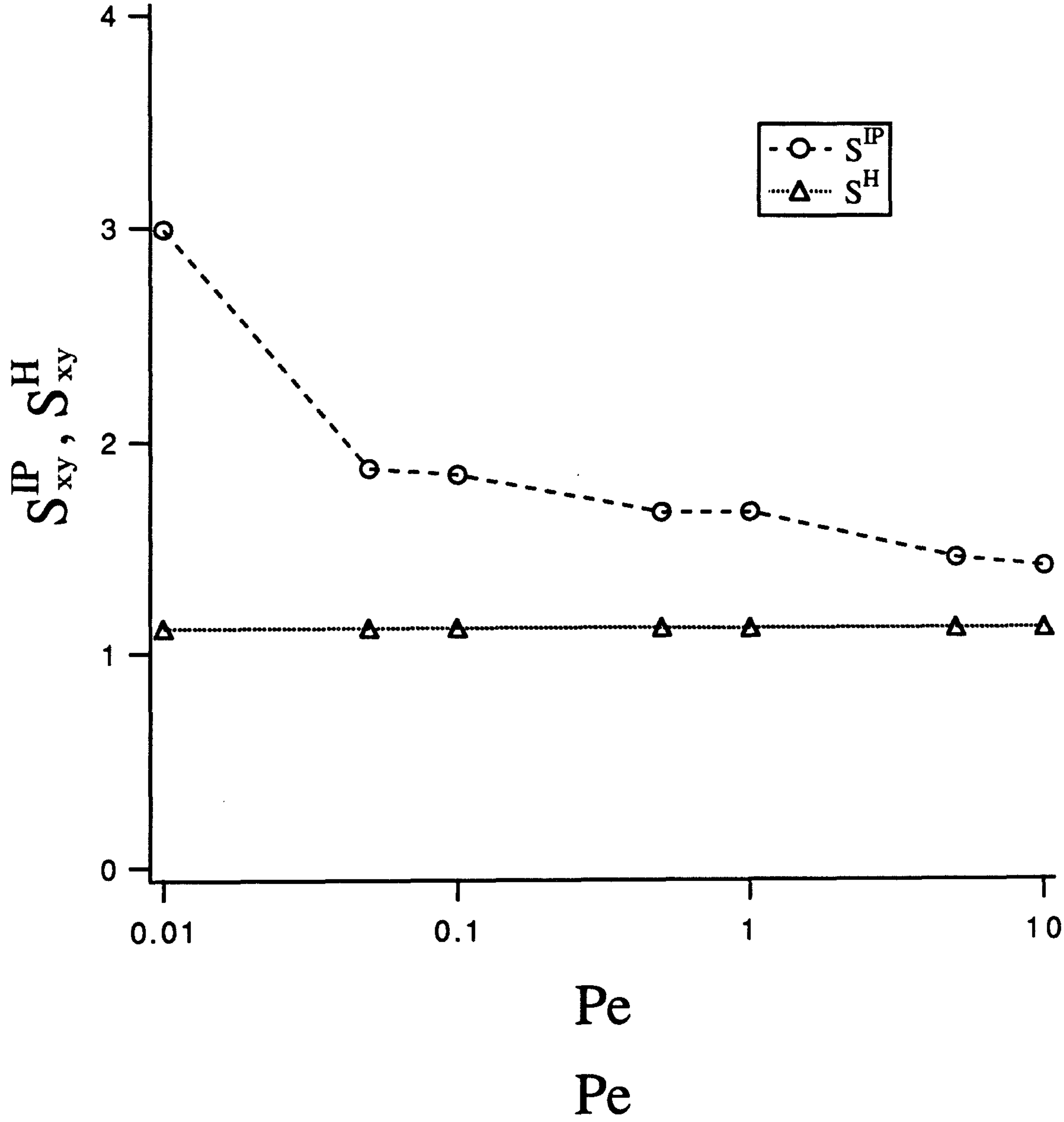

Figure (4.23)

Comparison of hydrodynamic and interparticle contributions to the stress for the Stokesian dynamics dumbbell. h*=0.25

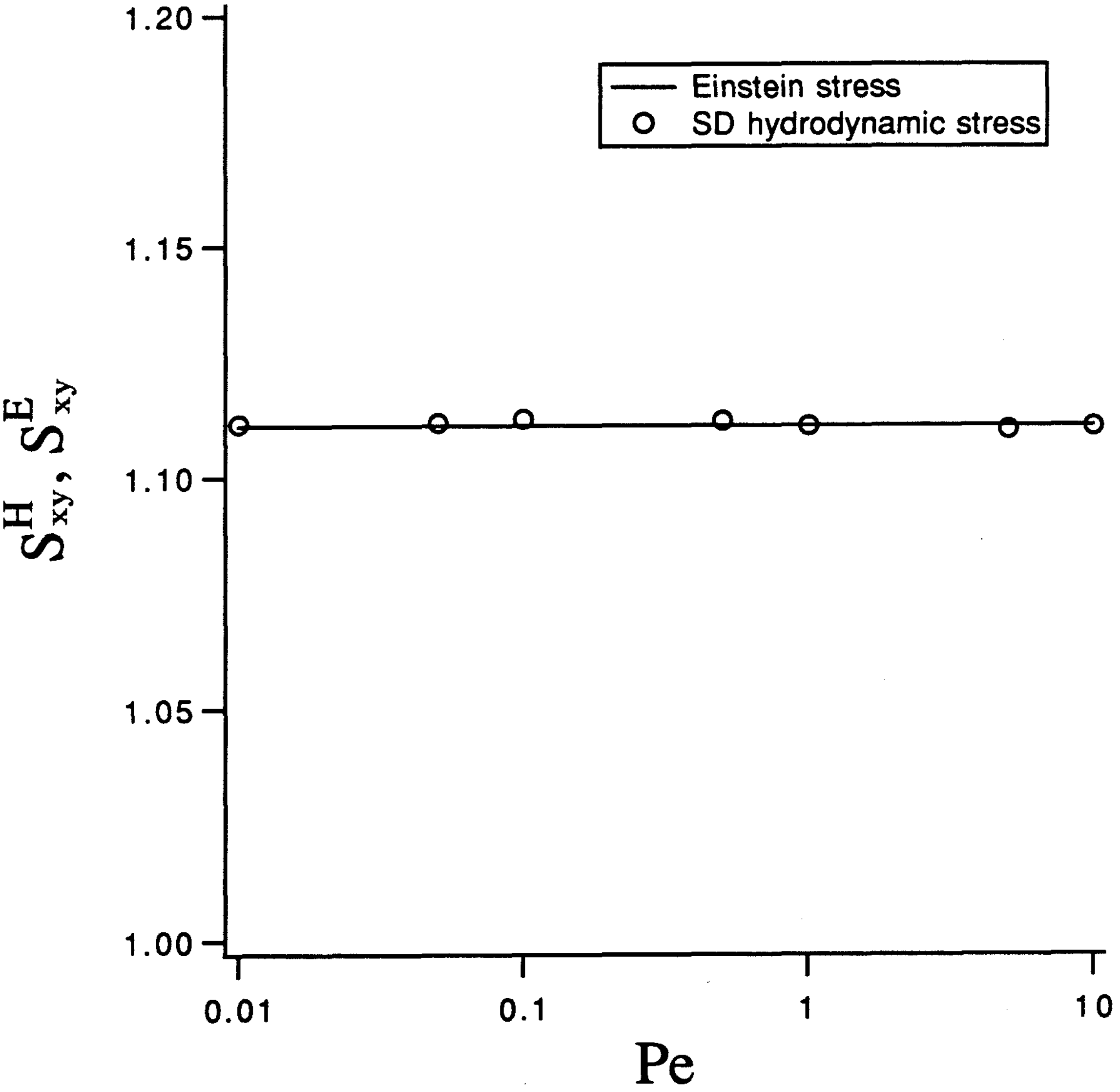

Figure (4.24)

Comparison between the Stokesian dynamics result and the Einstein prediction for the hydrodynamic stress as a function of Pe with h*=0.25 . The results for h*=0.15 are similar.

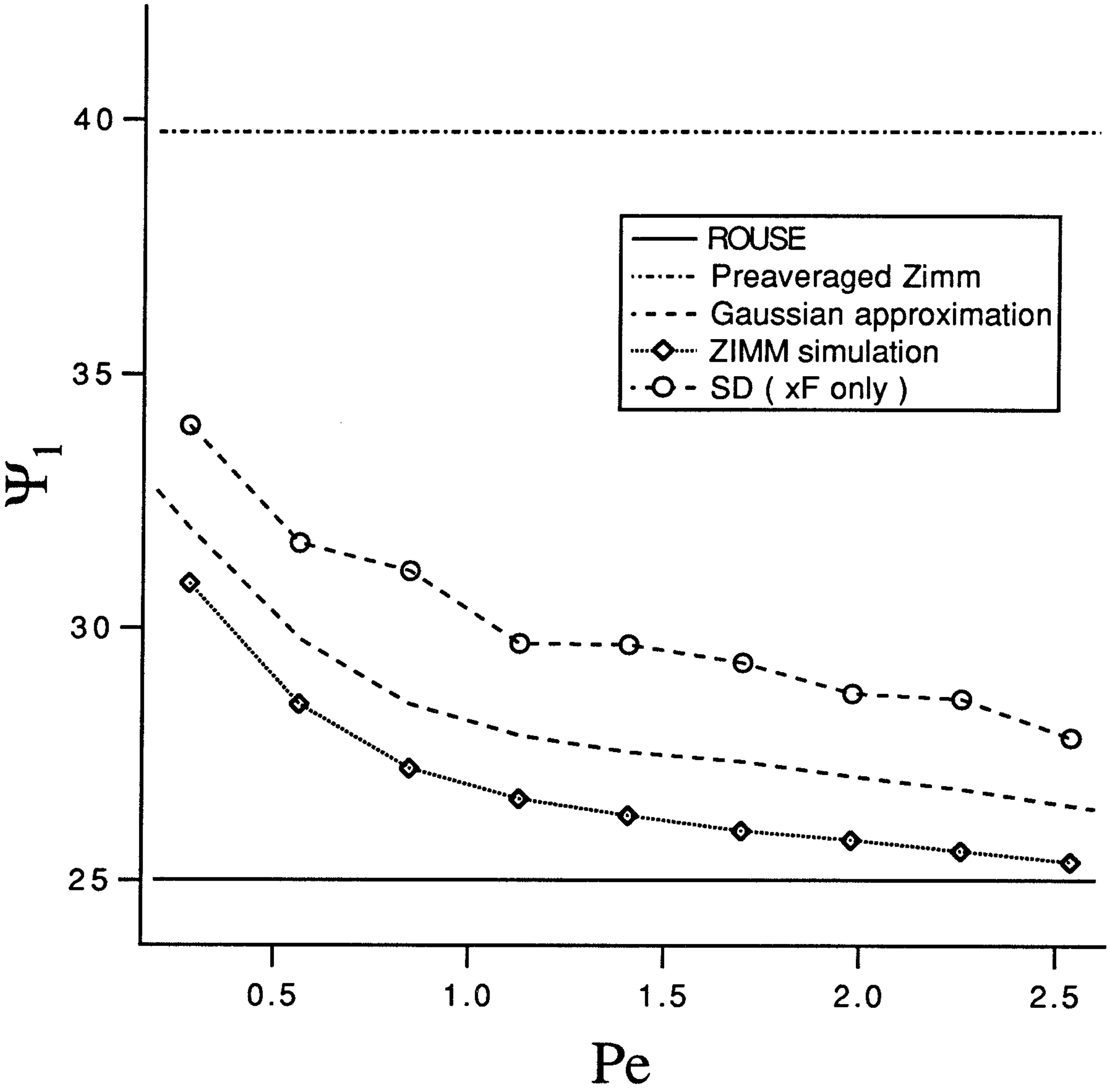

Figure (4.25)

Comparison between simulation results and various approximate analytical solutions for the shear-rate dependence of the first normal-stress difference. (h*=0.15)

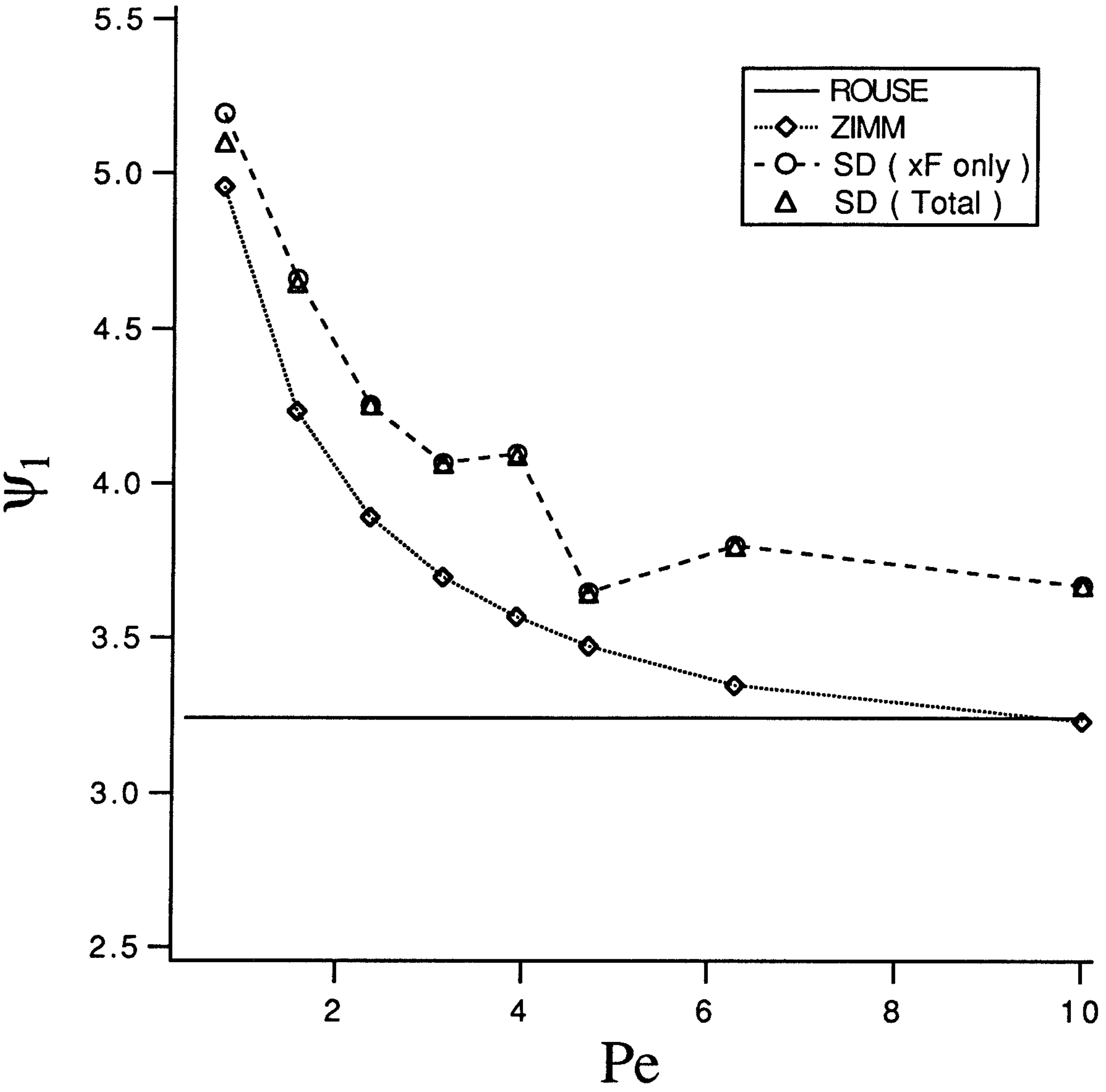

Figure (4.26)

Comparison between Rouse model and simulation results for the shear-rate dependence of the first normal-stress difference. (h*=0.25)

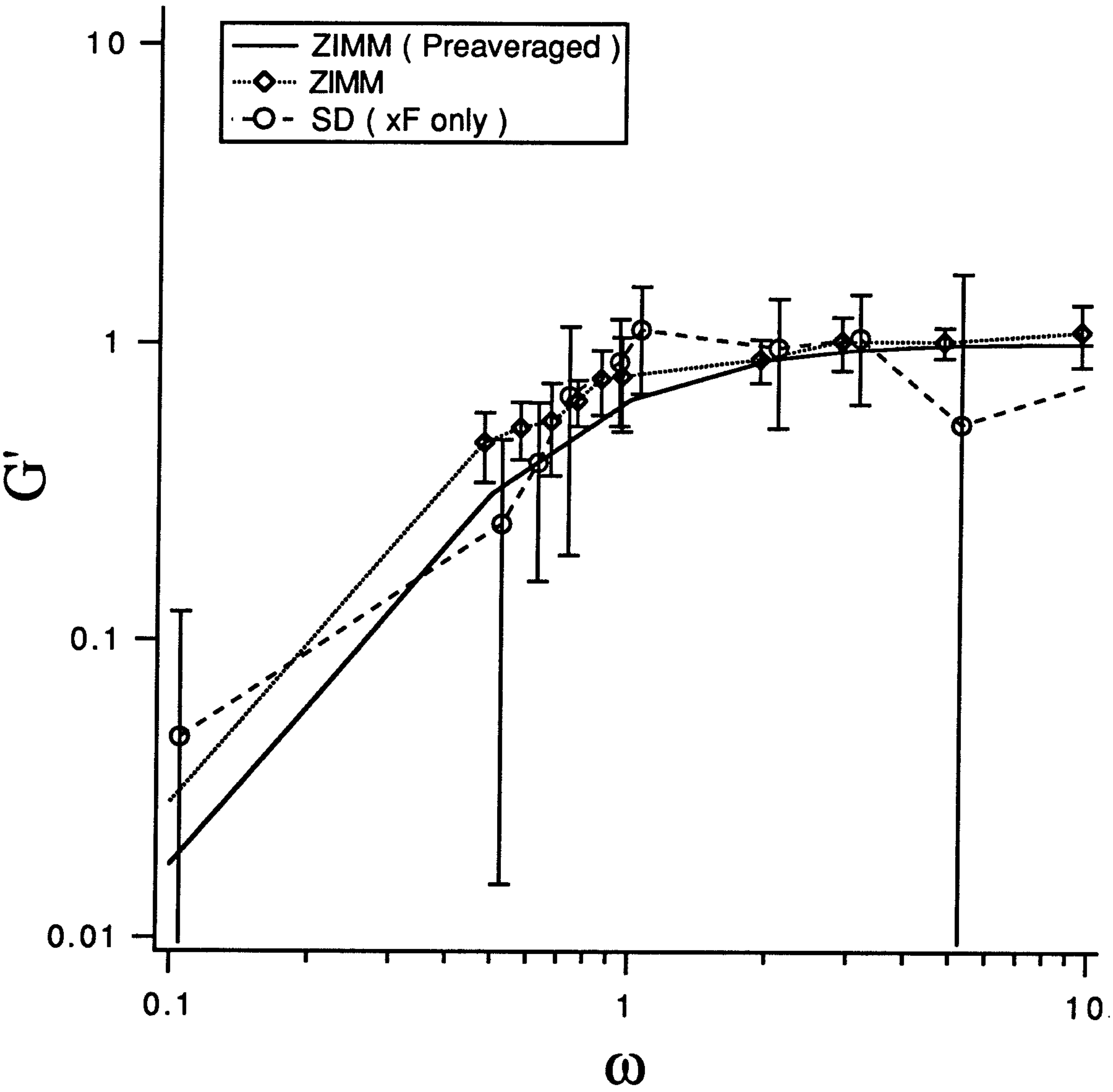

Figure (4.27)

Comparison between theory and simulation of the frequency dependence of the storage modulus. Pe = 0.1 and h* = 0.25 .

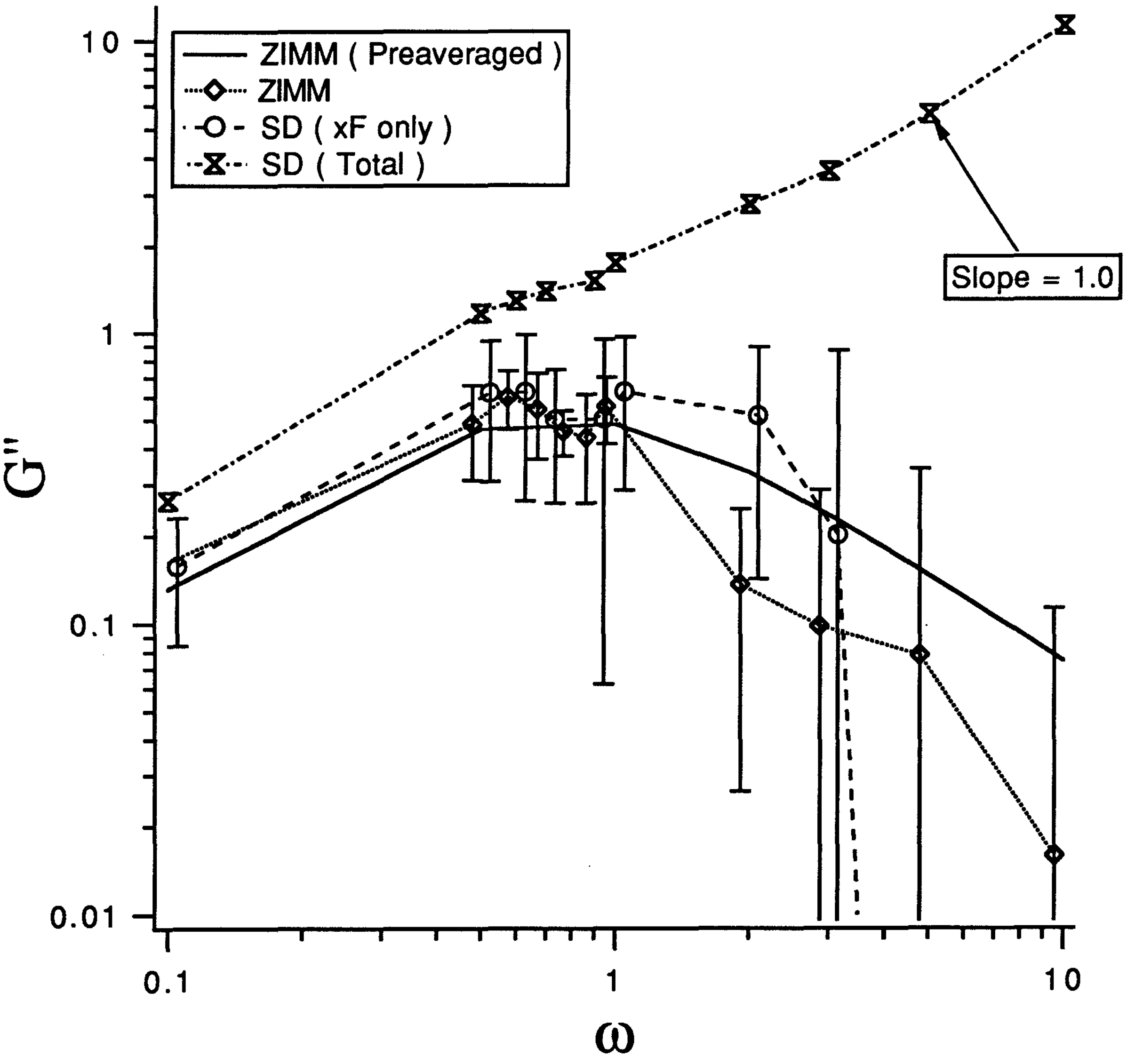

Figure (4.28)

Comparison between theory and simulation of the frequency dependence of the loss modulus. Note that with the inclusion of the hydrodynamic stress, the loss modulus goes to a slope of 1 at high frequency. Pe = 0.1 and h* = 0.25 .

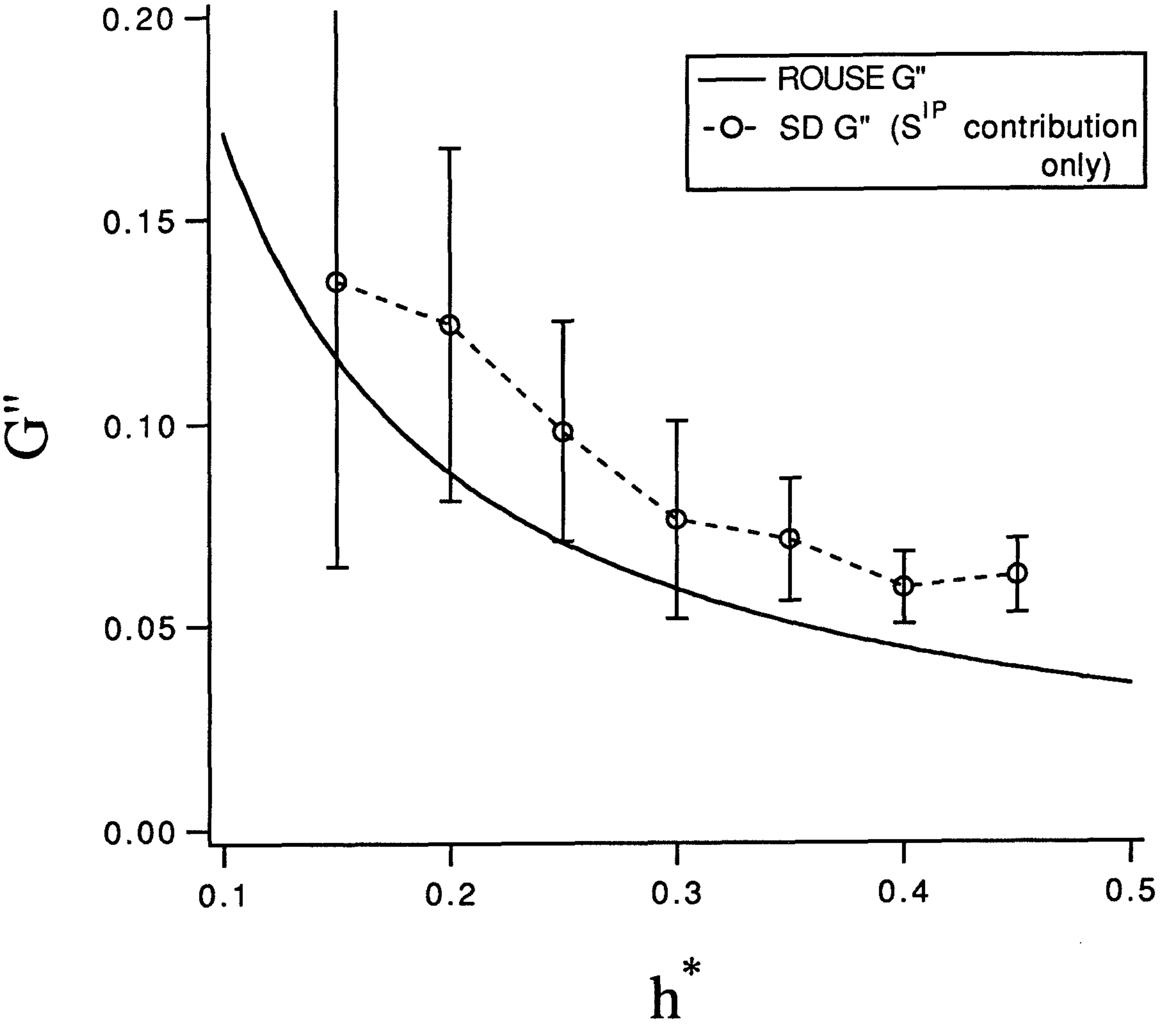

Figure (4.29)

Effect of excluded volume on the storage modulus of the dumbbell polymer model, plotted as a function of the hydrodynamic-interaction parameter. ω=0.0628 and Pe=0.628 .

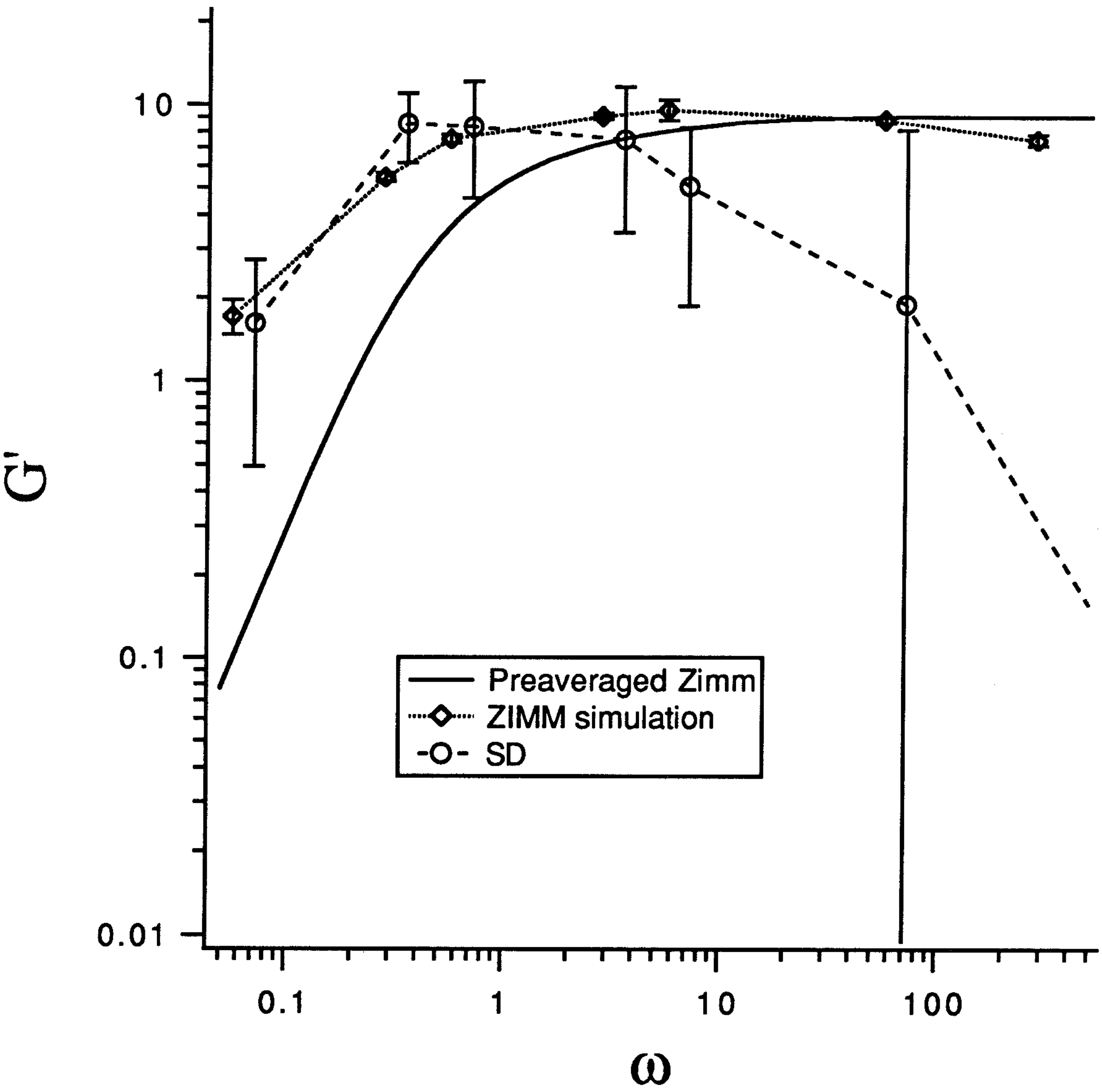

Figure (4.30)

Comparison between theory and simulation of the frequency dependence of the storage modulus for chains of 10 beads. Pe=0.628 and h*=0.15 . The decrease in the Stokesian dynamics result at high frequencies is a result of the relatively high Peclet number.

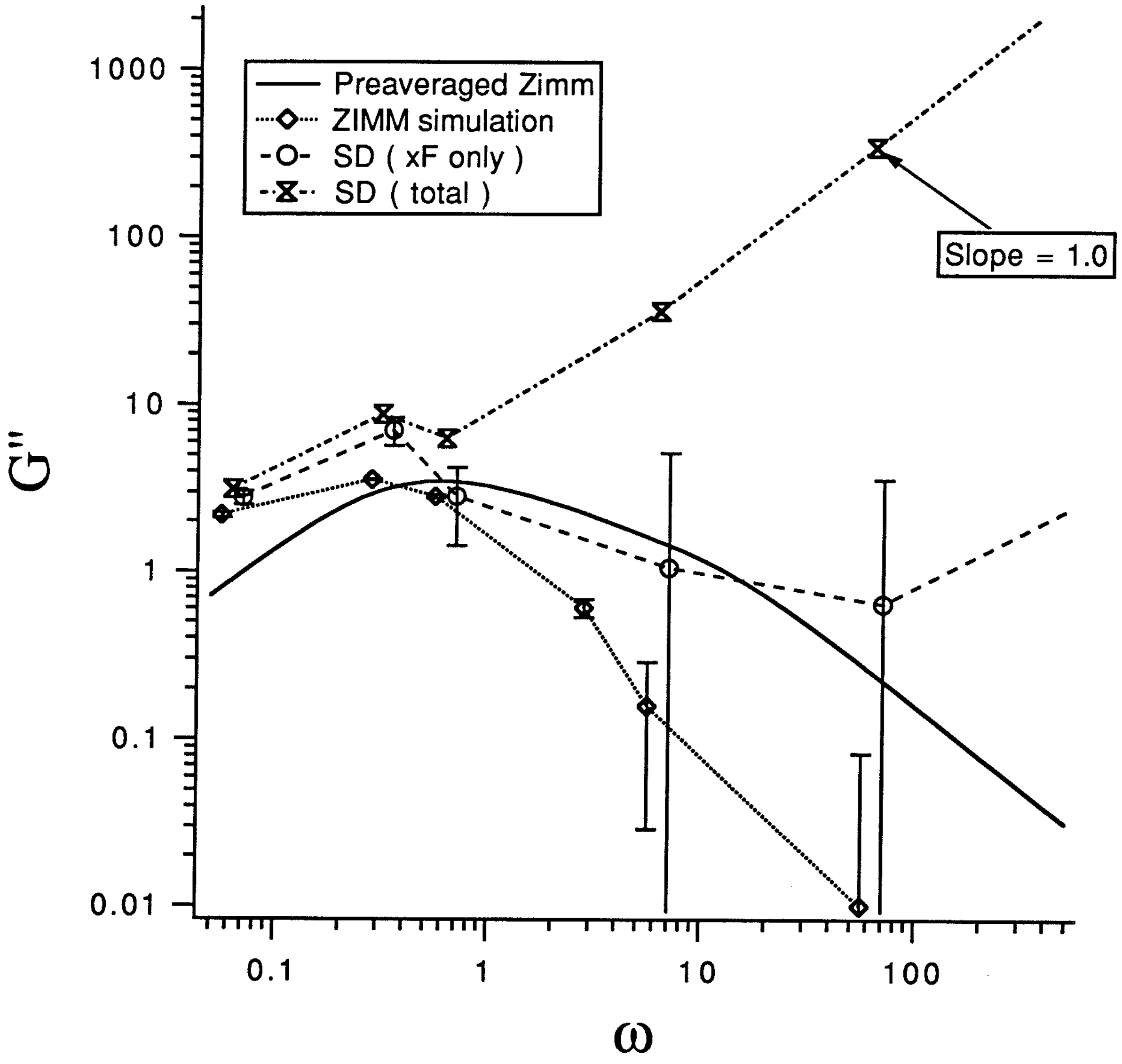

Figure (4.31)

Comparison between theory and simulation of the frequency dependence of the loss modulus for a chain of 10 beads. Note that with the inclusion of the hydrodynamic stress, the loss modulus goes to a slope of 1 at high frequency. Pe = 0.628 and h* = 0.15 . The high-frequency increase in the xF contribution from Stokesian dynamics is a result of the relatively high Peclet number.

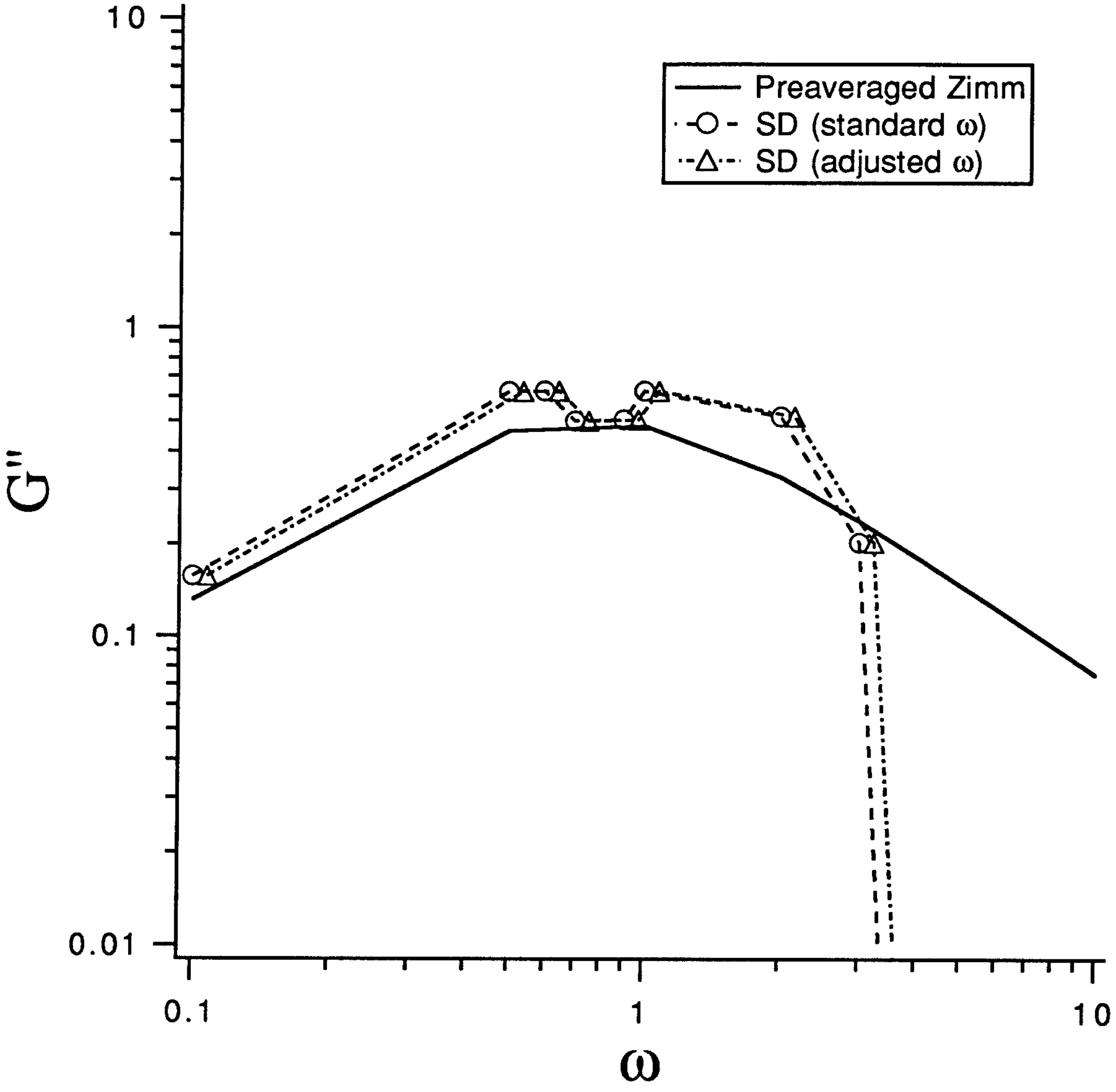

Figure (4.32)

Effect on loss modulus of renormalizing the frequency to account for the excluded-volume effect on the rest length of the connector spring. Pe = 0.1 and h* = 0.25 .

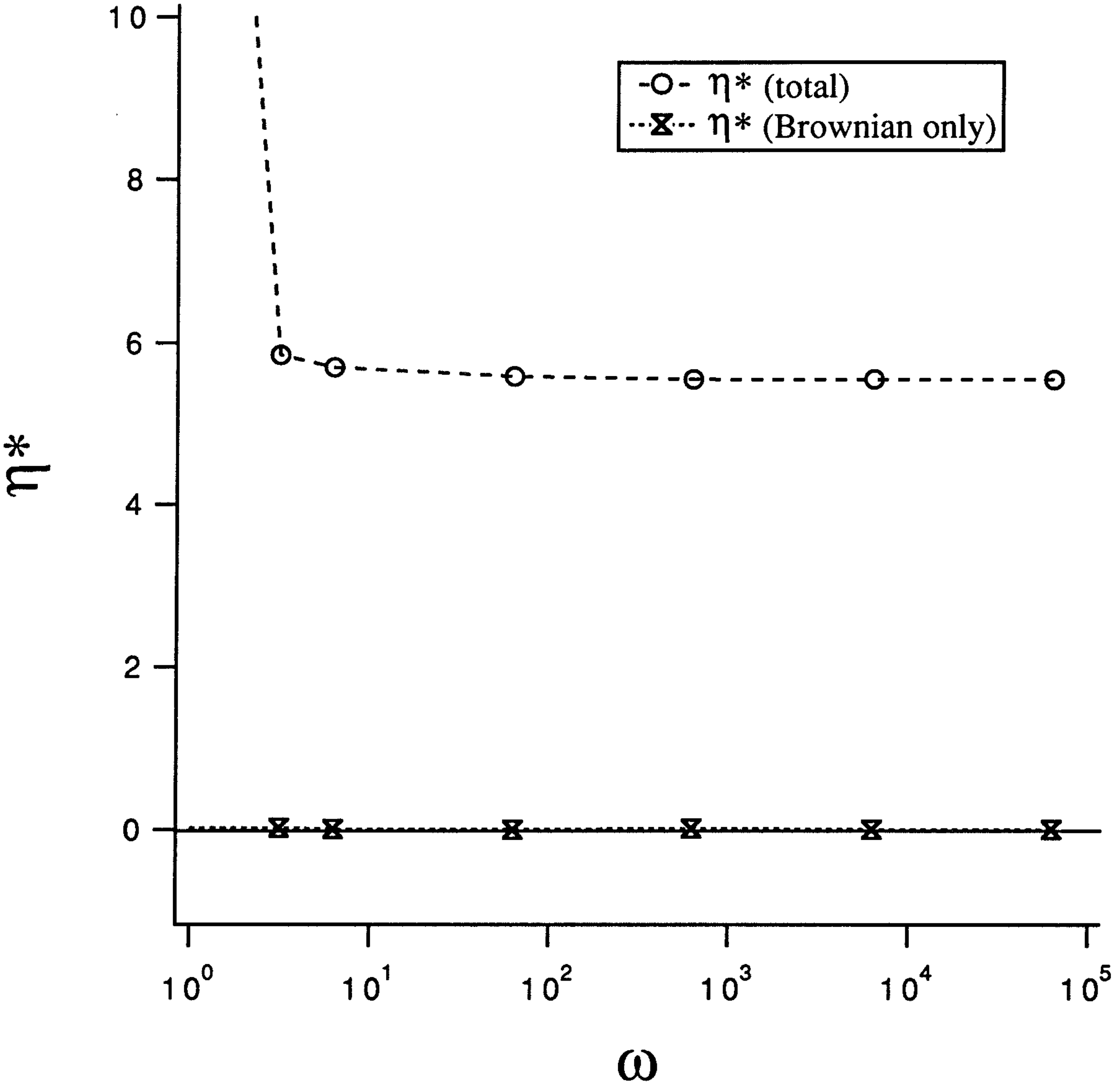

Figure (4.33)

Relative magnitude of the Brownian contribution to the complex viscosity for a 10-bead chain. Pe=0.628 and h*=0.15.

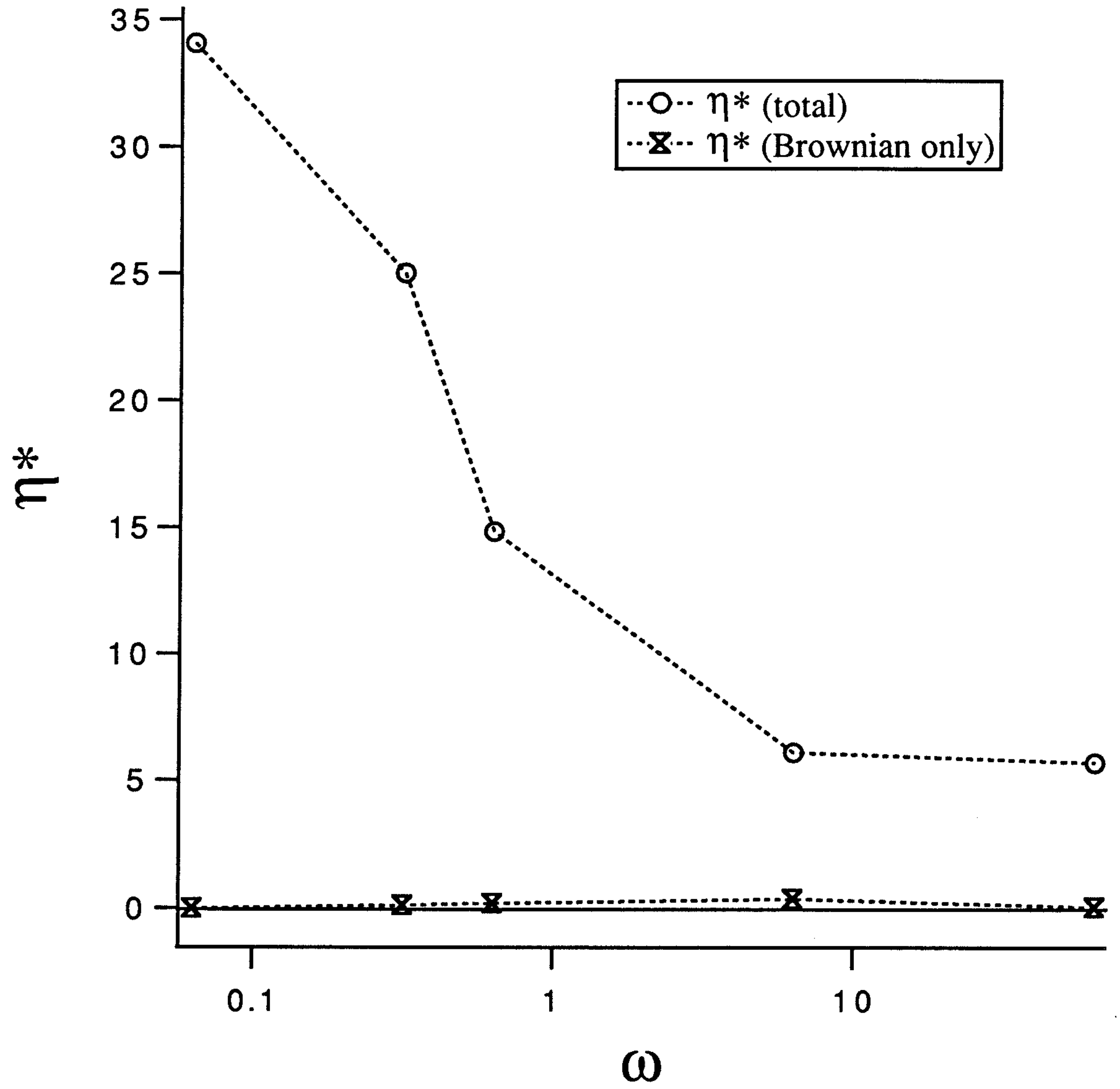

Figure (4.34)

Relative magnitude of the Brownian contribution to the complex viscosity for a 10-bead chain. Pe=0.628 and h*=0.25.

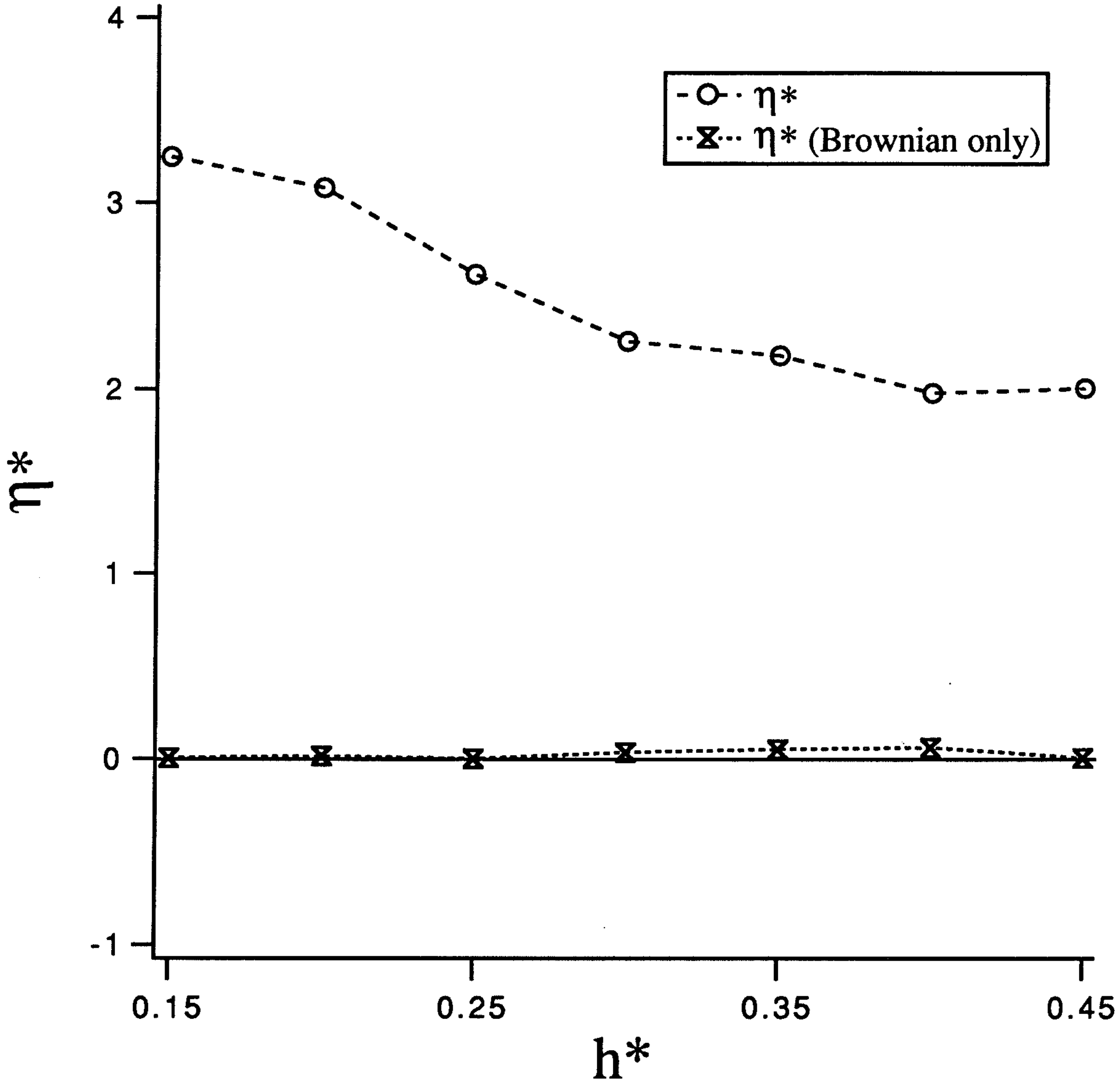

Figure (4.35)

Relative magnitude of the Brownian contribution to the complex viscosity of the Stokesian dynamics dumbbell as a function of the interaction parameter. Pe=0.628 and ω=0.0628 .

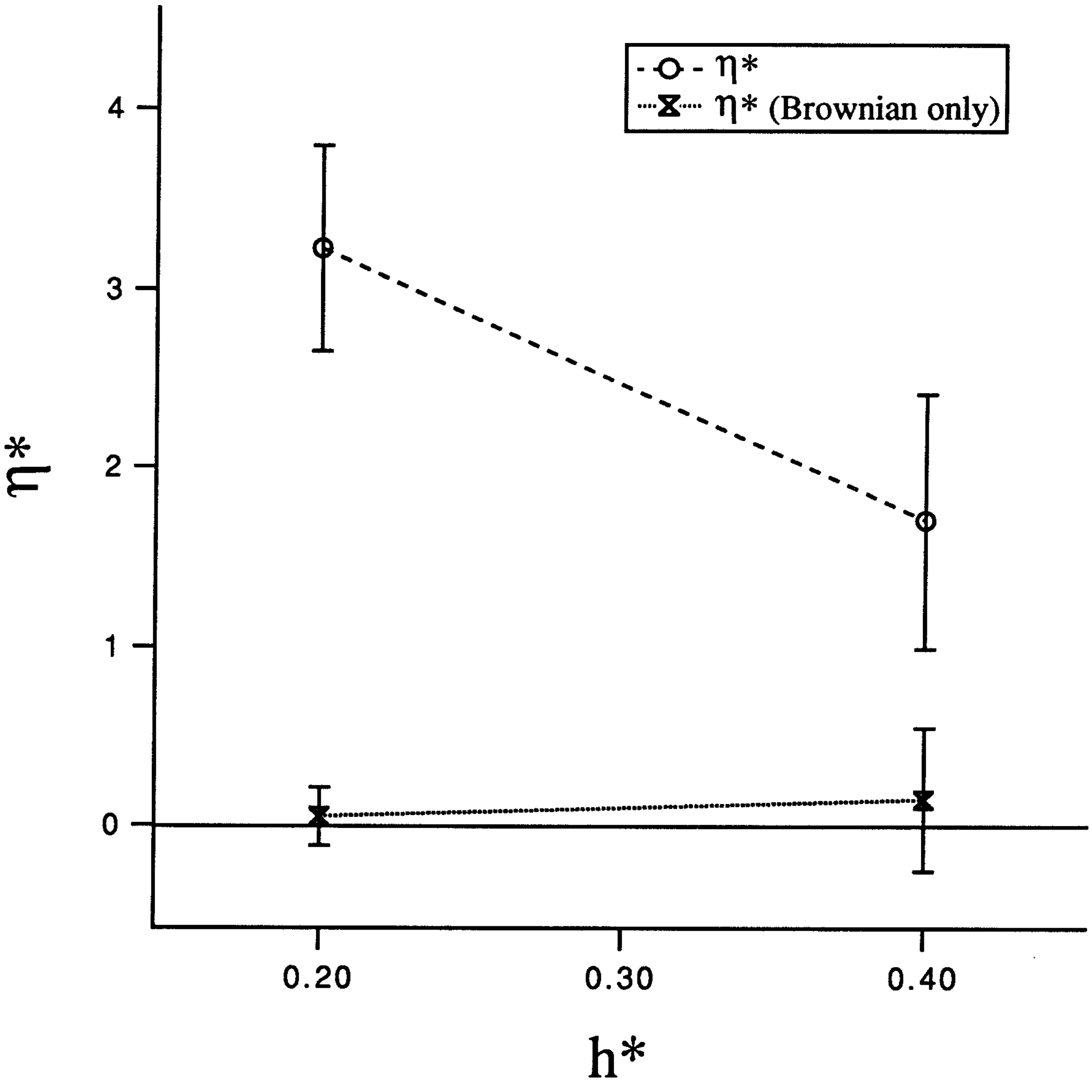

Figure (4.36)

Relative magnitude of the Brownian contribution to the stress as a function of the interaction parameter for the Stokesian dynamics dumbbell. Pe=0.10 and ω=0.0628 .

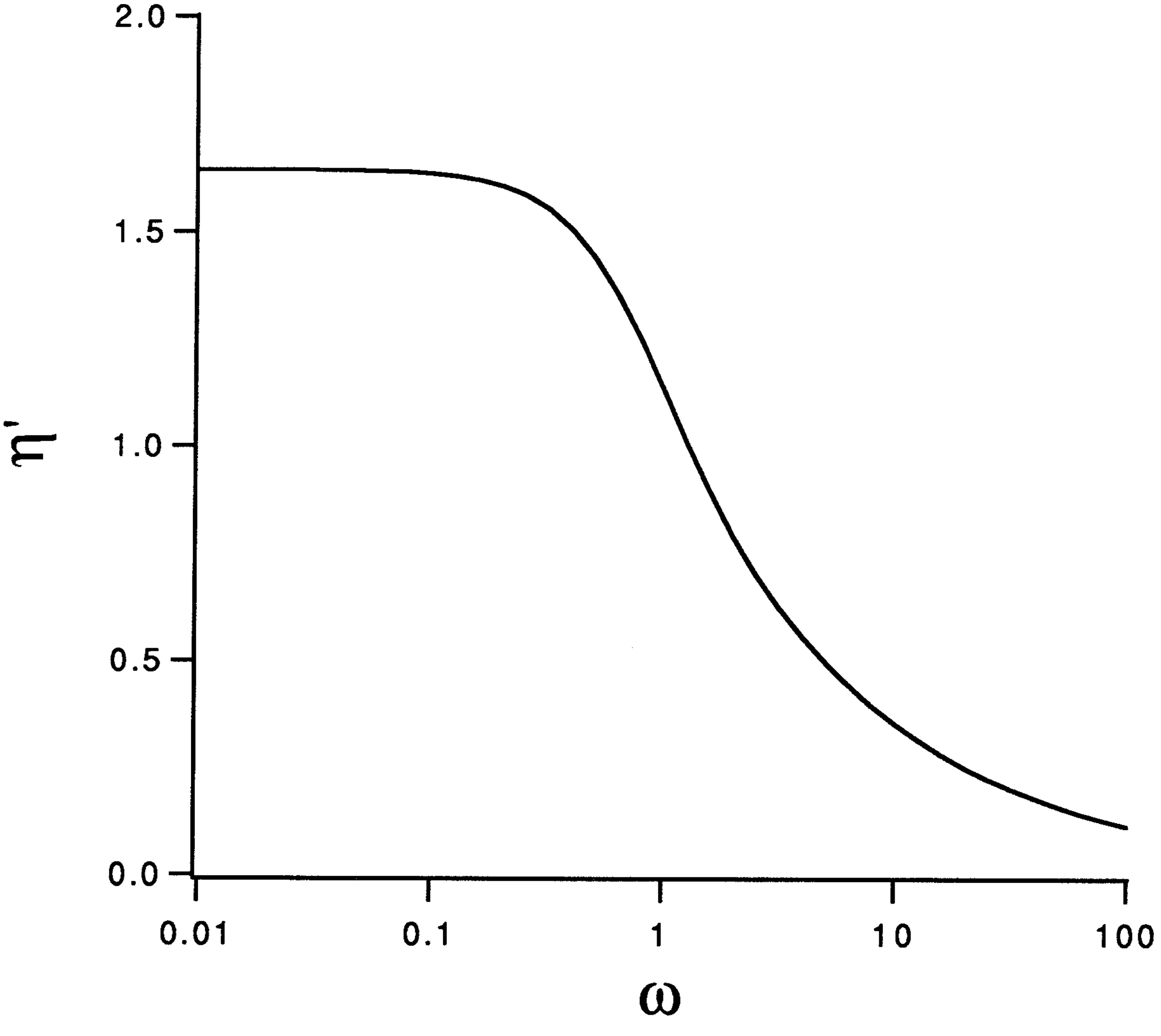

Figure (4.37)

Dissipative component of the complex viscosity predicted by the Rouse model for large N. The predictions of the Zimm model are similar.

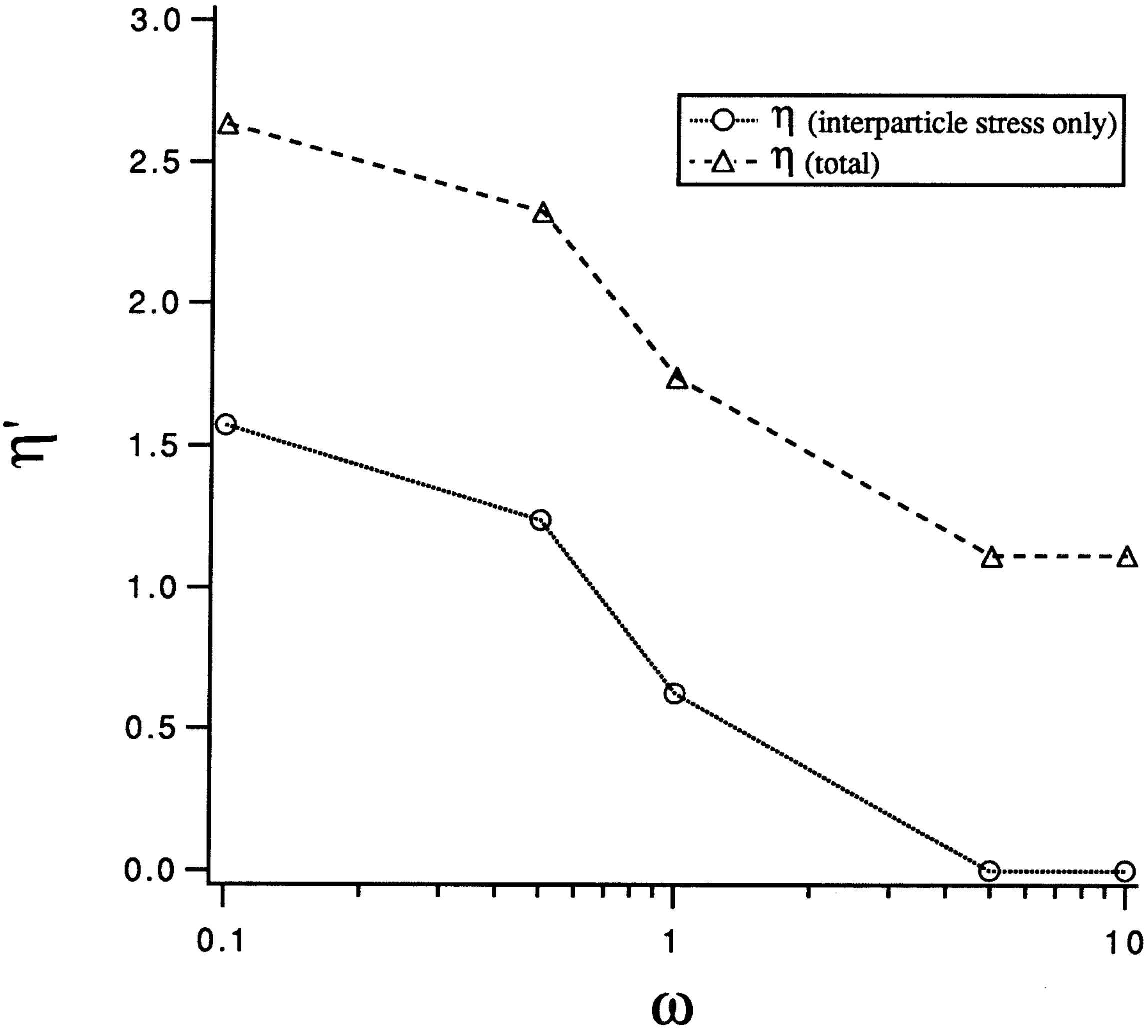

Figure (4.38)

Dissipative component of the complex viscosity predicted by the Stokesian dynamics dumbbell model for h*=0.25 .

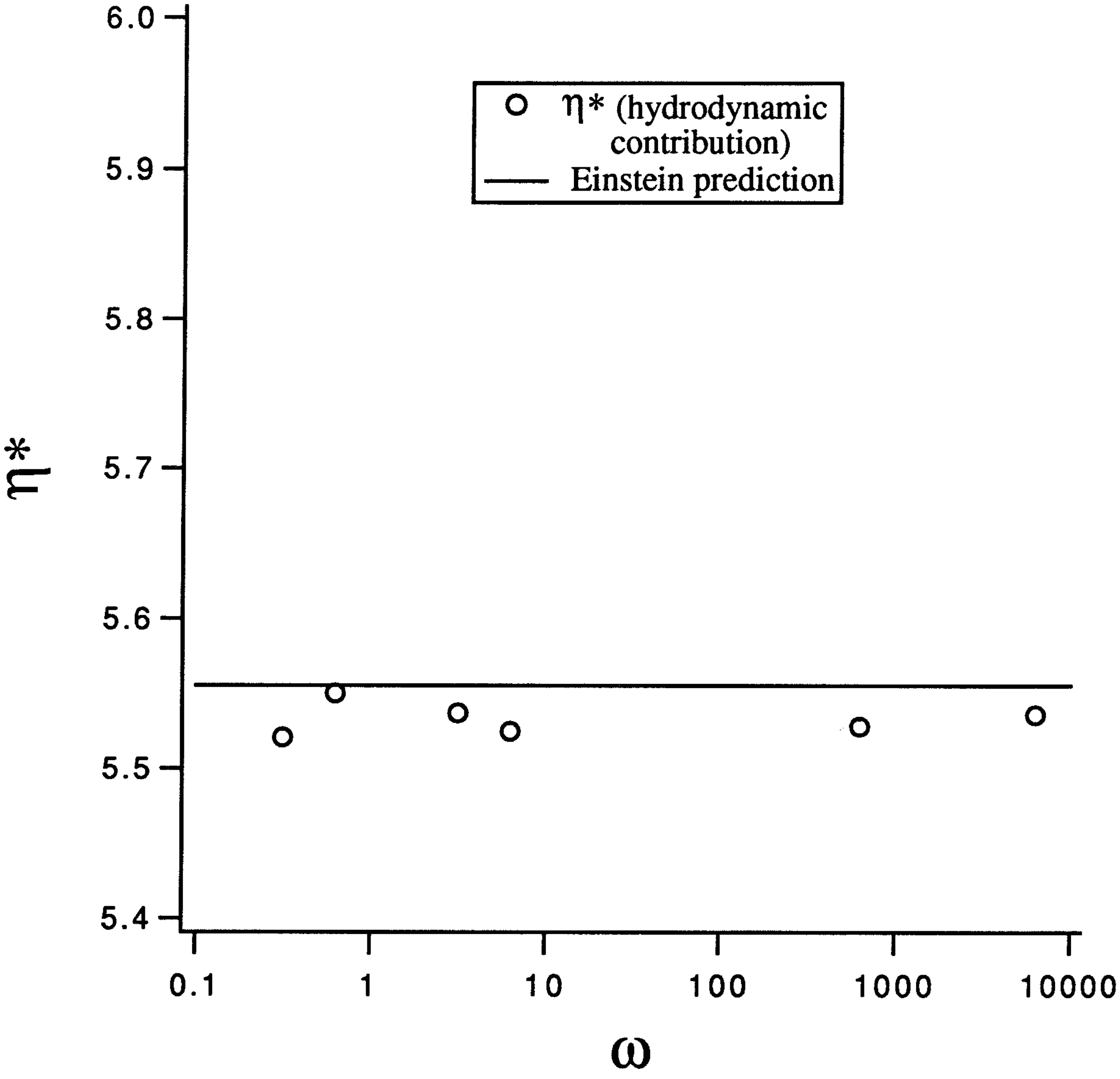

Figure (4.39)

Comparison between the Einstein viscosity prediction and the hydrodynamic contribution to the stress calculated by the Stokesian dynamics model for a chain of 10 beads. Pe=0.628 and h*=0.15 .

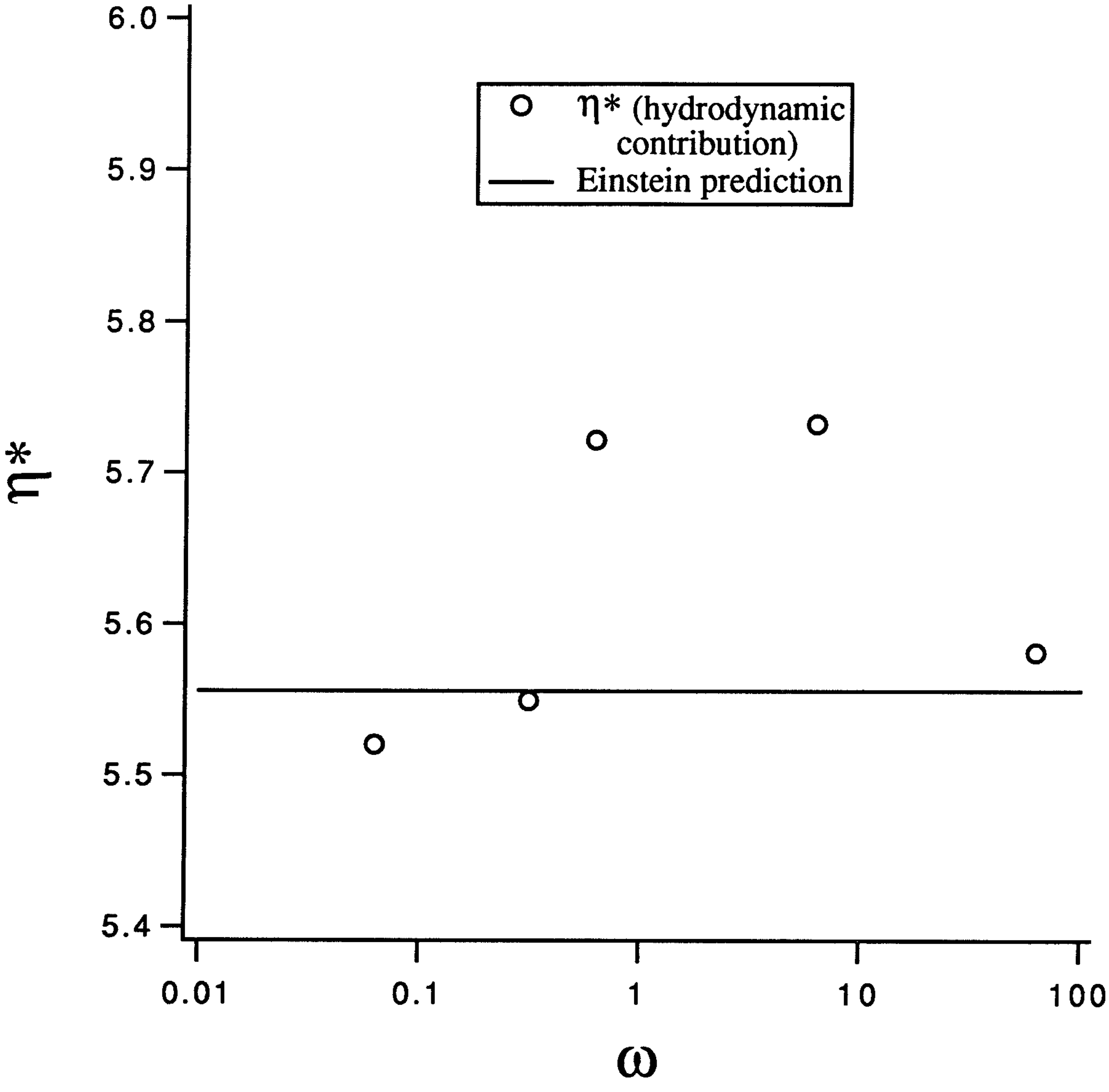

Figure (4.40)

Comparison between the Einstein viscosity prediction and the hydrodynamic contribution to the stress calculated by the Stokesian dynamics model for a chain of 10 beads. Pe=0.628 and h*=0.25 .

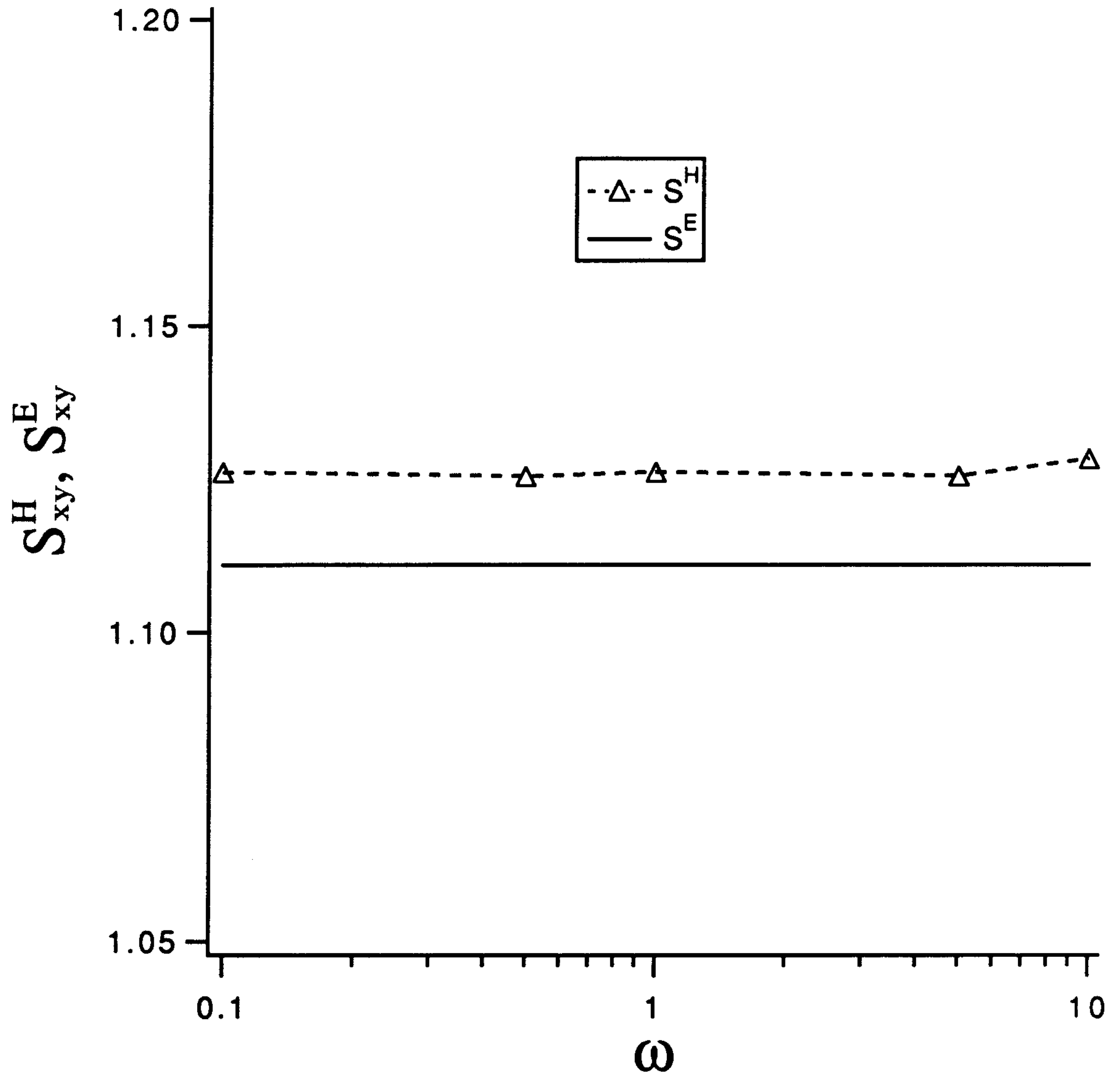

Figure (4.41)

Frequency dependence of the hydrodynamic stress predicted by the Stokesian dynamics dumbbell for h* = 0.25.

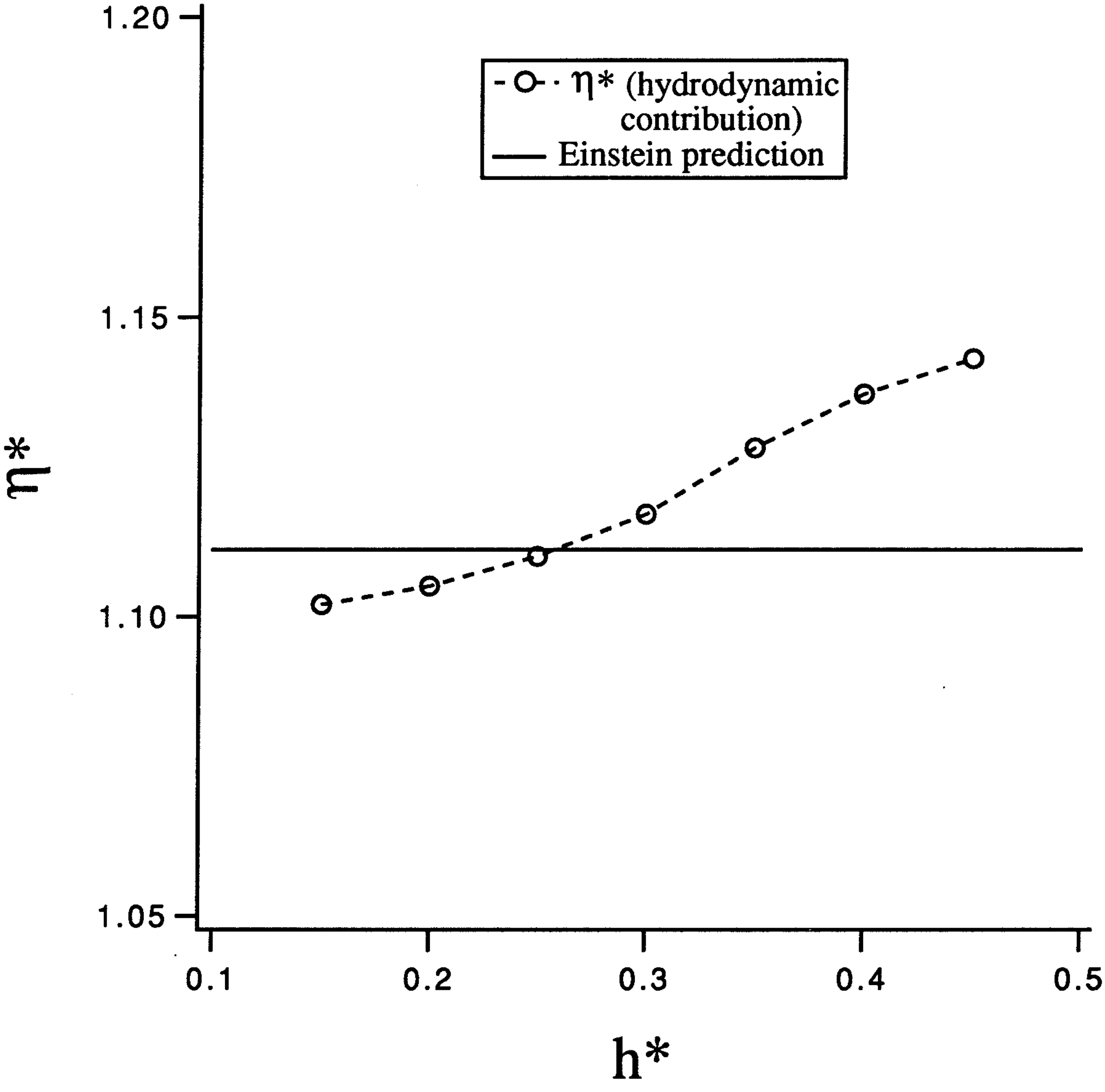

Figure (4.42)

Comparison between Einstein viscosity and hydrodynamic stress predicted by the Stokesian dynamics dumbbell as a function of interaction parameter for Pe=0.628 and ω=0.0628

5. NON-DILUTE RESULTS

5.1 Modeling of Non-dilute Solutions of Polymers

Simulations of non-dilute solutions of polymers were performed by placing 20 Stokesian dynamics bead-spring dumbbells into a cubic cell, and periodically replicating this volume throughout space. The concentration of the polymer solution was defined as the volume fraction of the beads in the control volume. The calculation of the interparticle forces was identical to the infinitely dilute case. The long-range hydrodynamic interactions between the periodically replicated beads of the dumbbells are summed using the renormalization method of O'Brien (1979) together with the Ewald summation technique. The details of the simulation are otherwise identical to the description in §2.2. An in-depth discussion of the modeling of suspensions using Stokesian dynamics may be found in Brady *et al.* (1988).

Unlike the infinitely dilute case, where the solvent viscosity differered from the pure-solvent viscosity by only a differential amount, a non-negligible viscosity contribution may be calculated from the non-dilute results. This is related to the stress contributions by the Einstein relation

$$\begin{aligned}\eta_{rel} &= 1 + \frac{\eta_p}{\eta_s} \\ &= 1 + \frac{5}{2}\phi\left\{\langle \mathbf{S}^{IP}\rangle + \langle \mathbf{S}^{H}\rangle + \langle \mathbf{S}^{B}\rangle\right\},\end{aligned} \tag{5.1}$$

where η_p is the contribution to the viscosity from the polymer and ϕ is the volume fraction of the beads in the solution.

The model solutions were subjected to an imposed, steady, simple shear flow for a period of 100,000 time steps. The first 20,000 time steps were discarded, and analyses of the configuration and of the stress were performed using the remaining

80,000 time steps. Because of increased computational difficulties associated with the concentrated solutions, the time step was 1/20 of the time step for the infinitely dilute analyses (dimensionless $\Delta t = 0.01$ for the infinitely dilute simulations and $\Delta t = 0.0005$ for the concentrated simulations). Thus, although the unit cells for the non-dilute solutions contained 20 distinct dumbbells, the 80,000 time steps actually represent a sampling of phase space only 2% as large as in the infinitely dilute case, where 4,000,000 data points were generated. For this reason there is a much higher degree of uncertainty in the analysis of the results for the non-dilute solutions.

5.2 Steady Simple Shear

Figures (5.1) - (5.7) present $Q_2(r)$ for the concentrated solutions of dumbbells for several volume fractions at $Pe = 1$ and $h^* = 0.25$. For the very low concentrations ($\phi \leq 0.01$) the distributions are only slightly disturbed from the infinitely dilute case. Instead of just one peak beyond contact, there are three, approximately at $r = 4$, 8 and 12. Even though the concentrations are very low, the presence of other dumbbells in the solution has a definite effect. Though the mean separation of the dumbbells is large, two of them come near contact often enough to perturb the distribution, effectively placing themselves between one another. At $\phi = 0.2$ and above, the effect on the distribution is striking. The peak at contact grows steadily, reflecting the difficulty of movement among the tightly packed beads. At $\phi = 0.45$, the peak at $r = 2$ rises to a magnitude of 3.2, nearly 30 times the size of the infinitely dilute peak. This increase in the time spent near contact has a great impact on the magnitude of the hydrodynamic and Brownian contributions to the stress.

Figures (5.8) - (5.10) show the angular-distribution function at an extension of $r = 5$ for $\phi = 0.1$, 0.2, and 0.45, respectively. These show that the concentrated solutions have a tilt toward the x-axis beyond that of the infinitely dilute case. This is not surprising, and is a result of the hindered rotation caused by the presence of other dumbbells. A large extension along the y-axis is not favorable, since it is likely to interfere with a neighboring dumbbell, as both try to rotate in the shear flow. As the concentration increases, the tilt toward the axis of shear is more pronounced. For a given concentration, the tilt is greater for larger values of r.

Figure (5.11) displays the magnitudes of the three contributions to the stress as a function of concentrations up to $\phi = 0.45$ for $Pe = 1$ and $h^* = 0.25$. $\mathbf{S}^{IP}$ appears to reach a maximum between $\phi = 0.1$ and $\phi = 0.2$. This shows that increasing the concentration of dumbbells has two competing effects on their extensions. Initially, the increased hydrodynamic and excluded-volume interactions act to pull the beads of the dumbbells apart, increasing the tension in the spring, and thus increasing $\mathbf{S}^{IP}$. As ϕ increases, the extension continues to increase, but it is offset by the increased tilt toward the x-axis. Finally, at $\phi = 0.45$, the beads become too tightly packed to be extended. They spend most of their time as nearly touching pairs, unable to be dragged apart despite the large hydrodynamic drag forces. This is another example of the importance of excluded volume. In a concentrated suspension of Zimm dumbbells (concentrated in number density, not volume fraction), there would be no such restriction to movement. The hydrodynamic drag from the surrounding dumbbells would dominate, and the extensions become large, as in the infinitely dilute case. At a concentration of $\phi = 0.2$, there is a transition from a regime where $\mathbf{S}^{IP}$ and $\mathbf{S}^{H}$ are of the same magnitude to a hydrodynamically dominated regime. This includes a large increase in the $\mathbf{S}^{B}$. At lower concentrations, $\mathbf{S}^{B}$ is consistently small relative to $\mathbf{S}^{IP}$, because conditions that induce order are accompanied by large extensions of the dumbbells. This shortcoming in the calculation of $\mathbf{S}^{B}$ was discussed in detail in §4.2. At higher concentrations the dumbbells still become ordered along the shear axis, but now the separation remains small, so that Brownian stresses calculated based on the beads become large. Figure (5.12) shows that the $\mathbf{S}^{IP}$ contribution to the stress changes the viscosity more quantitatively than qualitatively. Its biggest effect is to make the transition from low-ϕ viscosity to high-ϕ viscosity less smooth. This dampened effect of $\mathbf{S}^{IP}$ is a result of the restricted extension discussed above.

$\mathbf{S}^{IP}$ appears to have a much stronger effect on the shear-rate dependence of the viscosity of a suspension at a fixed volume fraction. Figure (5.13) displays the stress contributions for a suspension of dumbbells at a volume fraction of $\phi = 0.316$ for Pe=1, 10, and 100. Figure (5.14) plots the viscosity of the suspension for the same parameters. Just as in a suspension of spherical particles, $\mathbf{S}^{H}$ and $\mathbf{S}^{B}$ combine to produce shear thinning first, then shear thickening (e.g., Phung, 1991). The addition of interparticle forces, though, removes the shear-thickening behavior in the examined range of Pe. The decline in $\mathbf{S}^{IP}$ compensates for the increase in $\mathbf{S}^{H}$, and only shear thinning is present. This, however, is certainly only a temporary effect. As Pe increases further, $\mathbf{S}^{IP}$ no longer will make a substantial contribution to the stress. At $Pe = 100$, $\mathbf{S}^{IP}$ already is nearly zero. The hydrodynamic stress, though, will continue to increase with Pe, so the suspension will again shear thicken. The inclusion of interparticle forces has delayed the onset of shear thickening, and has also lessened the extent of shear thinning of the suspension.

It is important to note that the reported dominance of hydrodynamic forces over interparticle forces is in direct conflict with the observed experimental behavior of concentrated polymer solutions. The rheology of concentrated polymer solutions is better modeled by the Rouse model than by the Zimm model (Ferry, 1980), suggesting that concentrated-polymer rheology is actually dominated by the interparticle forces. This appears to be a shortcoming of the dumbbell model. Concentrated polymer solutions are subject to such multiple-length-scale phenomena as coiling and chain entanglements. The dumbbell model, with only one length scale, cannot address such issues.

As noted in §5.1, the amount of data collected for the solutions of the dumbbells is not large enough to justify firm statements about the results. In particular, it should be noted that all sets of initial configurations for $\phi \geq 0.1$ were chosen so that each dumbbell's initial extension was close to 2. The choice of short extensions, rather than random extensions, was based on the assumption that an equilibrium distribution would favor shorter extensions, as in the dilute case. To emphasize the sensitivity to initial conditions, Figure (5.15) presents $Q_2(r)$ for $\phi = 0.316$ and $Pe = 1$, based on an initial arrangement of slightly larger initial extensions than those shown in Figure (5.6). Apparently, several of the dumbbells became "trapped" at large separations, and were unable to move past the intervening dumbbells within the duration of the simulation. While this had a minimal effect on $\mathbf{S}^H$ and $\mathbf{S}^B$, the effect on $\mathbf{S}^{IP}$ was tremendous. The increased extension caused the interparticle stress to rise from 0.50 to 1.87, causing the predicted viscosity of the suspension to jump from 4.13 to 5.93, an increase of over 40%. While this result is still below the predicted viscosity for $\phi = 0.45$, it does illustrate the importance of obtaining a good sampling of phase space before drawing conclusions. Nonetheless, this "problem" represents a strength, not a weakness, of the Stokesian dynamics method. In a concentrated suspension of polymers, chain entanglements are expected to play a major role in determining the structure, and thus the rheology. Models based on far-field hydrodynamics and no excluded volume, such as the Rouse and Zimm models, cannot capture these steric effects. Stokesian dynamics can at least begin to address them.

Obviously, the imposed restriction to short extensions in this study is not necessarily correct. It may be the case that a wider distribution of extensions is correct, even if some dumbbells remain trapped at larger extensions. There may not even be a unique "equilibrium" distribution for all concentrations. The "relaxed" distribution as $t \to \infty$ could be completely dependent upon the initial configuration and the shear history. A more in-depth investigation using the Stokesian dynamics model should reveal that there is a critical concentration ϕ^* marking the onset of this behavior. Below ϕ^* all samples, regardless of the initial arrangement and shear history, will come to the same long-time, equilibrium distribution. Above ϕ^*, the spring forces acting to pull the dumbbells together will be insufficient to overcome the tight packing of the intervening beads. The distributions found after allowing the sample to "sit" for a long time will not be identical, but will be dependent upon the initial conditions and shear history.

This discussion of ϕ^* so far has considered the distribution of extensions found after the simulated suspension is allowed to relax, not subjected to any flow. There should also be critical concentrations for samples subjected to a shear flow for long times, i.e., a spectrum of $\phi^* = \phi^*(Pe)$. For instance, two different samples that were "locked" into distinct distributions at $\phi > \phi^*(0)$ may reach the same distribution after long-time exposure to a flow of $Pe = 10$. This would show that $\phi^*(10) > \phi^*(0)$. This information would be of use in industry, where the ultimate distribution of polymers in a material will affect the physical properties of the material. The knowledge of $\phi^*(Pe)$ could help processing to ensure that identical properties are obtained for all samples.

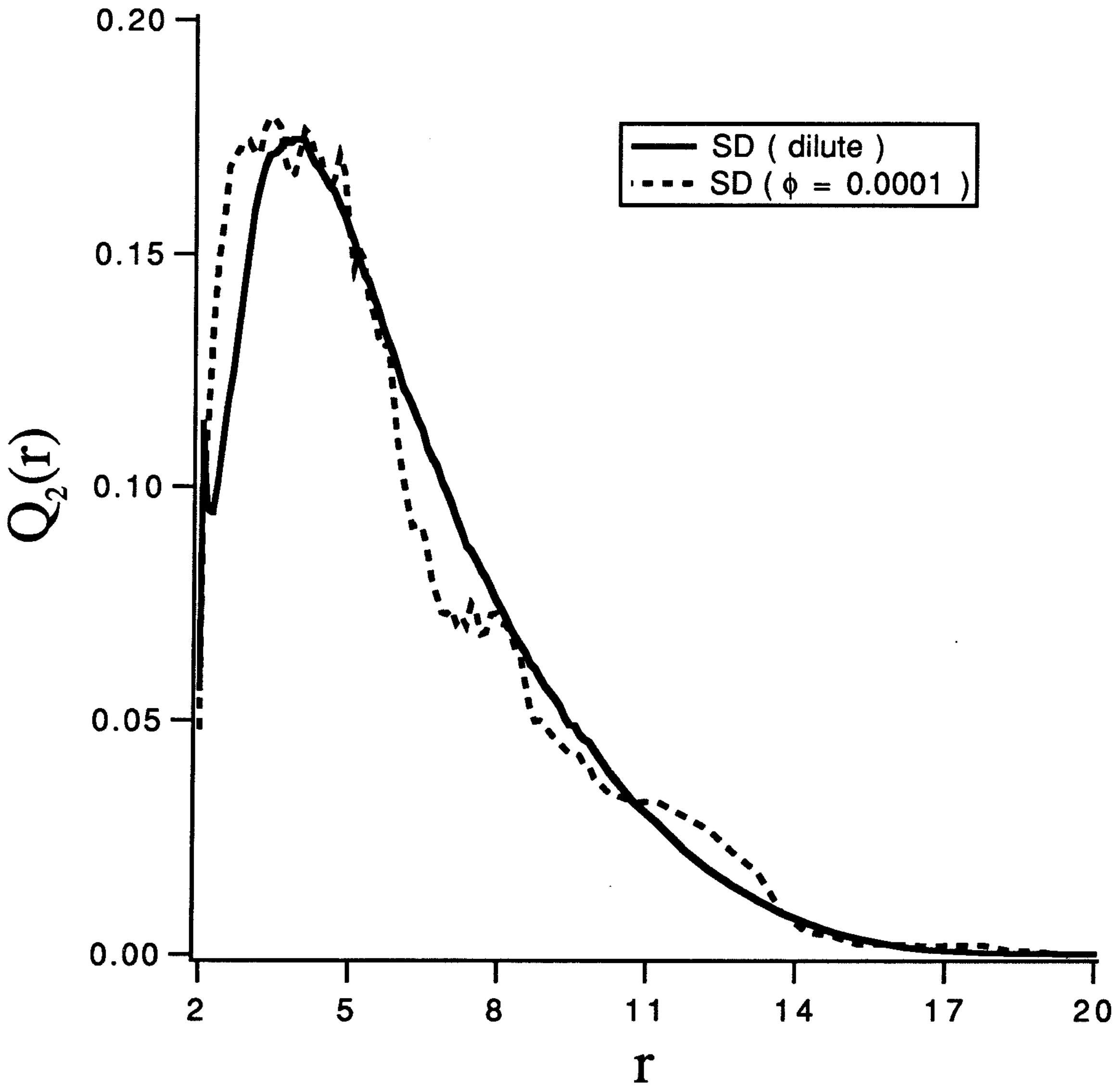

Figure (5.1)

Comparison of angularly averaged radial distribution functions of Stokesian dynamics dumbbells at infinite dilution and at a volume fraction $\phi = 10^{-4}$. Pe=1 and h*=0.25 .

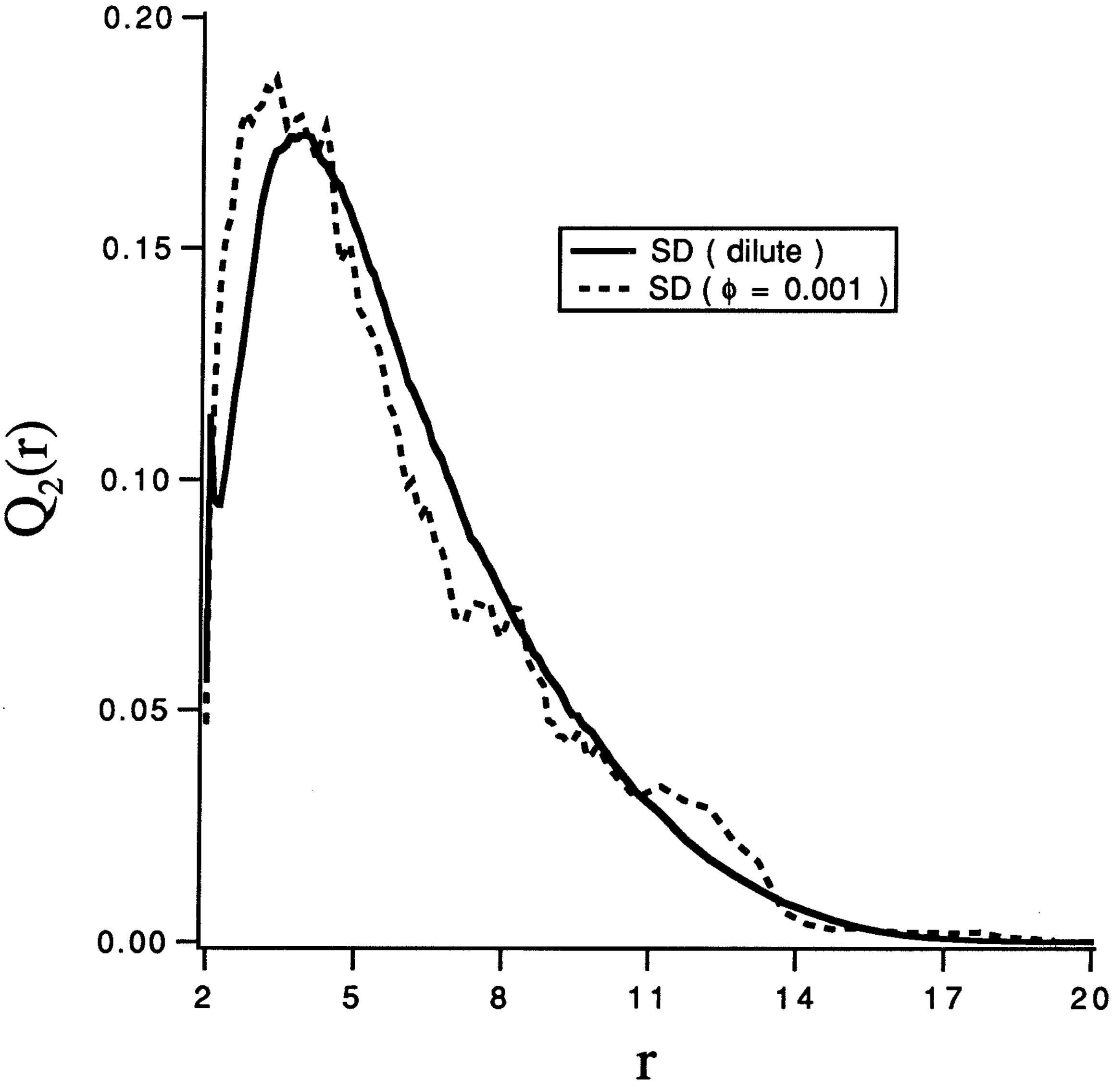

Figure (5.2)

Comparison of angularly averaged radial distribution functions of Stokesian dynamics dumbbells at infinite dilution and at a volume fraction $\phi = 10^{-3}$. Pe=1 and h*=0.25 .

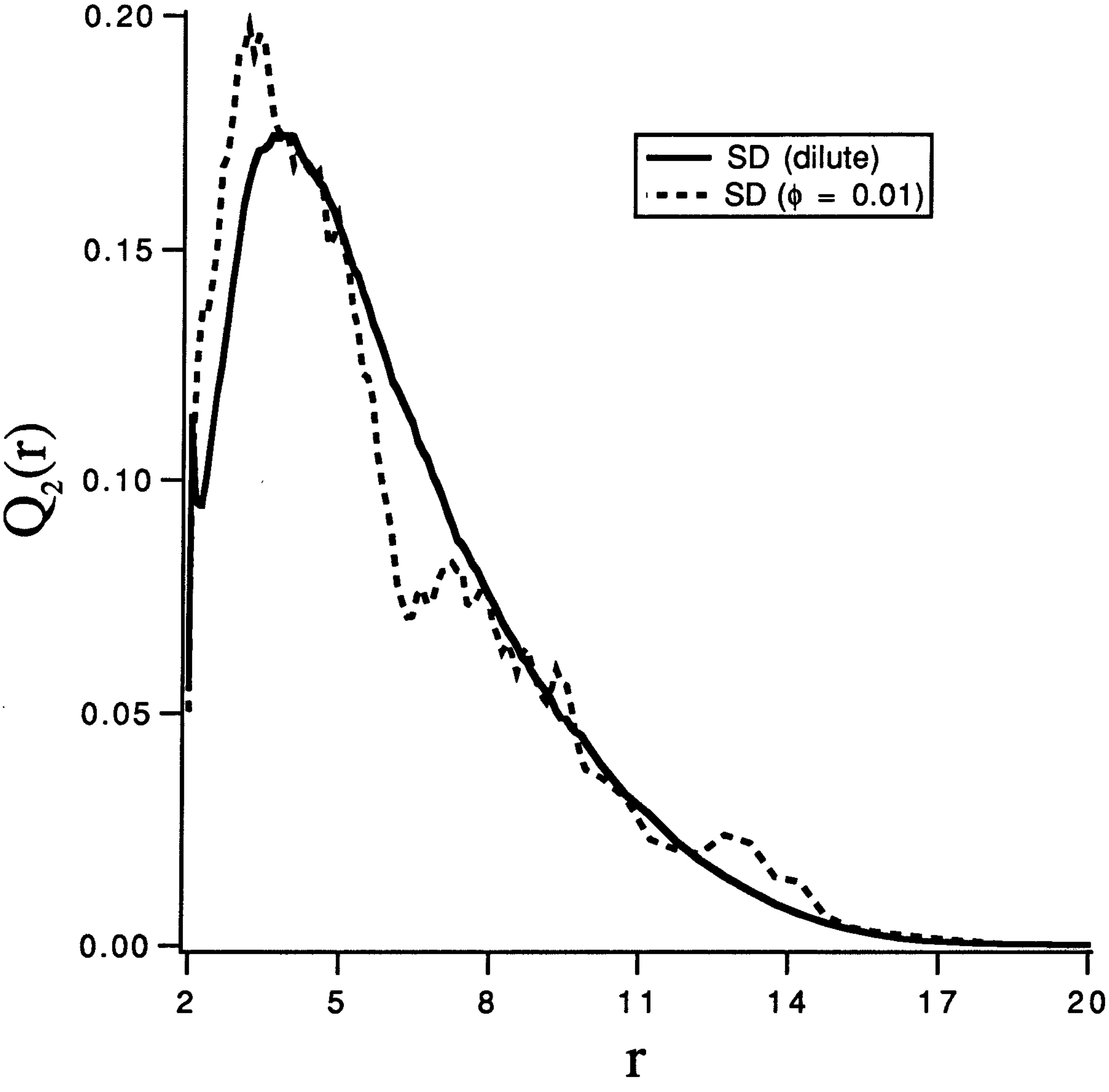

Figure (5.3)

Comparison of angularly averaged radial distribution functions of Stokesian dynamics dumbbells at infinite dilution and at a volume fraction $\phi = 10^{-2}$. Pe=1 and h*=0.25 .

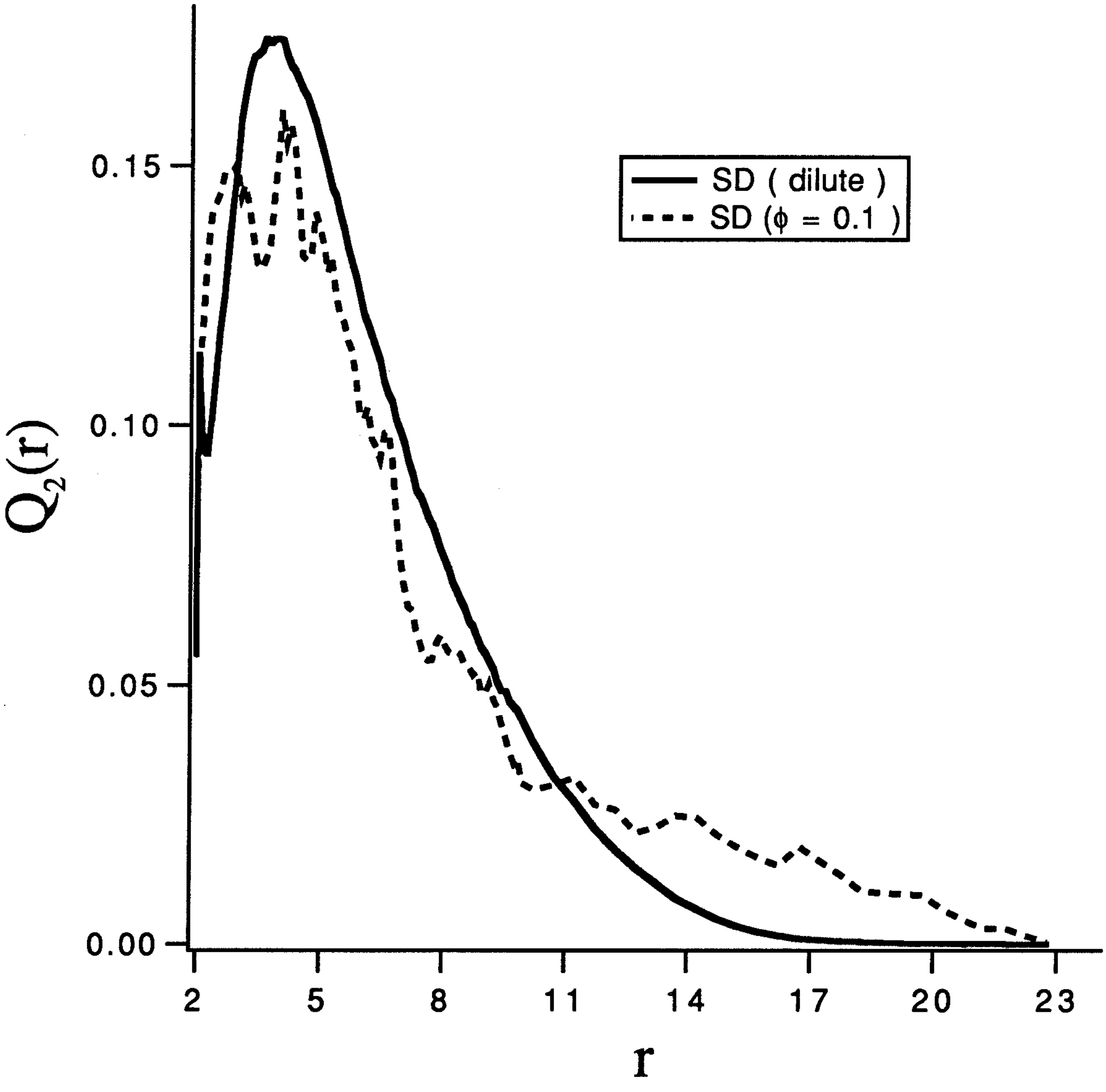

Figure (5.4)

Comparison of angularly averaged radial distribution functions of Stokesian dynamics dumbbells at infinite dilution and at a volume fraction $\phi = 0.1$. Pe=1 and h*=0.25 .

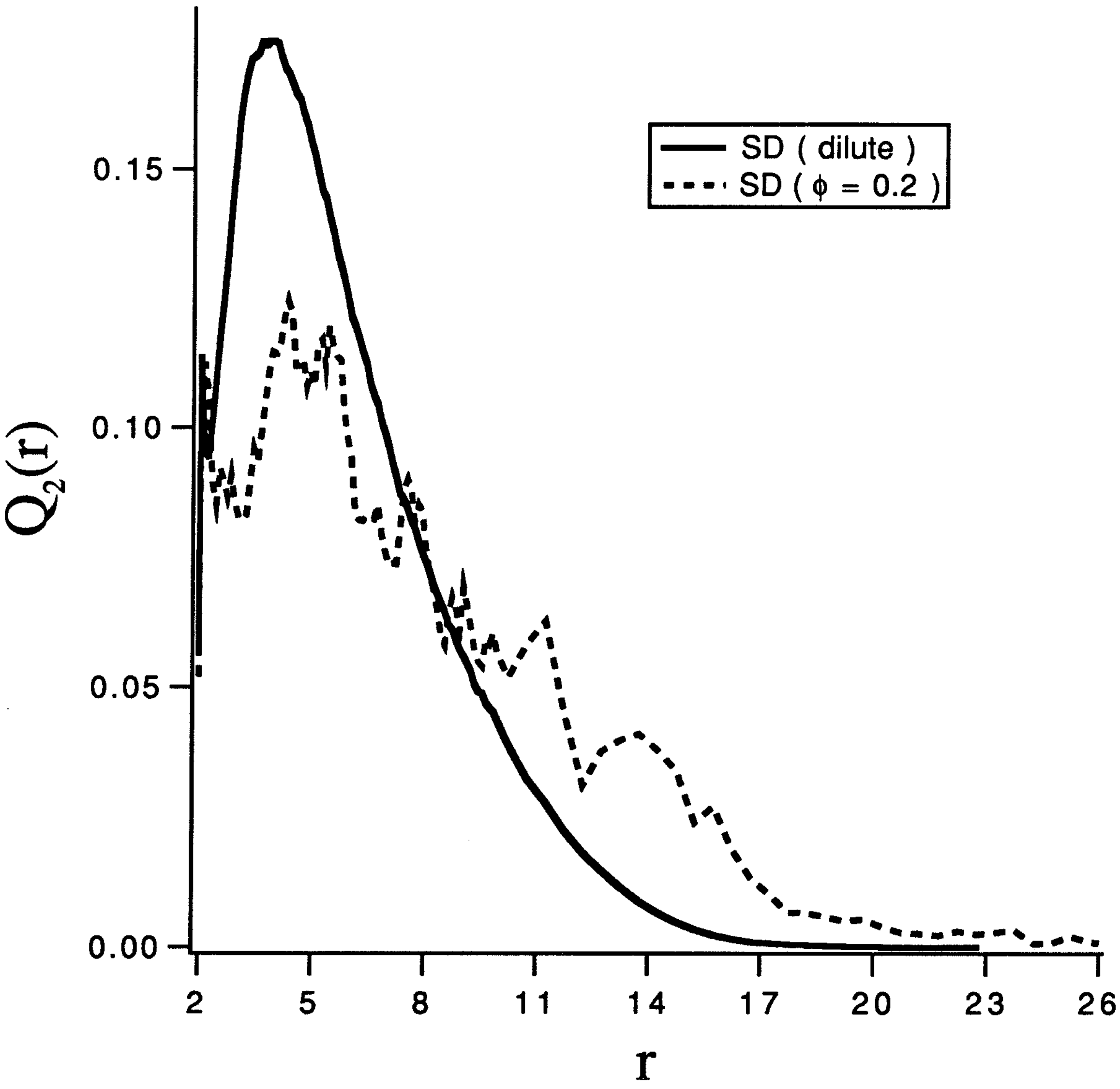

Figure (5.5)

Comparison of angularly averaged radial distribution functions of Stokesian dynamics dumbbells at infinite dilution and at a volume fraction $\phi = 0.2$. Pe=1 and $h^*=0.25$.

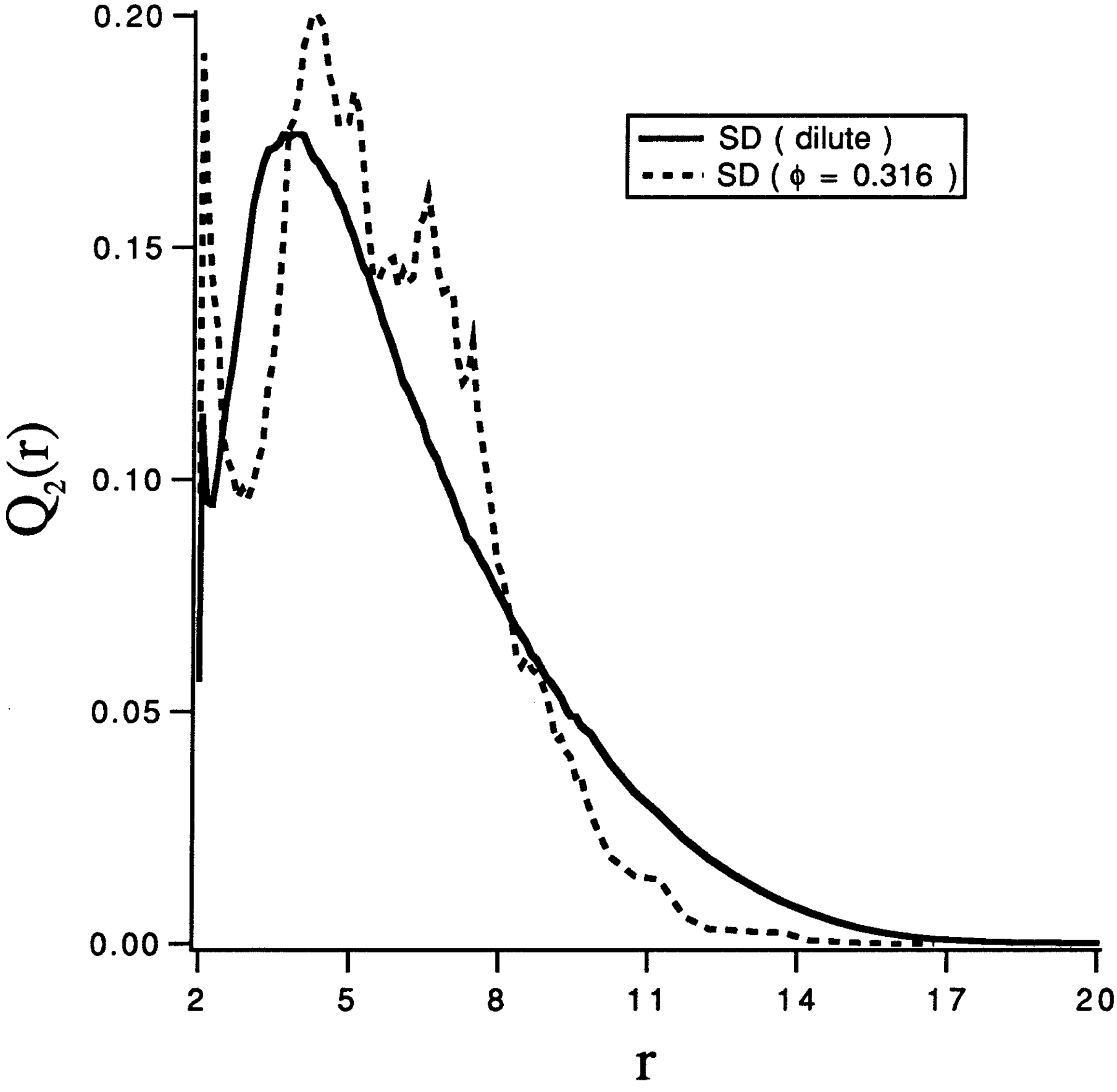

Figure (5.6)

Comparison of angularly averaged radial distribution functions of Stokesian dynamics dumbbells at infinite dilution and at a volume fraction $\phi = 0.316$. Pe=1 and h*=0.25 .

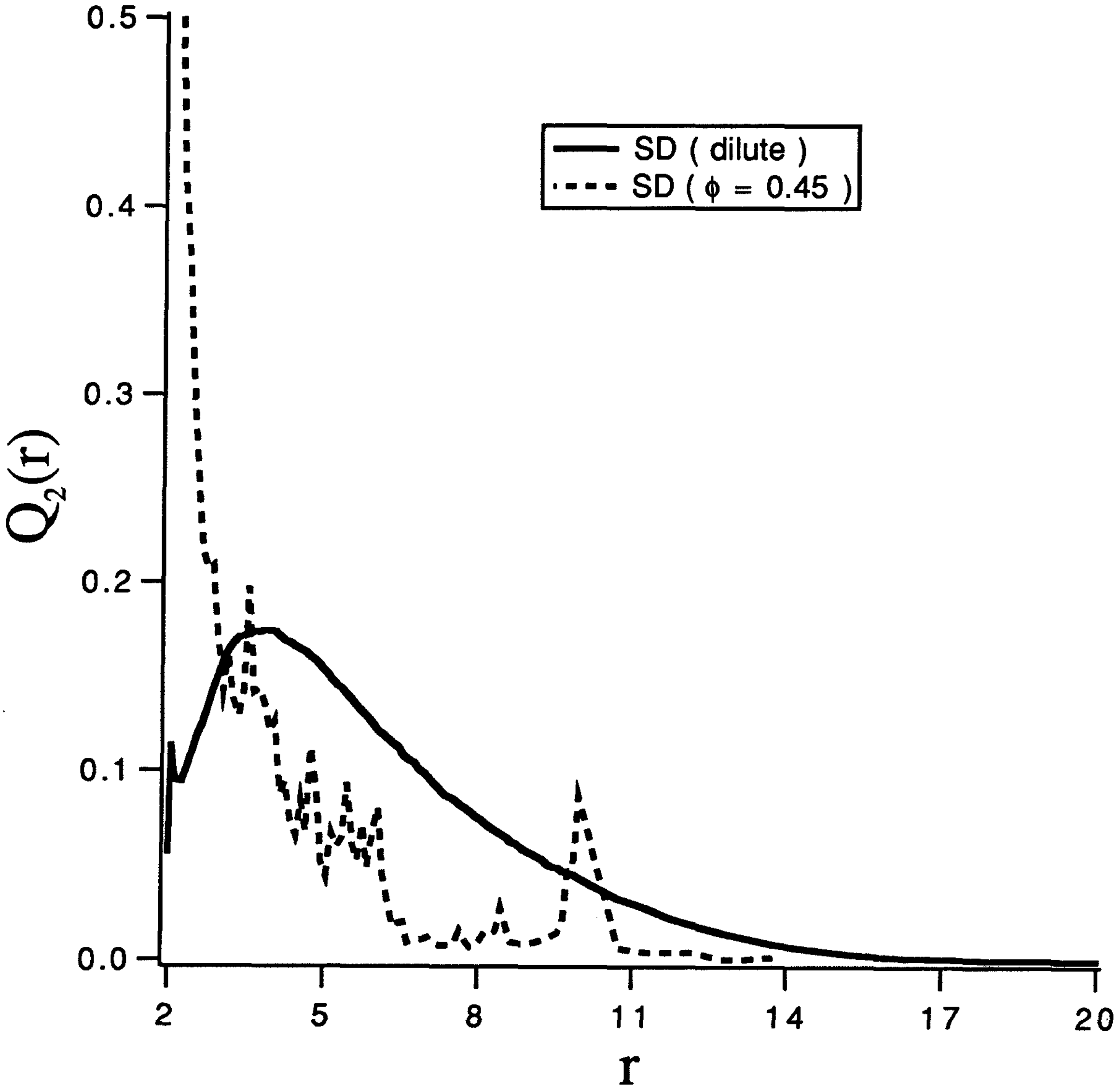

Figure (5.7)

Comparison of angularly averaged radial distribution functions of Stokesian dynamics dumbbells at infinite dilution and at a volume fraction $\phi = 0.45$. Pe=1 and h*=0.25 . The peak at r=2 reaches a maximum value of 3.2 .

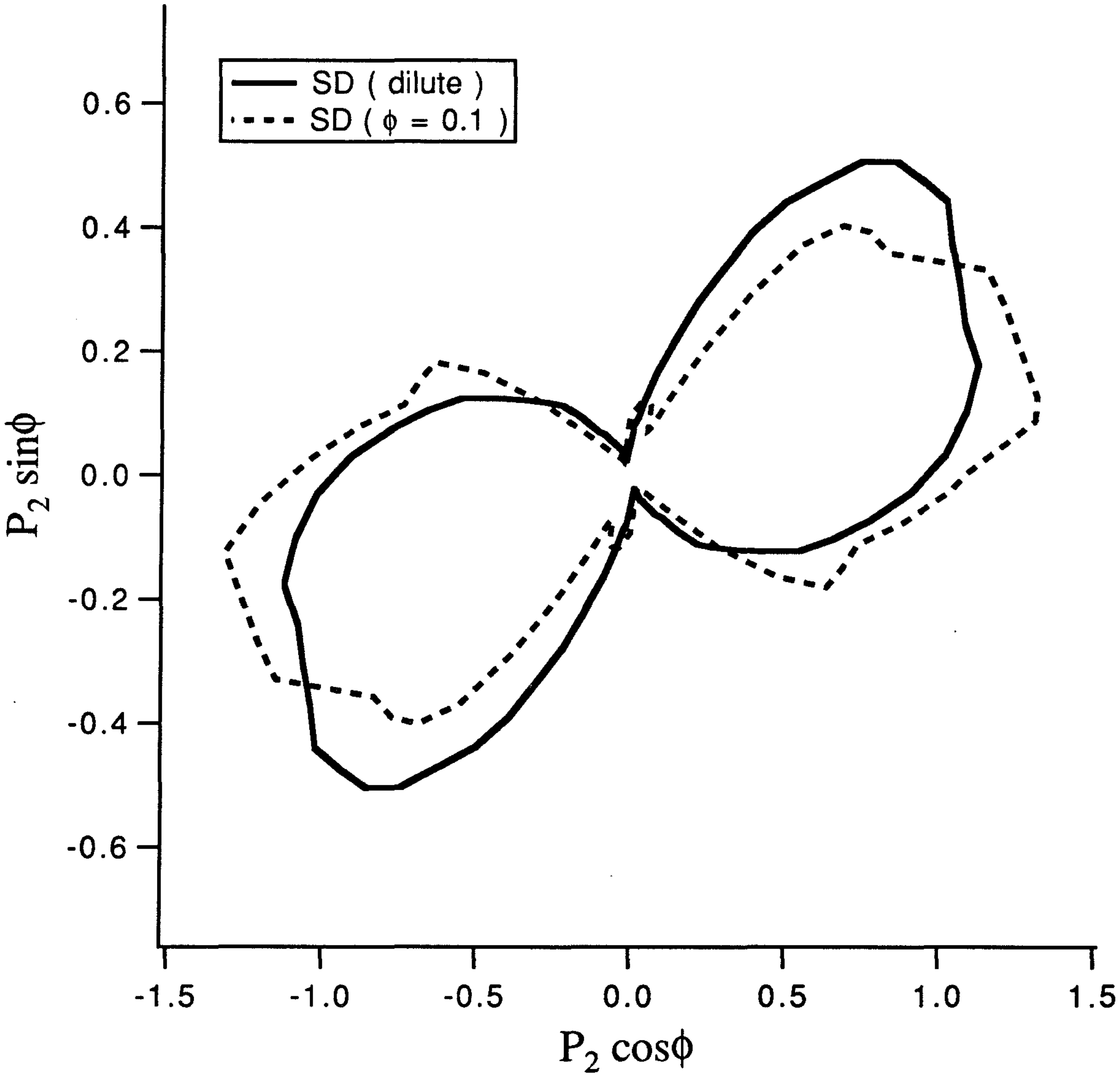

Figure (5.8)

Comparison between angular distribution functions of Stokesian dynamics dumbbells at infinite dilution and at a volume fraction ϕ=0.1 for an extension r=5. Pe=1 and h*=0.25 .

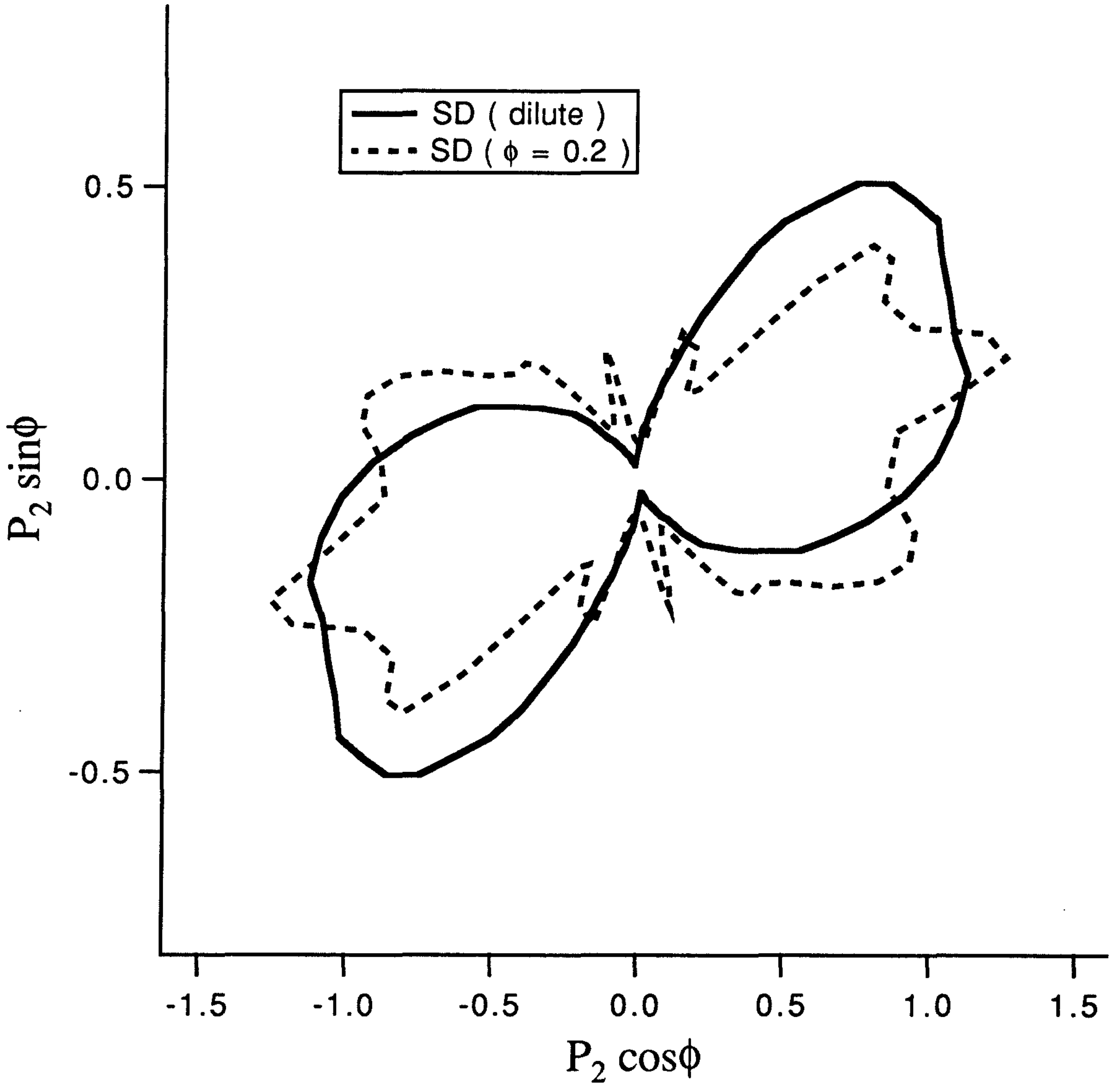

Figure (5.9)

Comparison between angular distribution functions of Stokesian dynamics dumbbells at infinite dilution and at a volume fraction ϕ=0.2 for an extension r=5. Pe=1 and h*=0.25 .

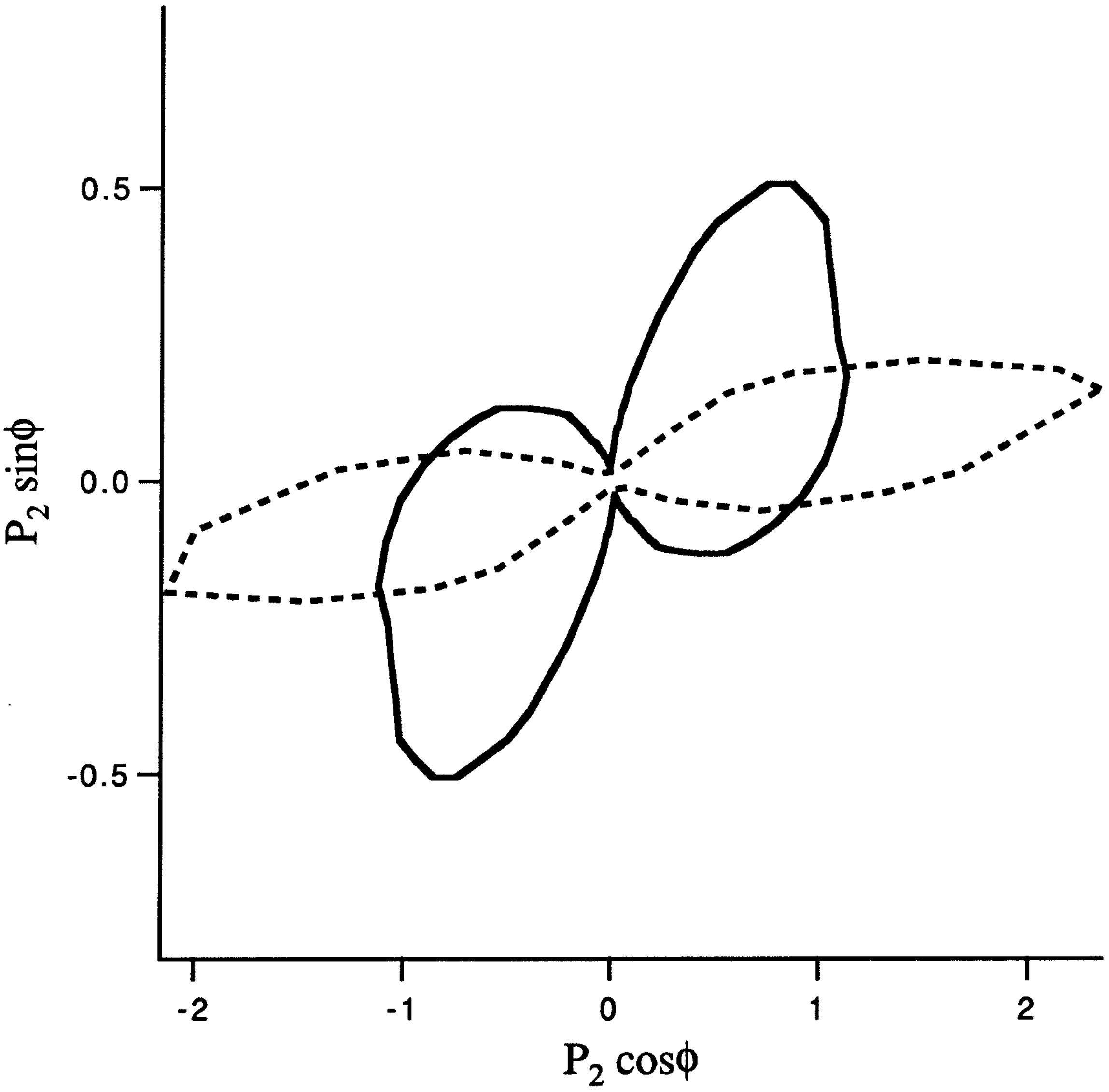

Figure (5.10)

Comparison between angular distribution functions of Stokesian dynamics dumbbells at infinite dilution and at a volume fraction ϕ=0.45 for an extension r=5. Pe=1 and h*=0.25 .

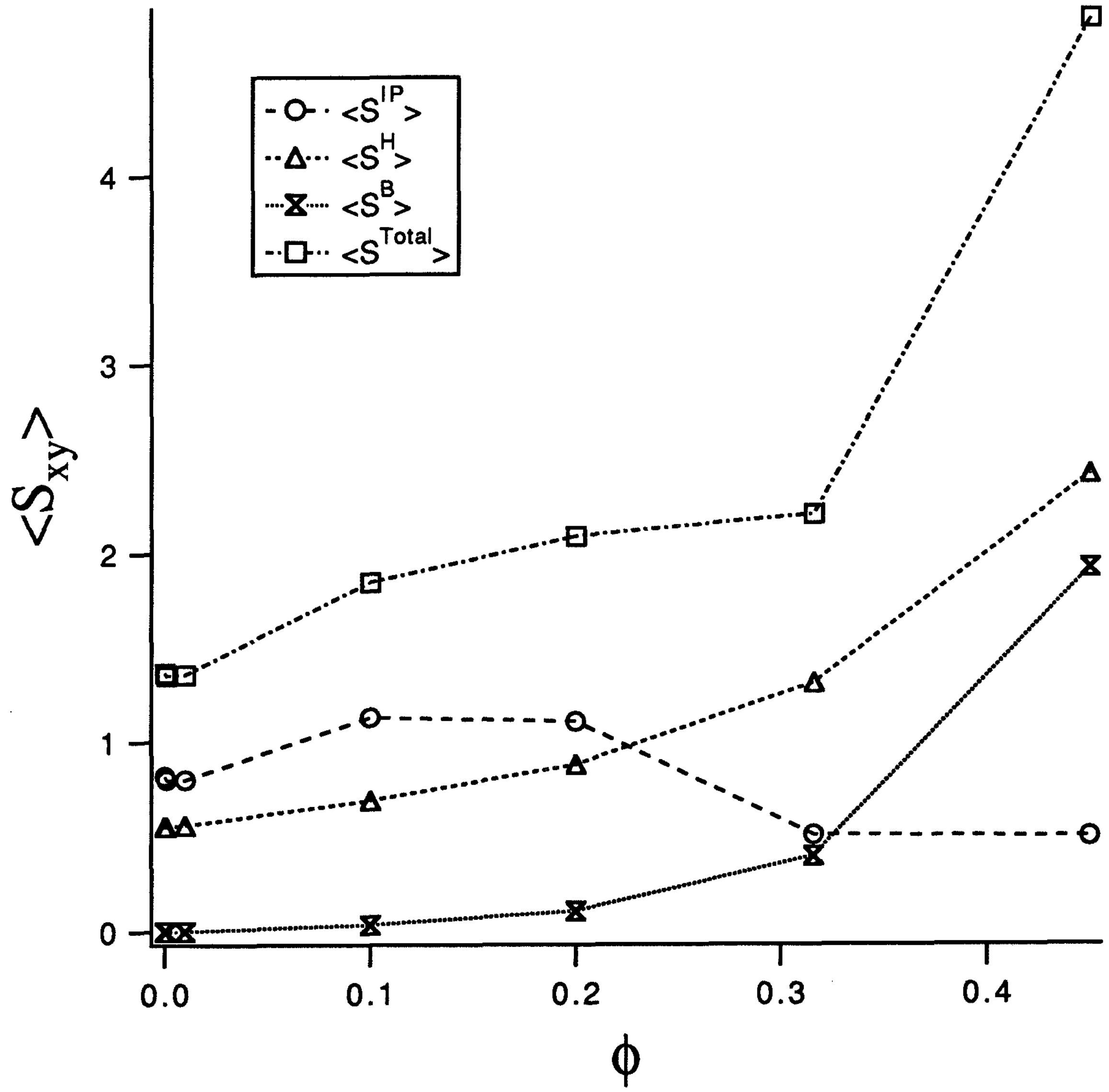

Figure (5.11)

Concentration dependence of the various stress contributions in a suspension of Stokesian dynamics dumbbells. Pe=1 and h*=0.25.

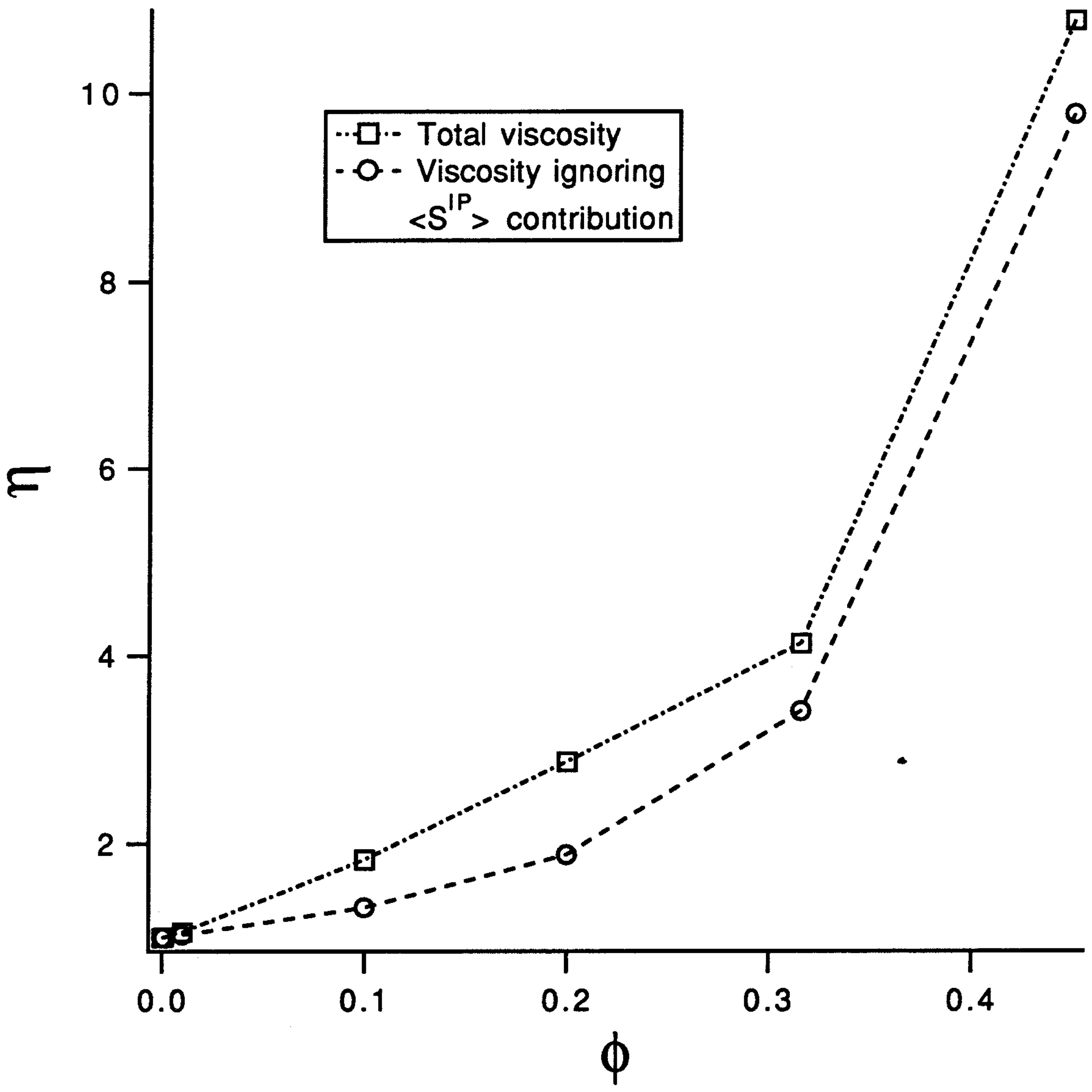

Figure (5.12)

Viscosity as a function of concentration in a suspension of Stokesian dynamics dumbbells. Pe=1 and h*=0.25.

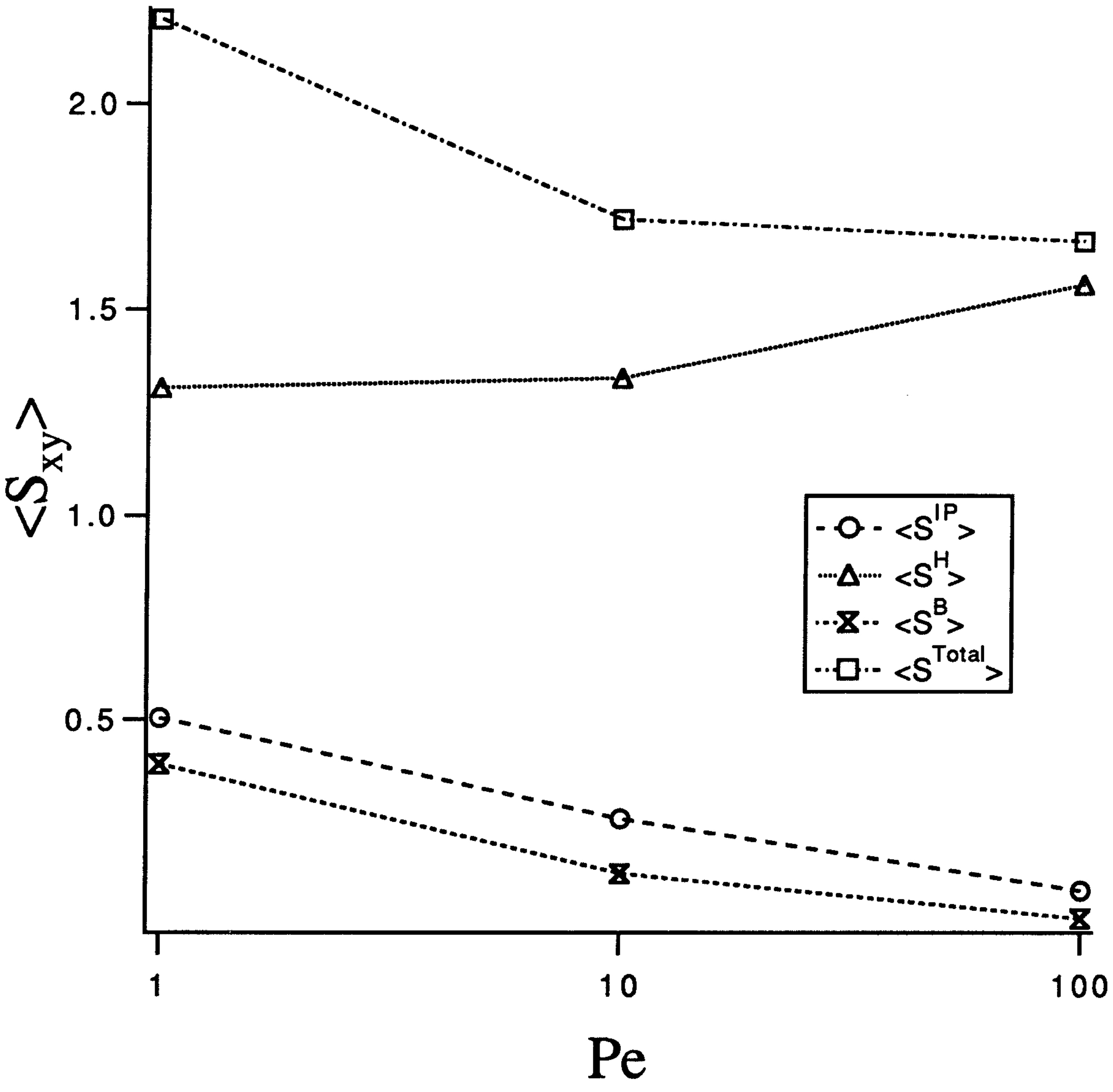

Figure (5.13)

Stress contributions as a function of Pe in a suspension of Stokesian dynamics dumbbells. The volume fraction is 0.316 and h*=0.25.

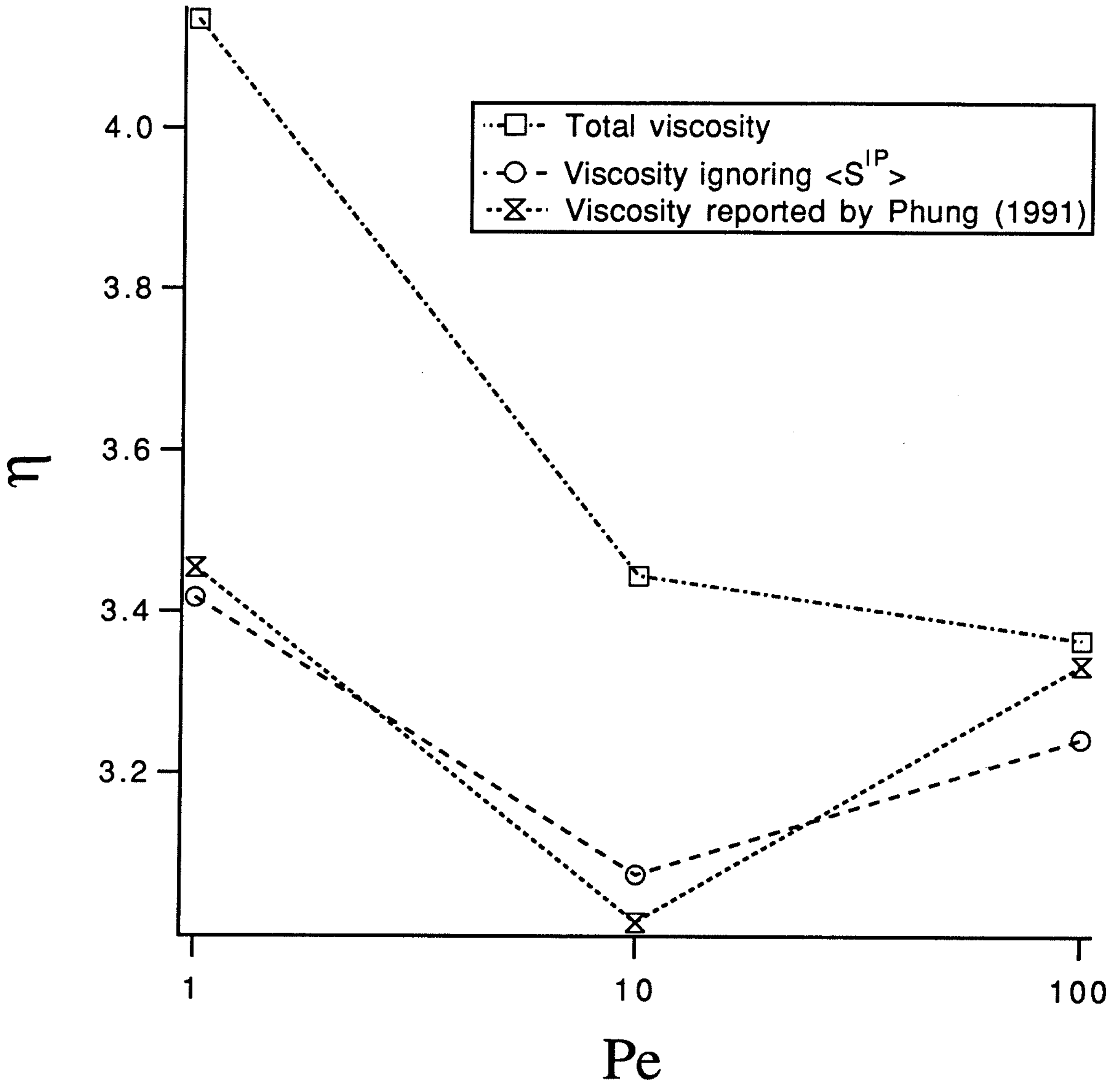

Figure (5.14)

Effect of interparticle forces on the hydrodynamical contributions to viscosity. The hydrodynamic and Brownian contributions from the Stokesian dynamics dumbbells are nearly identical to the results of Phung (1991) for a suspension of spheres at the same volume fraction. The volume fraction is 0.316 and h* = 0.25 for the dumbbells.

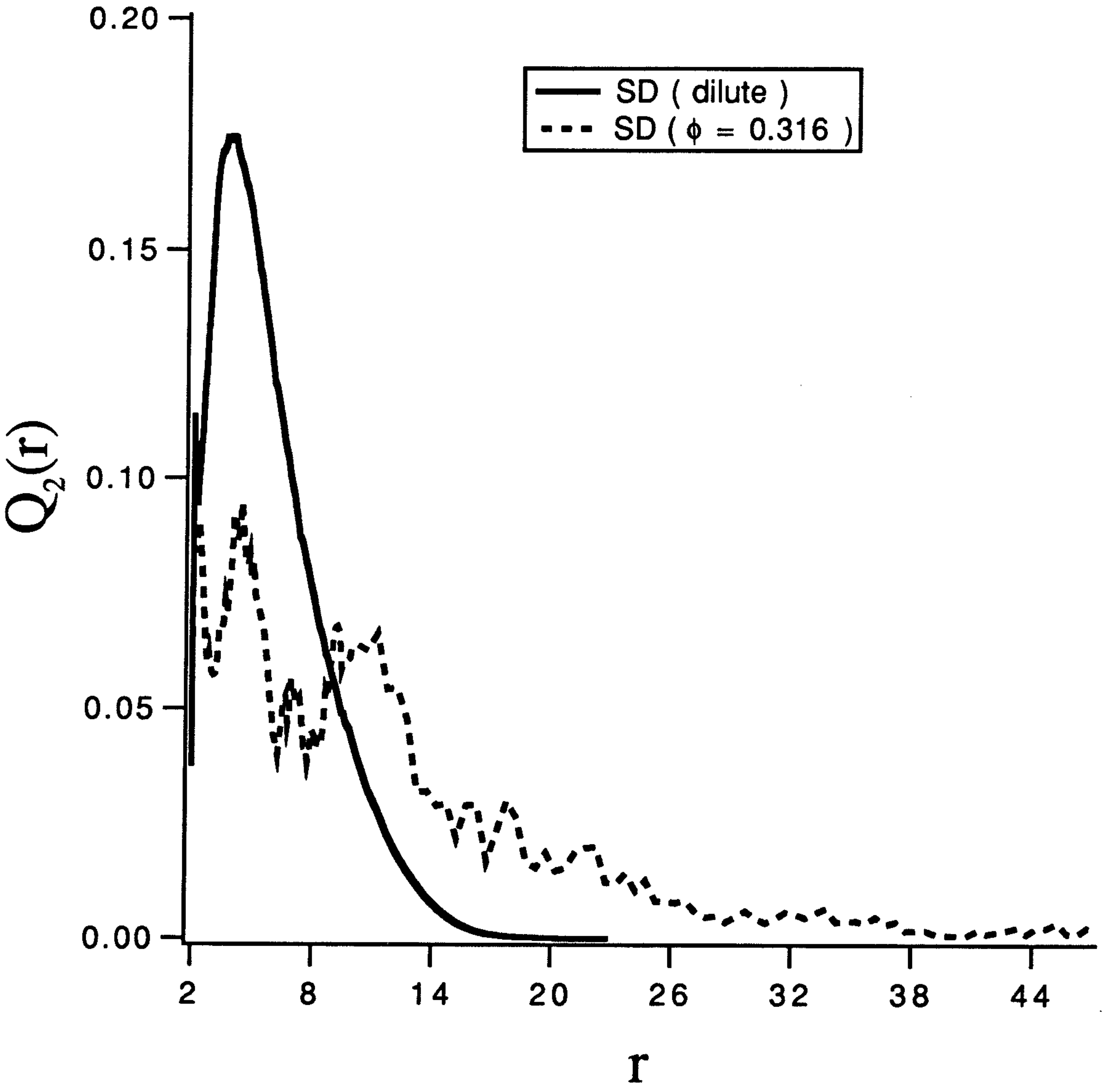

Figure (5.15)

Additional comparison of angularly averaged radial distribution function for a volume fraction φ = 0.316 . Pe=1 and h*=0.25 .

6. CONCLUSIONS

A new method of studying polymer dynamics that intensively calculates the full hydrodynamics has been compared to existing models. The Stokesian dynamics bead-spring model was compared to the Rouse and Zimm models for steady and oscillatory shear, and also compared to Öttinger's Gaussian approximation for steady shear.

For the dumbbell model of polymers, the Stokesian dynamics model provides no advantages over the dynamical Zimm model or the Gaussian approximation. It is computationally more expensive, yet gives similar results. Nonetheless, an analysis of the predictions of the Stokesian dynamics model does suggest several ways in which the simpler models may be improved. Stokesian dynamics calculates the full hydrodynamics of the dumbbell, including the hydrodynamic stress, $\mathbf{S}^H$. Under both the steady shear and the oscillatory shear, $\mathbf{S}^H$ is predicted to be nearly equal to the Einstein-stress contribution, $\mathbf{S}^E$. This suggests that $\mathbf{S}^E$ may be added to the results of Zimm and the Gaussian approximations without complicating their solutions. This is particularly attractive in the case of oscillatory flow. The Stokesian dynamics results predict that $\mathbf{S}^H$ is the sole contributor to the high-frequency viscosity addition in a polymer solution. The Rouse and Zimm models both predict the high-frequency viscosity to be zero.

An analysis of the microstructures of the Rouse, Zimm and Stokesian dynamics models reveals that shear thinning is the result of a change in orientation. Hydrodynamic interaction causes the angular orientation to shift toward the axis of shear. This tilt increases with Pe. This shift in the orientation reduces the contribution of the interparticle force to the measured stress. Hence, the viscosity decreases with increasing shear rate. This shear thinning as the result of change in orientation suggests a way by which shear thinning may be studied in the Rouse model. The increased time spent along the axis of shear by the Zimm and Stokesian dynamics models suggests behavior that would be expected in a flow with greater extensional character. In shear flow, rotation balances extension. Analyzing the Rouse model in a flow where the extensional effect is of greater magnitude than the rotational effect should mimic the increase in time spent near the shear axis. Studying the effect of increased extension on the stress predicted by the Rouse model could provide additional insight into the roles of configuration and extension in the stress contributions of polymers.

An additional investigation suggested by the orientationally induced shear thinning involves flow birefringence. As stated in Onuki and Doi (1986), the intrinsic birefringence in a polymer solution is proportional to the anisotropy of the stress tensor. Since the stress tensor is directly dependent upon the polymer orientation, this implies that intrinsic-birefringence measurements will provide information about the orientational distribution of a polymer solution subjected to a flow. Examining intrinsic-birefringence data for dilute polymer solutions over a range of Pe will provide another point of reference for determining when the Stokesian dynamics model is an appropriate model and when the Zimm (or another, simpler model) will suffice.

The Brownian stress calculated by the Stokesian dynamics model is negligible for almost all examined flows. Rather than confirming that $\mathbf{S}^B$ is unimportant, this points to a shortcoming in the stress calculations of all bead-spring models, including the present Stokesian dynamics model. None of the models consider the entropy of the orientation of the interparticle springs. In the theory of rodlike polymers, the entropy of the rod orientation is the only source of stress. Equal consideration should be given to the springs in the bead-spring model. To better see why the Stokesian dynamics formulation does not capture this stress, consider a concentrated suspension of randomly packed spheres. There is little order in the system. Now, connect pairs of spheres such that the connecting vectors are nearly identical in orientation. The system has become highly ordered, but the Stokesian dynamics prediction of $\mathbf{S}^B$ has not changed. The Stokesian dynamics formulation may be able to capture the contribution to $\mathbf{S}^B$ by allowing the beads to rotate only about the axis of the spring, since this would induce rotational coupling among the bead pairs.

Despite the numerous improvements in polymer modeling suggested by the Stokesian dynamics model, it is not an efficient model in the case of a dumbbell. The dynamical Zimm model and Öttinger's Gaussian approximation give essentially the same results with much less effort. This is not true for multibead representations, or for the modeling of concentrated solutions. In both of these cases the lubrication forces and many-body effects calculated by Stokesian dynamics become important, and are not provided by the other models. Dumbbells often rotate as a unit, with little relative motion and thus little hydrodynamic stress. The beads in multibead models, particularly in high-frequency flows, will be forced to move relative to one another, inducing additional hydrodynamic stress. The Stokesian dynamics model may also capture some aspects of the so-called "internal viscosity" of polymers. Internal viscosity refers to a polymer's resistance to a sudden extension. If included in a model, it is in the form of a "dashpot," or a term proportional to the rate of extension rather than to the magnitude of the extension. Lubrication effects from nearly touching beads may provide a similar effect in the Stokesian dynamics model – – again, an aspect of polymer physics which simpler models cannot address.

In concentrated solutions these hydrodynamic and excluded-volume effects become even more apparent. At high concentrations, the hydrodynamic and Brownian stresses provided by the Stokesian dynamics model allow analysis of chain entanglements. This important qualitative aspect of concentrated-solution behavior cannot be addressed by previous dynamical models that do not include these forces. However, the present results show that even the Stokesian dynamics model is not appropriate for concentrated-solution analysis if the simple dumbbell model is used. Chain entanglement is a multiple-length-scale phenomenon, and the dumbbell model is inherently a single-length-scale model. In addition, the concentrated solutions require long simulation times to ensure that a good sampling of configuration space is obtained, and this preliminary study has not satisfied that criterion. The results obtained are strongly dependent upon the initial configurations. Without examining longer runs it is impossible to state whether this dependence on initial conditions is real or is a consequence of the short simulation times. It is anticipated that there exists a critical concentration ϕ^*, above which the orientational distribution of the solution as $t \to \infty$ will always be determined by the initial arrangement and the shear history. With the rapid increase in speed of modern computers, the practical use of multibead models to answer such questions is not far away.

APPENDIX A

Calculation of preaveraged time constants.

As noted in §2.1, the Oseen tensor is unsuitable for numerical simulations of polymers because it predicts negative mobilities for small bead separations. For this reason most studies, including this one, use the Rotne-Prager interaction tensor. For comparison with the preaveraged results, however, prior studies still have compared to the preaveraged Oseen tensor, assuming that the differences between Oseen and Rotne-Prager will be small. For the dumbbell case this assumption is unnecessary, since it is trivial to calculate the preaveraged results for *any* interaction tensor, as shown below. This development draws upon the the work of Thurston and Morrison (1969).

From Eq. (2.11*b*), for two beads,

$$\begin{aligned}\langle \mathcal{J} \rangle_{eq} &= \frac{1}{6\pi\eta_s}\langle\frac{1}{r}\rangle, \\ &= C_{\mathcal{J}}. \end{aligned} \tag{A.1}$$

The choice of the hydrodynamic-interaction description does not change $\langle 1/r \rangle$ (an equilibrium characteristic), but it can change the constant in front. Thus, for a given hydrodynamic-interaction tensor χ, the average interaction is

$$\begin{aligned}\langle \chi \rangle_{eq} &= \int \chi \Psi_{eq} d\mathbf{r}, \\ &= C_{\chi}. \end{aligned} \tag{A.2}$$

For example, Ψ_{eq} between the two beads of a Hookean dumbbell with no excluded volume is given by

$$\Psi_{12} = \left(\frac{K}{2\pi}\right)^{3/2} e^{-\frac{1}{2}Kr^2}. \tag{A.3}$$

It is simple to determine C_χ numerically for any χ, an advantage for such interaction tensors as Rotne-Prager, where the different form of the interaction for different ranges of r may make analytic solution difficult or impossible. This leads to a general definition for the off-diagonal elements of the matrix **H**,

$$\begin{aligned} H &= \zeta C_\chi, \\ &= H_\chi. \end{aligned} \tag{A.4}$$

To solve for the time constant of the dumbbell, the eigenvalues of $\mathbf{HA} - \lambda\mathbf{I}$ are required, where **A** is defined in Eq.(2.3) of §2. For the dumbbell case,

$$\mathbf{HA} = \begin{pmatrix} 1 - H_\chi & H_\chi - 1 \\ H_\chi - 1 & 1 - H_\chi \end{pmatrix}, \tag{A.5}$$

so

$$\mathbf{HA} - \lambda\mathbf{I} = \begin{pmatrix} 1 - H_\chi - \lambda & -(1 - H_\chi) \\ (1 - H_\chi) & 1 - H_\chi - \lambda \end{pmatrix}, \tag{A.6}$$

This leads to a relaxation time constant λ_1 for the dumbbell,

$$\lambda_1 = 2(1 - H_\chi). \tag{A.7}$$

As shown above, C_χ is a function of h^*, and thereby a function of the spring constant K. Thus, the relaxation time for any given χ and h^* is determined by calculating C_χ and inserting in Eq.(A.7), then using the resulting λ_1 in the equations for G' and G'' given in §3.3.

For a chain of N beads ($N > 2$), Eq.(A.7) no longer applies, but the eigenvalues of $\mathbf{HA} - \lambda\mathbf{I}$ can still be found. If the beads have no excluded volume, then the distance between bead i and bead j is given by

$$\Psi_{ij} = \left(\frac{K}{2\pi|i-j|}\right)^{3/2} e^{-\frac{1}{2}K|i-j|r^2}. \tag{A.8}$$

The components of the complex moduli obtained using both the preaveraged Oseen tensor and the preaveraged Rotne-Prager tensor are plotted in Figure (A.1) for the case $N = 10$. This plot validates the assumption that Oseen and Rotne-Prager are negligibly different in the preaveraged case. This example may be repeated for any value of N. The limiting step is the length of time required to solve for the eigenvalues of the $N \times N$ matrix.

Although no analytical equations exist for a chain of N beads with excluded volume, preaveraged time constants for such a chain may still be calculated. Monte Carlo simulations can be run for any length of chain, and a numerical equivalent to Eq.(A.8) can be calculated for Ψ_{eq}. This numerical Ψ_{eq} can then be used to form the $\mathbf{H}$ matrix, and eigenvalues of $\mathbf{HA} - \lambda\mathbf{I}$ calculated. The limiting step becomes the length of time required to get a good estimate of Ψ_{eq} from the Monte Carlo runs. For the case of $N = 2$, $\Psi_{eq} = P_2^0$ from Eq.(3.3), §3. Using this distribution function, λ_1 can be calculated. For the Rotne-Prager interaction, it is found to be 1.440, as compared to 1.336 for the non-excluded-volume case. The components of the complex moduli for the dumbbell with and without excluded volume, using the Rotne-Prager interaction, are plotted in Figure (A.2).

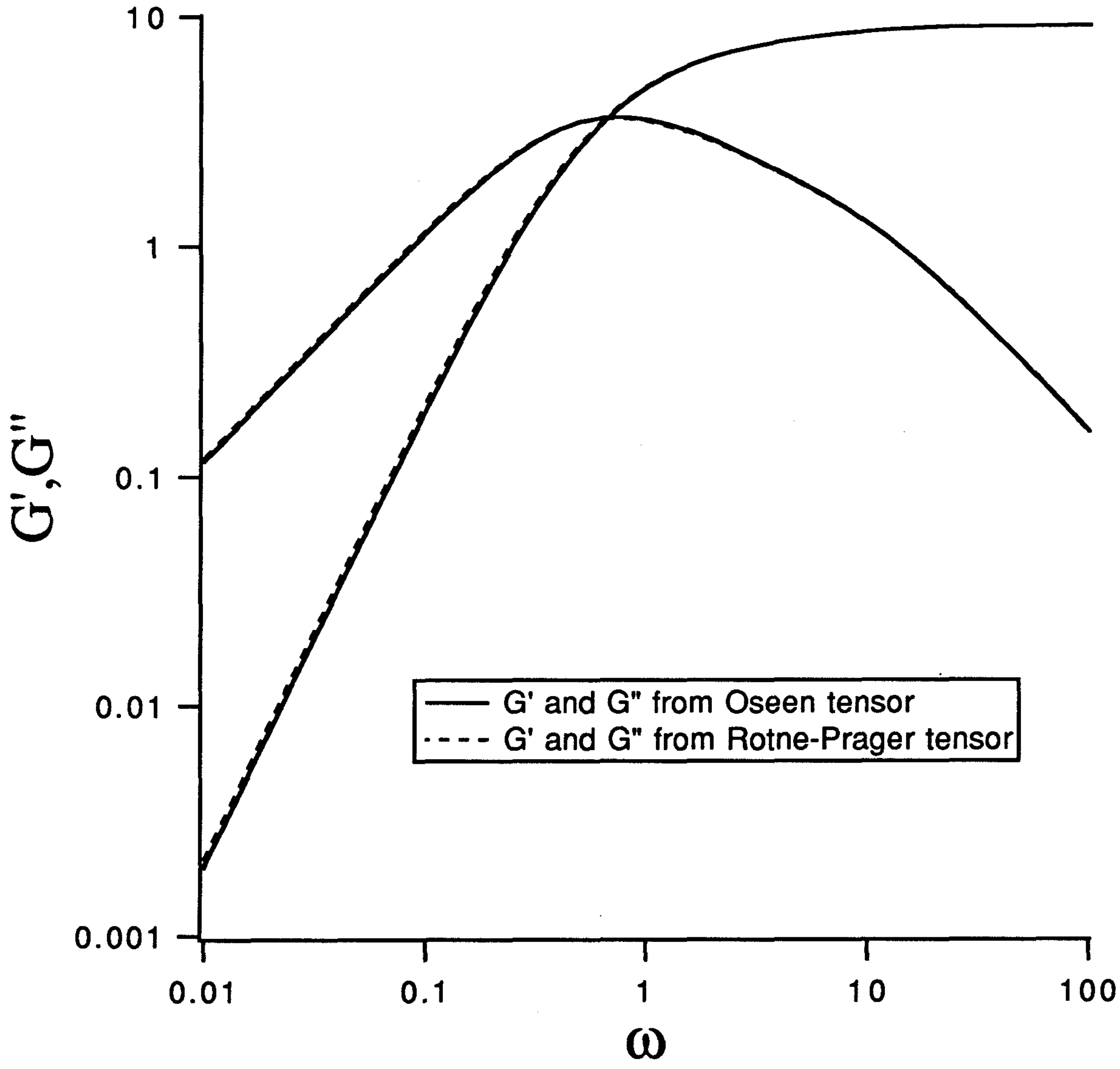

Figure (A.1)

Complex moduli for a chain of 10 beads based on the preaveraged Oseen tensor and the preaveraged Rotne-Prager tensor. h*=0.25

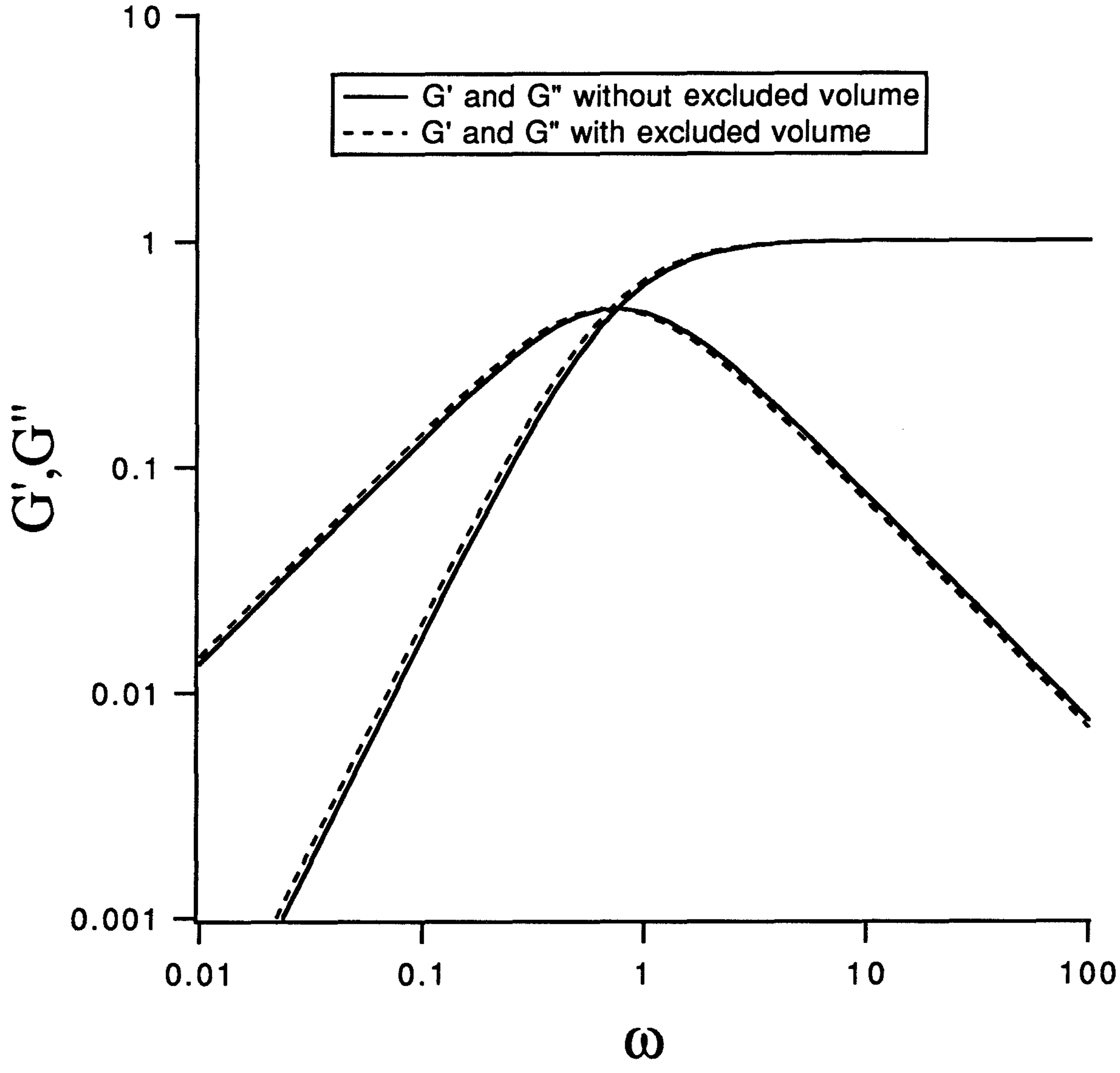

Figure (A.2)

Complex moduli for a dumbbell with and without excluded volume, using the preaveraged Rotne-Prager tensor. h*=0.25

APPENDIX B

Low Péclet departure from equilibrium of P_2 for the Stokesian dynamics dumbbell.

The equilibrium radial-distribution function for the Stokesian dynamics dumbbell is

$$P_2^0(\mathbf{r}) = \begin{cases} P_0 e^{-\frac{1}{2}Kr^2} & (r > 2a); \\ 0 & (r \le 2a). \end{cases} . \tag{B.1}$$

For the Stokesian dynamics model in low-Péclet, steady, simple shear flow, an ordinary differential equation may be solved for the exact departure of the radial-distribution function P_2 from the equilibrium distribution P_2^0. Introducing the disturbance quantity f_2, defined by

$$P_2 = P_2^0 + Pef_2, \tag{B.2}$$

Eq.(3.1) of §3.1 becomes, to leading order in Pe,

$$\frac{\partial f_2}{\partial t} - \nabla \cdot \mathbf{D}_2 \cdot \nabla f_2 - \nabla \cdot \mathbf{D}_2 \cdot (\nabla V_2) f_2 = -\nabla \cdot \mathrm{U}_2 P_2^0, \tag{B.3}$$

where $\mathbf{D} \equiv kT\mathbf{M}$ is the relative diffusivity. Note that the third term on the left-hand side of (B.3) arises because the disturbance function f_2 in (B.2) has been defined independent of P_2^0, as opposed to the f_2 of Russel and Gast (1986) and Bossis, Brady and Mathis (1988), which was defined as

$$P_2 = P_2^0 + \mathrm{Pe} P_2^0 f_2. \tag{B.4}$$

Since $\mathbf{F}^{IP}$ for the polymer problem grows rather than decays with $\mathbf{r}$, the introduction of Eq. (B.4) as the disturbance quantity results in a differential equation with ill-posed boundary conditions. Hence, (B.2) must be introduced to allow solution of the problem.

Because the equilibrium state is isotropic, the non-dimensional, hydrodynamic, relative diffusivity and velocity can be written as

$$\mathbf{D}_2(\mathbf{r}) = 2\{\hat{\mathbf{r}}\hat{\mathbf{r}}G(r) + (\mathbf{I} - \hat{\mathbf{r}}\hat{\mathbf{r}})H(r)\}, \tag{B.5}$$

$$\mathbf{U}_2(r) = r\hat{\mathbf{r}} \cdot \mathbf{E}^\infty - r\hat{\mathbf{r}} \cdot \mathbf{E}^\infty\{\hat{\mathbf{r}}\hat{\mathbf{r}}A(r) + (\mathbf{I} - \hat{\mathbf{r}}\hat{\mathbf{r}})B(r)\}, \tag{B.6}$$

where $\mathbf{E}^\infty$ is the non-dimensional rate-of-strain tensor of the imposed linear shear flow, and $\hat{\mathbf{r}} = \mathbf{r}/r$. G, H, A, and B are the hydrodynamic-interaction functions for two particles given by Batchelor (1976). The same expressions are used as in Bossis, Brady and Mathis (1988). These expressions are given at the end of this appendix.

From the form of the relative velocity for steady shear flow, $f_2(\mathbf{r},t)$ can be written as

$$f_2(\mathbf{r},t) = -\frac{1}{2}f(r)\hat{\mathbf{r}} \cdot \mathbf{E}^\infty \cdot \hat{\mathbf{r}}, \tag{B.7}$$

where $f(r)$ satisfies

$$\begin{aligned} &\frac{d}{dr}\left(G\frac{df}{dr}\right) + \left(\frac{\delta_{ii}}{r} - \frac{3}{r} + Kr\right)G\frac{df}{dr} \\ &+ \left[\left(\frac{4}{r^2} - \frac{2\delta_{ii}}{r^2} + \delta_{ii}K\right)G - \left(\frac{2}{r} + Kr\right)\frac{dG}{dr} - \frac{2\delta_{ii}}{r^2}H\right] f \\ &= -WP_2^0 - \frac{dP_2^0}{dr}r(1 - A), \end{aligned} \tag{B.8}$$

where

$$W(r) = -\delta_{ii}(A - B) - r\frac{dA}{dr} \quad , \tag{B.9}$$

and δ_{ii} is the trace of the identity matrix, $\delta_{ii} = 3$ for the three-dimensional problem. Note that this differential equation is substantially different from those of Russel and Gast; Bossis *et al.*; and Batchelor because of the change in the definition of f_2.

The boundary conditions to be imposed on f are zero distortion at infinity,

$$f \sim 0 \quad \text{as} \quad r \to \infty, \tag{B.10}$$

and no flux at contact,

$$G\left(\frac{df}{dr}+Krf\right)=0 \quad \text{at} \quad r=2, \tag{B.11}$$

which uses the fact that $A \sim 1$ as $r \to 2$. Furthermore, examination of Eq. (B.1) reveals that not only must $f \sim 0$ asymptotically, but f must decay exponentially. Since P_0 decays exponentially, a slower rate of decay for f would eventually cause the disturbance to exceed P_0, thus violating the initial assumption of a small perturbation. Equation (B.7) must be solved numerically. Solution of the equation follows the procedure of Russel & Gast (1986).

The asymptotic solution of Eq. (B.8) satisfying the boundary conditions as $r \to \infty$ can be written as

$$f = c_1 f_{H1} + c_2 f_{H2} + f_P, \tag{B.12}$$

where $c_i f_{Hi}$ is a homogeneous, asymptotic solution and f_P is a particular solution. One of the homogeneous solutions decays algebraically and is discarded. This investigation found, as the remaining solutions,

$$f_H = e^{-\frac{1}{2}Kr^2}\left[1+\frac{3}{K}r^{-2}+\frac{3}{2K}r^{-3}+\left(\frac{3}{K^2}+\frac{9}{16K}\right)r^{-4}\right], \tag{B.13}$$

$$f_P = P_0 e^{-\frac{1}{2}Kr^2}\left[-\frac{1}{2}r^2-\frac{3}{2}r-\frac{9}{4}\ln r-\left(\frac{27}{4K}+\frac{21}{8}\right)r^{-1}\right]. \tag{B.14}$$

The integration is started at $r = 20$ for the homogeneous equation, and the full equation, with the solutions (B.13) and (B.14), respectively. A fourth-order predictor-corrector is used with $\Delta r = 10^{-4}$. The integration is continued up to $r = 2.0001$, at which time the unknown constant in the homogeneous solution is found by substitution of the combined solution into (B.11). The solutions of (B.13) and (B.14) for $K = 0.19635$ are plotted in Figures (B.1) and (B.2), respectively. The full solution for $K = 0.19635$ is plotted in Figure (B.3).

The expressions for G, H, A and B depend upon the value of r. For $r \geq 4$, they are given by

$$A = 5r^{-3} - 8r^{-5} + 25r^{-6}, \tag{B.15a}$$

$$B = \frac{16}{3}r^{-5}, \tag{B.15b}$$

$$G = 1 - \frac{3}{2}r^{-1} + r^{-3} - \frac{15}{4}r^{-4} + \frac{11}{2}r^{-6}, \tag{B.15c}$$

$$H = 1 - \frac{3}{4}r^{-1} - \frac{1}{2}r^{-3} - \frac{17}{16}r^{-6}. \tag{B.15d}$$

For $2.01 \leq r < 4$, the functions are given by

$$A = \frac{2}{r}\left(x^a_{11} - x^a_{12}\right)\left(X^G_{11} - X^G_{12}\right), \tag{B.16a}$$

$$B = \frac{4}{r}\left[\left(y^a_{11} - y^a_{12}\right)\left(Y^G_{11} - Y^G_{12}\right) - \left(y^b_{11} - y^b_{12}\right)\left(Y^H_{11} - Y^H_{12}\right)\right], \tag{B.16b}$$

$$G = x^a_{11} - x^a_{12}, \tag{B.16c}$$

$$H = y^a_{11} - y^a_{12}, \tag{B.16d}$$

where the functions in these equations are either mobility functions (small letters) or resistance functions (capital letters) for two spheres. The calculation of the functions is based on the collocation method given by Kim and Mifflin (1985). For $r < 2.01$, the following lubrication approximations are used:

$$A = 1 - 4.148\xi + 3.290\xi^{3/2}, \tag{B.17a}$$

$$B = 0.406 - \frac{0.9121}{\ln \xi^{-1}} + \frac{0.7804}{\left(\ln \xi^{-1}\right)^2}, \tag{B.17b}$$

$$G = 2\xi + 1.8\xi^2 \ln \xi - 4\xi^2, \tag{B.17c}$$

$$H = 0.402 - \frac{0.532}{\ln \xi}, \tag{B.17d}$$

where $\xi = r - 2$.

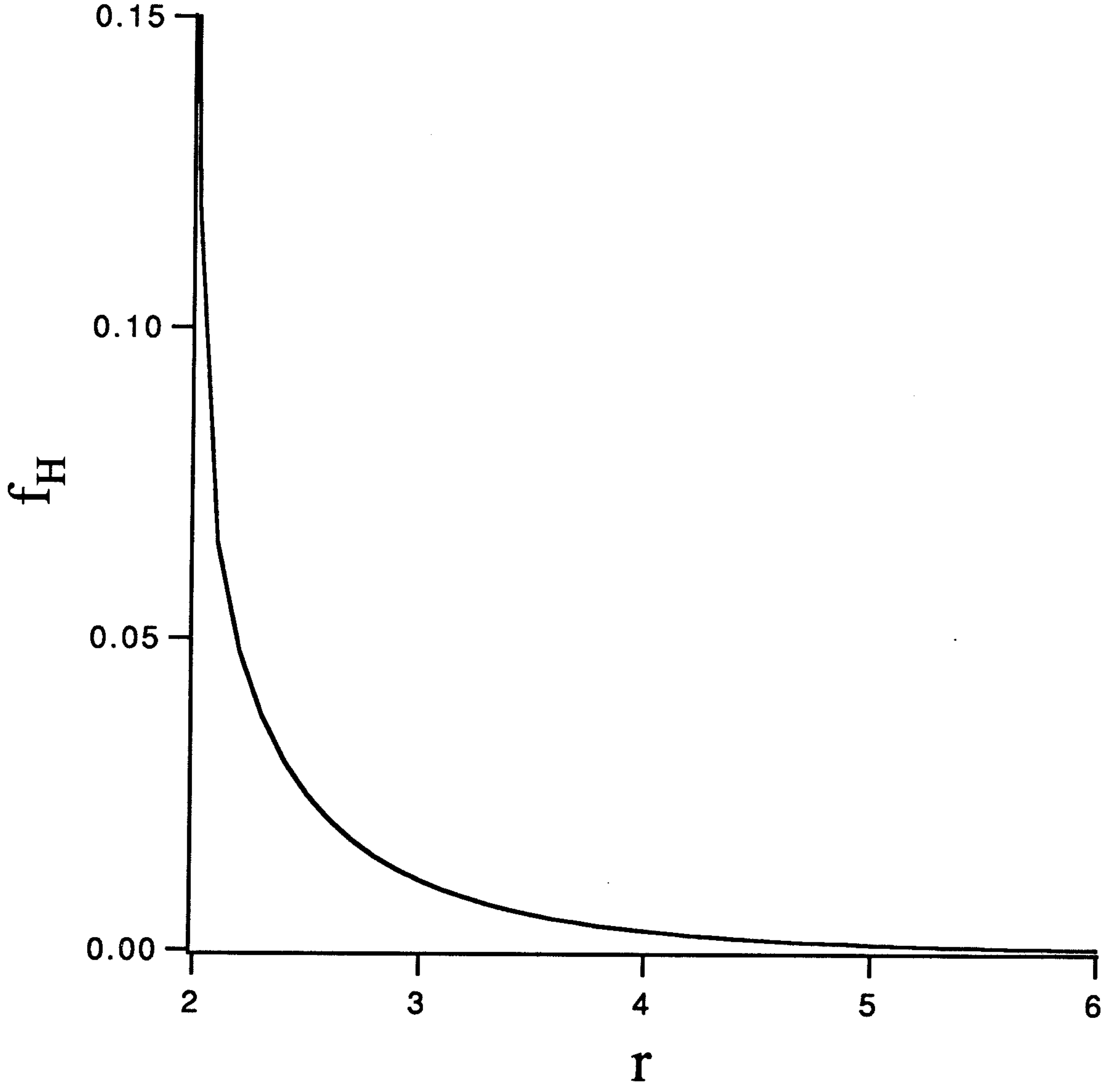

Figure (B.1)

Homogeneous solution of Equation (B.8) describing the low-Pe disturbance to the Stokesian dynamics dumbbell distribution function in steady shear.

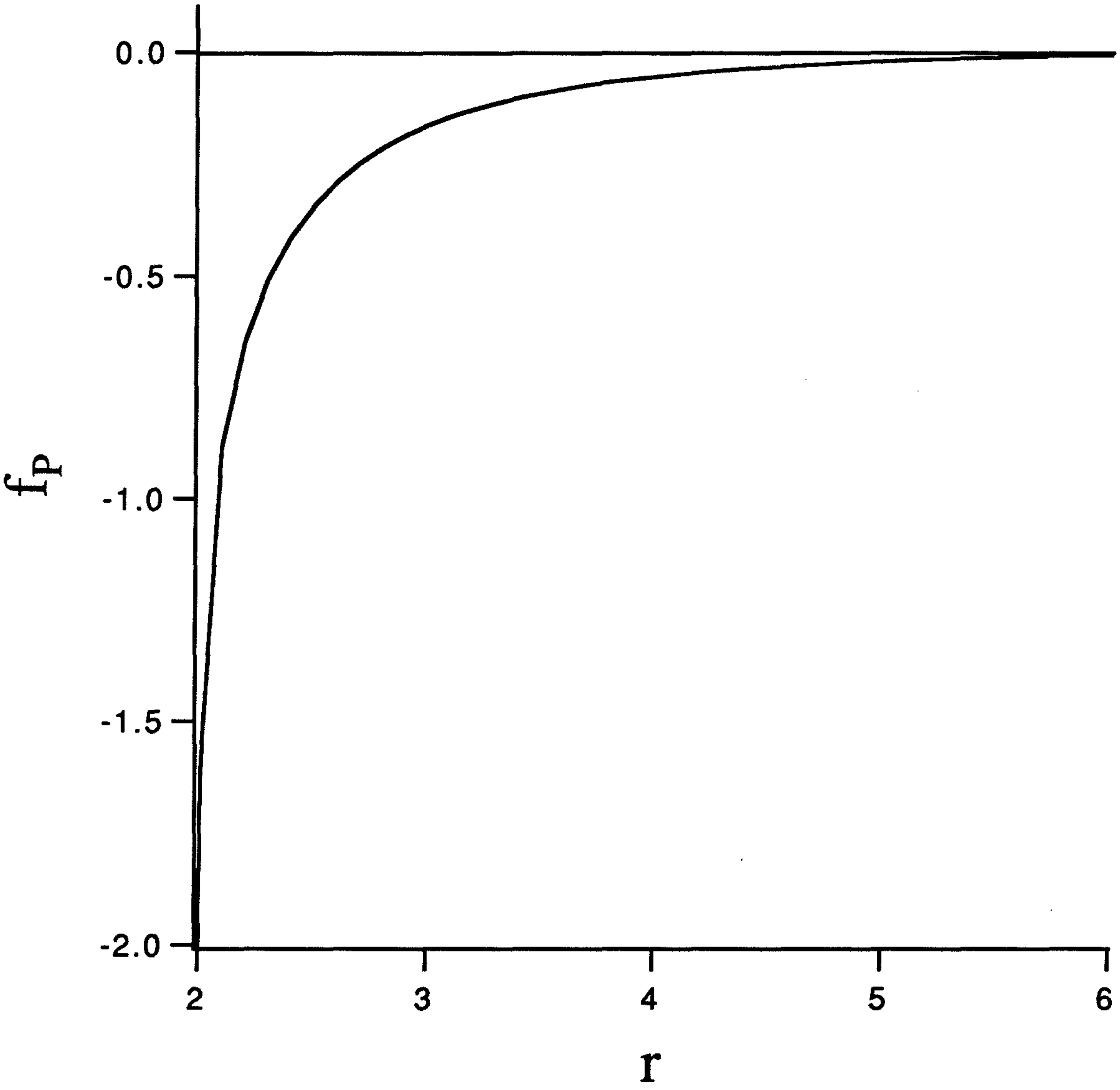

Figure (B.2)

Particular solution of Equation (B.8) describing the low-Pe disturbance to the Stokesian dynamics dumbbell distribution function in steady shear.

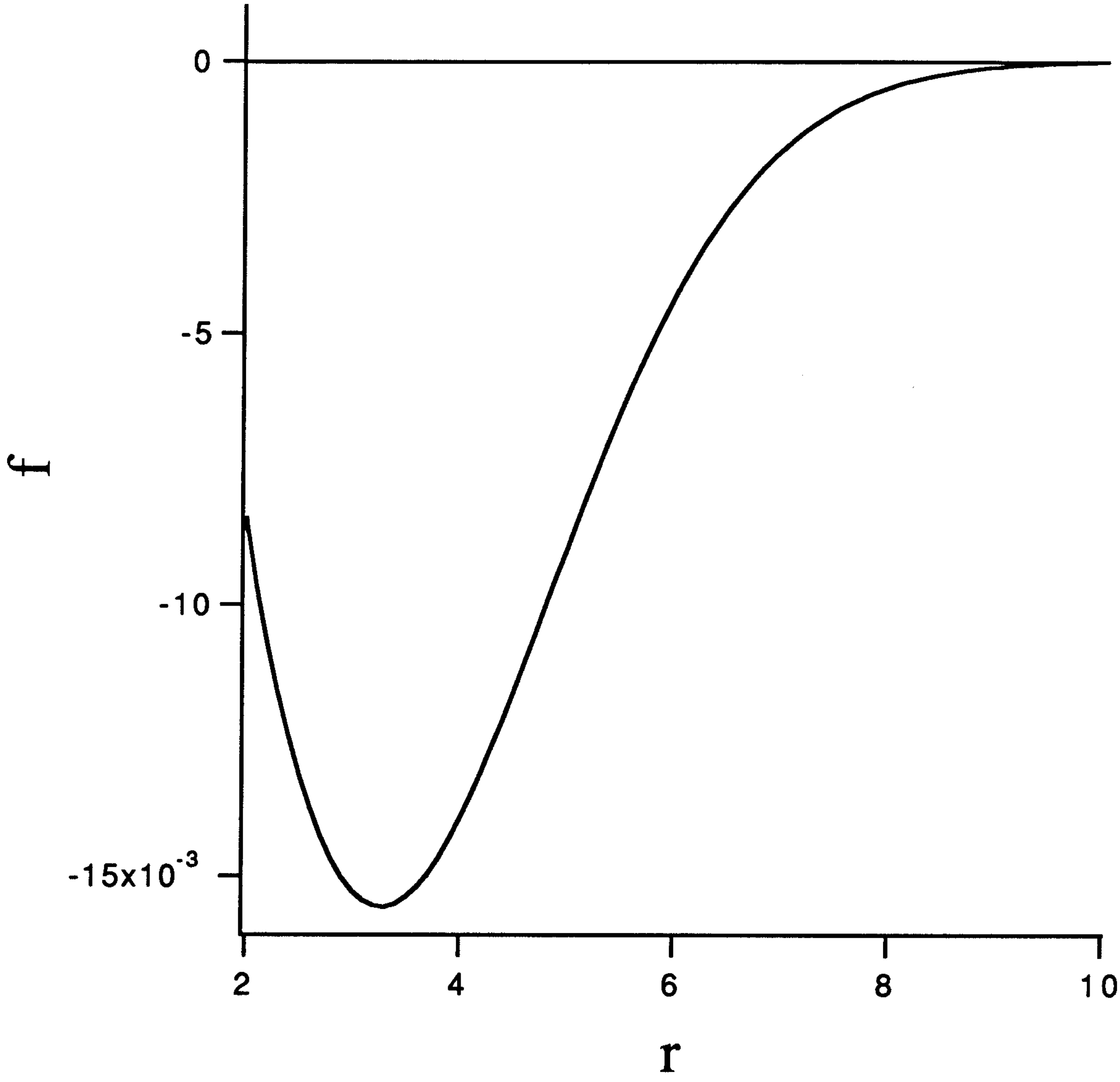

Figure (B.3)

Complete solution of Equation (B.8) describing the low-Pe disturbance to the Stokesian dynamics dumbbell distribution function in steady shear.

APPENDIX C

Calculation of $\nabla \cdot \mathbf{R}_{FU}^{-1}$ for Brownian motion

$\nabla \cdot \mathbf{R}_{FU}^{-1}$ is needed for the calculation of the Brownian-displacement term in Stokesian dynamics, Eq.(2.29*a*). $\mathbf{R}_{FU}^{-1}$ does not exist in analytical form, so the divergence is calculated using the identity

$$\nabla \cdot \mathbf{R}_{FU}^{-1} = -\mathbf{R}_{FU}^{-1} \cdot \nabla \mathbf{R}_{FU} : \mathbf{R}_{FU}^{-1}, \tag{C.1}$$

or using index notation,

$$\frac{\partial R_{ij}^{-1}}{\partial x_j} = -R_{ij}^{-1} \frac{\partial R_{jk}}{\partial x_l} R_{kl}^{-1}. \tag{C.2}$$

$\mathbf{R}_{FU}$ also does not exist in a closed form. It must be extracted from

$$\mathcal{R} = \mathcal{M}^{-1} + \mathcal{R}_{lub} = \begin{pmatrix} \mathbf{R}_{FU} & \mathbf{R}_{FE} \\ \mathbf{R}_{SU} & \mathbf{R}_{SE} \end{pmatrix}, \tag{C.3}$$

where $\mathcal{M}$ is the $11N \times 11N$ grand mobility matrix defined in Eq.(2.36) and $\mathcal{R}_{lub} = \mathbf{R}_{2b} - \mathbf{R}_{2b}^{\infty}$ from Eq.(2.38). Hence, the solution requires the calculation of

$$\nabla \mathcal{R} = \nabla \mathcal{M}^{-1} + \nabla \mathcal{R}_{lub}, \tag{C.4}$$

of which the $\mathbf{R}_{FU}$ portion is used. However, $\nabla \mathcal{M}^{-1}$ is not known analytically either, but must be calculated using the identity

$$\nabla \mathcal{M}^{-1} = -\mathcal{M}^{-1} \cdot \nabla \mathcal{M} \cdot \mathcal{M}^{-1}, \tag{C.5}$$

which, using index notation, is

$$\frac{\partial \mathcal{M}_{jk}^{-1}}{\partial x_l} = -\mathcal{M}_{jn}^{-1} \frac{\partial \mathcal{M}_{np}}{\partial x_l} \mathcal{M}_{pk}^{-1}. \tag{C.6}$$

Thus, the final result is

$$\begin{aligned}\nabla \cdot \mathbf{R}_{FU}^{-1} &= \frac{\partial R_{ij}^{-1}}{\partial x_j} \\ &= -R_{ij}^{-1} \frac{\partial R_{jk}}{\partial x_l} R_{kl}^{-1} \\ &= -R_{ij}^{-1} \left[-M_{jm}^{-1} \frac{\partial M_{mp}}{\partial x_l} M_{pk}^{-1} + \frac{\partial R_{jk}^{lub}}{\partial x_l} \right] R_{kl}^{-1} . \qquad \text{(C.7)}\end{aligned}$$

As it stands, this calculation of $\partial R_{ij}^{-1}/\partial x_j$ is an $O(N^6)$ operation, which is unacceptable. It is broken down into separate operations, none of which are larger than $O(N^3)$. Also note that although i, j, k and l in (C.7) range from $1 - 6N$, the use of $\mathcal{M}^{-1}$ in calculating $\mathbf{R}_{FU}$ requires that m and p range from $1 - 11N$; i.e., the full FTS mobility matrix must be used.

Start with the $\mathcal{M}^{-1}$ portion. Define vectors **A** and **T** and matrix **Q** as follows:

$$A_i = R_{ij}^{-1} \mathcal{M}_{jm}^{-1} \frac{\partial \mathcal{M}_{mp}}{\partial x_l} \mathcal{M}_{pk}^{-1} R_{kl}^{-1}, \qquad \text{(C.8)}$$

$$Q_{im} = R_{ij}^{-1} \mathcal{M}_{jm}^{-1} \quad , \quad (O(N^3)) \qquad \text{(C.9)}$$

and similarly,

$$Q_{lp} = \mathcal{M}_{pk}^{-1} R_{kl}^{-1} . \qquad \text{(C.10)}$$

Thus,

$$A_i = Q_{im} \frac{\partial \mathcal{M}_{mp}}{\partial x_l} Q_{lp} . \qquad \text{(C.11)}$$

Now define

$$\hat{T}_m = \frac{\partial \mathcal{M}_{mp}}{\partial x_l} Q_{lp} \quad , \quad (O(N^3)) \qquad \text{(C.12)}$$

which gives the final result for the $\mathcal{M}^{-1}$ portion,

$$A_i = Q_{im} \hat{T}_m \quad . \quad (O(N^2)) \qquad \text{(C.13)}$$

For the $\mathbf{R}^{lub}$ portion, define vectors **B** and **P** as

$$B_i = -R_{ij}^{-1} \frac{\partial R_{jk}^{lub}}{\partial x_l} R_{kl}^{-1}, \qquad \text{(C.14)}$$

and

$$P_j = \frac{\partial R^{lub}_{jk}}{\partial x_l} R^{-1}_{kl} \quad , \quad \big(O(N^3)\big) \tag{C.15}$$

thus,

$$B_i = -R^{-1}_{ij} P_j \quad . \quad \big(O(N^2)\big) \tag{C.16}$$

So $\nabla \cdot R^{-1}_{ij}$ is formed by

$$\frac{\partial R^{-1}_{ij}}{\partial x_j} = A_i + B_i. \tag{C.17}$$

APPENDIX D

Calculation of $\nabla \cdot \left(\mathbf{R}_{SU} \cdot \mathbf{R}_{FU}^{-1}\right)$ for Brownian Stress

For Brownian stress, $\nabla \cdot \left(\mathbf{R}_{SU} \cdot \mathbf{R}_{FU}^{-1}\right)$ is required, given by

$$\left\{\nabla \cdot \left(\mathbf{R}_{SU} \cdot \mathbf{R}_{FU}^{-1}\right)\right\}_i = \frac{\partial (R_{SU})_{ij}}{\partial x_k} \left(R_{FU}^{-1}\right)_{jk} + (R_{SU})_{ij} \frac{\partial \left(R_{FU}^{-1}\right)_{jk}}{\partial x_k}, \tag{D.1}$$

where the $\partial \left(R_{FU}^{-1}\right)_{jk} / \partial x_k$ term in brackets has already been calculated in Appendix C. As in Appendix C, the divergence term is broken down into a mobility and a lubrication portion,

$$\frac{\partial (R_{SU})_{ij}}{\partial x_k} = \frac{\partial}{\partial x_k} \left[\mathcal{M}_{ij}^{-1} + R_{ij}^{lub}\right], \tag{D.2a}$$

$$= -\mathcal{M}_{im}^{-1} \frac{\partial \mathcal{M}_{mp}}{\partial x_k} \mathcal{M}_{pj}^{-1} + \frac{\partial R_{ij}^{lub}}{\partial x_k}, \tag{D.2b}$$

where only the SU terms are kept in Eq.(D.2). As with the Brownian-displacement calculation, the full Brownian-stress calculation is broken into several steps, none of which require more than $O(N^3)$ operations. The full expression is

$$\left\{\nabla \cdot \left(\mathbf{R}_{SU} \cdot \mathbf{R}_{FU}^{-1}\right)\right\}_i =$$

$$\left[-\mathcal{M}_{im}^{-1} \frac{\partial \mathcal{M}_{mp}}{\partial x_k} \mathcal{M}_{pj}^{-1} + \frac{\partial R_{ij}^{lub}}{\partial x_k}\right]^{SU} (R_{FU})_{jk}^{-1} + (R_{SU})_{ij} \frac{\partial \left(R_{FU}^{-1}\right)_{jk}}{\partial x_k}. \tag{D.3}$$

Note that $i = 1, 5N$, m and $p = 1, 11N$, and j and $k = 1, 6N$. From Appendix C,

$$\hat{T}_m = \frac{\partial \mathcal{M}_{mp}}{\partial x_k} \mathcal{M}_{pj}^{-1} \left(R_{FU}^{-1}\right)_{jk}^{-1} \quad . \quad (O(N^3)) \tag{D.4}$$

Now introduce vectors $\hat{\mathbf{A}}$, $\hat{\mathbf{B}}$ and $\hat{\mathbf{C}}$:

$$\hat{A}_i = -\mathcal{M}_{im}\hat{T}_m \quad , \quad \left(O(N^2)\right) \tag{D.5}$$

$$\hat{B}_i = \frac{\partial \left(R^{lub}_{SU}\right)_{ij}}{\partial x_k} \left(R^{-1}_{FU}\right)_{jk} \quad , \quad \left(O(N^3)\right) \tag{D.6}$$

$$\hat{C}_i = \left(R_{SU}\right)_{ij} \frac{\partial \left(R^{-1}_{FU}\right)_{jk}}{\partial x_k} \quad . \quad \left(O(N^2)\right) \tag{D.7}$$

Eqs.(D.5), (D.6) and (D.7) are combined to give

$$\left\{\nabla \cdot \left(\mathbf{R}_{SU} \cdot \mathbf{R}^{-1}_{FU}\right)\right\}_i \quad = \quad \hat{A}_i + \hat{B}_i + \hat{C}_i. \tag{D.8}$$

REFERENCES

Batchelor, G.K. 1970 The stress system in a suspension of force-free particles. *J. Fluid Mech.* **41**, 545-570.

Batchelor, G.K. 1972 Sedimentation in a dilute dispersion of spheres. *J. Fluid Mech.* **52**, 245-268.

Batchelor, G.K. and Green, J. T. 1972 The hydrodynamic interaction of two small freely-moving spheres in a linear flow field. *J. Fluid Mech.* **56**, 375-400.

Batchelor, G.K. 1976 Brownian diffusion of particles with hydrodynamic interaction. *J. Fluid Mech.* **74**, 1-29.

Batchelor, G.K. 1977 The effect of Brownian motion on the bulk stress in a suspension of spherical particles. *J. Fluid Mech.* **83**, 97-117.

Batchelor, G.K. 1982 Sedimentation in a dilute polydisperse system of interacting spheres. Part 1: General theory. *J. Fluid Mech.* **119**, 379-408.

Bird, R. B. and Curtiss, C. F. 1985 Molecular theory expressions for the stress tensor in flowing polymeric liquids. *J. Poly. Sci.; Polym. Symp. 73.*, 187-199.

Bird, R. B., Armstrong, R. C. and Hassager, O. 1987 *Dynamics of Polymeric Liquids, Vol. I, Fluid Mechanics.* J. Wiley and Sons, New York.

Bird, R. B., Curtiss, C. F., Armstrong, R. C. and Hassager, O. 1987 *Dynamics of Polymeric Liquids, Vol. II, Kinetic Theory.* J. Wiley and Sons, New York.

Bird, R. B. and Wiest, J. M 1984 Anisotropic effects in dumbbell kinetic theory. *J. Rheol.* **29**, 519-532.

Bossis, G. and Brady, J.F. 1984 Dynamic simulation of sheared suspensions. I. General Method. *J. Chem. Phys.* **80**, 5141-5154.

Bossis, G. and Brady, J. F. 1987 Self-diffusion of Brownian particles in concentrated suspensions under shear. *J. Chem. Phys.* **87**, 5437-5448.

Bossis, G., Brady, J. F. and Mathis, C. 1988 Shear-induced structure in colloidal suspensions. I. Numerical Simulation. *J. Colloid Interface Sci.* **126**, 1-15

Brady, J. F. and Bossis, G. 1988 Stokesian dynamics. *Ann. Rev. Fluid Mech.* **20**, 111-157.

Brady, J.F., Phillips, R.J., Lester, J.C. and Bossis G. 1988 Dynamic simulation of hydrodynamically interacting suspensions. *J. Fluid Mech.* **195**, 257-280.

Brenner, H. and O'Neill, M.E. 1972 On the Stokes resistance of multiparticle systems in a linear shear field. *Chem. Eng. Sci.* **27**, 1421-1439.

Debye, P. and Bueche, A. M. 1948 Intrinsic viscosity, diffusion, and sedimentation rate of polymers in solution. *J. Chem. Phys.* **16**, 573-579.

Durlofsky, L., Brady, J. F. and Bossis, G. 1987 Dynamic simulation of hydrodynamically interacting particles. *J. Fluid Mech.* **180**, 21-49.

Ermak, D.L. and McCammon, J.A. 1978 Brownian dynamics with hydrodynamic interactions. *J. Chem. Phys.* **69**, 1352-1360.

Ferry, J. D., 1980 *Viscoelastic Properties of Polymers.* J. Wiley and Sons, New York.

Fixman, M. 1981 Inclusion of hydrodynamic interaction in polymer dynamical simulations. *Macromolecules* **14**, 1710-1717.

Hinch, E. J. 1975 Application of the Langevin equation to fluid mechanics. *J. Fluid. Mech.* **72**, 499-511.

Huggins, M. L. 1939 The viscosity of dilute solutions of long-chain molecules. II. *J. Phys. Chem.* **43**, 439-456.

Jeffrey, D. J. and Onishi, Y. 1984 Calculation of the resistance and mobility functions for two unequal rigid spheres in low-Reynolds-number flow. *J. Fluid Mech.* **139**, 261-290.

Kramers, H. A. 1946 The behavior of macromolecules in inhomogeneous flow. *J. Chem. Phys.* **14**, 415-424.

Kim, S. and Mifflin, R.T. 1985 The resistance and mobility functions of two equal spheres in low-Reynolds-number flow. *Phys. Fluids* **28**, 2033-2045.

Kirkwood, J. G., 1967 *Macromolecules.* Gordon and Breach, New York.

Kirkwood, J. G. and Riseman, J. 1948 The intrinsic viscosities and diffusion constants of flexible macromolecules in solution. *J. Chem. Phys.* **16**, 565-573.

Kuhn, W. 1932 Über teilchenform und teilchengrösse aus viscosität und strömungsdoppelbrechung. *Zeits. f. Phys. Chem.* **161**, 1-32.

Lin, C. J., Lee, K. J. and Sather, N.F. 1970 Slow motion of two spheres in a shear field. *J. Fluid Mech.* **43**,35-47.

Liu, T. W. and Öttinger, H. C. 1987 Bead-spring rings with hydrodynamic interaction. *J. Chem. Phys.* **87**, 3131-3136.

Lodge, A. S. and Wu, Y. 1971 Constitutive equations for polymer solutions derived from the bead/spring model of Rouse and Zimm. *Rheol. Acta* **10**, 539-553.

Miller, M. L. 1966 *The Structure of Polymers.* Reinhold, New York.

O'Brien, R. W. 1979 A method for the calculation of the effective transport properties of suspensions of interacting particles. *J. Fluid Mech.* **91**, 17-39.

Onuki, A. and Doi, M. 1986 Flow birefringence and dichroism of polymers. I. General theory and application to the dilute case *J. Chem. Phys.* **85**, 1190-1197.

Öttinger, H. C. 1985 Consistently averaged hydrodynamic interaction for Rouse dumbbells in steady shear flow. *J. Chem. Phys.* **83**, 6535-6536.

Öttinger, H. C. 1986*a* Consistently averaged hydrodynamic interaction for Rouse dumbbells. Series expansions. *J. Chem. Phys.* **84**, 4068-4073.

Öttinger, H. C. 1986*b* Consistently averaged hydrodynamic interaction for Rouse dumbbells. The rheological equation of state. *J. Chem. Phys.* **85**, 1669-1671.

Öttinger, H. C. 1987 Consistently averaged hydrodynamic interaction for Rouse dumbbells. Translational diffusivity. *J. Chem. Phys.* **87**, 6185-6190.

Öttinger, H. C. 1989 Gaussian approximation for Rouse chains with hydrodynamic interaction. *J. Chem. Phys.* **90**, 463-473.

Öttinger, H. C. 1987 Translational diffusivity from the Zimm model. *J. Chem. Phys.* **87**, 3156-3165.

Phillips, R. 1986 (private communication).

Phung, T. 1991 (private communication).

Pyun, C. W. and Fixman, M. 1965 Intrinsic viscosity of polymer chains. *J. Chem. Phys.* **42**, 3838-3844.

Pyun, C. W. and Fixman, M. 1966 Perturbation theory of the intrinsic viscosity of polymer chains. *J. Chem. Phys.* **44**, 2107-2115.

Rallison, J.M. and Hinch, J. 1986 The effect of particle interactions on dynamic light scattering from a dilute suspension. *J. Fluid Mech.* **167**, 131-168.

Russel, W. B. 1981 Brownian motion of small particles suspended in liquids. *Ann. Rev. Fluid Mech.* **13**, 425-455.

Russel, W. B. and Gast, A. 1986 Nonequilibrium statistical mechanics of concentrated colloidal dispersions: Hard spheres in weak flows. *J. Chem. Phys.* **84**, 1815-1826.

Rouse, P.E. 1953 A theory of the linear viscoelastic properties of dilute solutions of coiling polymers. *J. Chem. Phys.* **21**,1272-1280.

Staudinger, H. 1932 *Die Hochmolecularen Organischen Verbindungen.* Verlag Julius Springer, Berlin.

Thurston, G. B. and Morrison, J. D. 1969 Eigenvalues and the intrinsic viscosity of short Gaussian chains. *Polymer* **10**, 421-438.

Wiest, J. M., Wedgewood, L. E. and Bird, R. B. 1989 On coil-stretch transitions in dilute polymer solutions. *J. Chem. Phys.* **90**, 587-594.

Yoon, B. J. and Kim, S. 1987 Note on the direct calculation of mobility functions for two equal-sized spheres in Stokes flow. *J. Fluid Mech.* **185**, 437-446.

Zimm, B. H. 1956 Dynamics of polymer molecules in dilute solution: viscoelasticity, flow birefringence and dielectric loss. *J. Chem. Phys.* **24**, 269-278.

Zylka, W. and Öttinger, H.C. 1989 A comparison between simulations and various approximations for Hookean dumbbells with hydrodynamics interaction. *J. Chem. Phys.* **90**, 474-480.

Zylka, W. 1991 Gaussian approximation and Brownian dynamics simulations for Rouse chains with hydrodynamic interaction undergoing simple shear flow. *J. Chem. Phys.* **94**, 4628-4636.